

UCLA

UCLA Electronic Theses and Dissertations

Title

Design of Electrically Small Loop Antennas with Wide-Band Frequency Tuning Capability to Facilitate Mars Exploration

Permalink

<https://escholarship.org/uc/item/9qv4p25b>

Author

Cai, Yubin

Publication Date

2019

Peer reviewed|Thesis/dissertation

UNIVERSITY OF CALIFORNIA

Los Angeles

Design of Electrically Small Loop Antennas with Wide-Band Frequency Tuning Capability
to Facilitate Mars Exploration

A thesis submitted in partial satisfaction
of the requirements for the degree
Master of Science in Electrical and Computer Engineering

by

Yubin Cai

2019

© Copyright by
Yubin Cai
2019

ABSTRACT OF THE THESIS

Design of Electrically Small Loop Antennas with Wide-Band Frequency Tuning Capability
to Facilitate Mars Exploration

by

Yubin Cai

Master of Science in Electrical and Computer Engineering

University of California, Los Angeles, 2019

Professor Yahya Rahmat-Samii, Chair

For decades, it was believed that the Martian subsurface contains no liquid water but only shallow ground ice. Nevertheless, over the past few years scientists have been discovering on Mars new evidence of liquid water, which is an essential ingredient for life. Post processing high-resolution pictures taken by NASA's Mars Reconnaissance Orbiter (MRO) revealed sheets of water ice located in the Martian subsurface. To obtain the dielectric spectroscopy of these potential water bodies, a demand has arisen for electrically small loop antennas that can be used on the broadband dielectric spectrometer for future Mars rover missions. The hope among the scientific community is that by sweeping the frequencies of the transmitting electromagnetic waves from 0.8 to 10MHz, the presence of water and hydrated minerals can leave some signature in the reflected wave.

To provide the scientists with the "ears" to listen to the flow of water underneath the Martian surface, proposed in this work are two novel electrically small loop antenna designs for 0.8-10MHz wide-band operation: a single-turn loop antenna with a continuous mechanical frequency tuning capability (Chapter 2) and a reconfigurable multi-turn loop antenna with an electrical frequency tuning capability (Chapter 3). The usage of lumped elements, RF MEMS switch, varactor diodes, transformers, and RF balun in the realm of small antenna designs is investigated. Prototypes have been fabricated, tested and measured (Chapter 4).

The thesis of Yubin Cai is approved.

Jonathan Chau-Yan Kao

Yuanxun Ethan Wang

Yahya Rahmat-Samii, Committee Chair

University of California, Los Angeles

2019

*To the memory of my grandfather, without whom I would have never been enlightened to
be an engineer.*

TABLE OF CONTENTS

1	Introduction	1
1.1	Background	1
1.2	Design Overview and Challenges	3
1.2.1	Research Goals and Requirements	3
1.2.2	Proposed Designs	4
2	Single-Turn Electrically Small Loop Antennas with Mechanical Frequency Tuning Capability	6
2.1	Overview	6
2.2	Design Specifications	7
2.2.1	Radiation Characteristics of Single-Turn Small Loops	8
2.2.2	Equivalent Circuit Model	9
2.3	Narrow-band Impedance Matching Network Design	11
2.3.1	T-type Impedance Matching Network	11
2.3.2	Equivalent Circuit Model of Matched Electrically Small Loop	12
2.3.3	Continuous Frequency Tuning	13
2.4	Near-field Electric Field and Magnetic Field of an Electrically Small Single-turn Loop Antenna at 1MHz	15
2.4.1	Analytic Solution	15
2.4.2	Modification of Analytical Solution	19
2.5	Two Single-turn Loop Antennas	22
2.5.1	Decoupling Technique	22
2.5.2	S-12 Performance with loading	24

2.6	Required Tuning Capacitance Reduction	27
2.6.1	Methodology	28
2.6.2	Switchable Varactor Banks Methodology	29
2.7	Copper Tube Single-Turn Loop Antenna	31
3	Reconfigurable Multi-Turn Electrically Small Loop Antennas with Elec-	
	trical Frequency Tuning Capability	35
3.1	Motivations	35
3.2	Design Specifications	36
3.2.1	Loop Antenna Design	36
3.2.2	Resonant Frequency Tuning	39
3.3	Switching Technologies	41
3.3.1	Overview	41
3.3.2	MEMS Switch	42
3.3.3	MEMS Switch Integration	44
3.4	Impedance Matching network Design	46
3.4.1	Transmission-Line Transformers	48
3.4.2	Varactors and Biasing Structure	52
3.5	Near-field Electric Field and Magnetic Field of an Electrically Small Multi-	
	turn Loop Antenna at 1MHz	59
4	Fabrication and Measurements	63
4.1	Single-Turn Electrically Small Loop Antennas with Mechanical Frequency	
	Tuning Capability	63
4.1.1	Single Loop Antenna	63
4.1.2	Two Loop Antennas	65

4.2	Reconfigurable Multi-Turn Electrically Small Loop Antennas with Electrical Frequency Tuning Capability	68
4.2.1	Measurement Using Fixed Capacitors as the Tuning Element	69
4.2.2	Measurement on the Reconfigurable Multi-Turn Loop Antenna Using Varactors	71
5	Conclusions and Future Works	75
A	Transformer Fabrication	77
B	Efforts Toward Directional Radiation Pattern	80
	References	100

LIST OF FIGURES

1.1	Images of Mars and Martian mantle decomposition[6]	2
1.2	Demonstration of where the loop antennas are mounted on the Mars rover and an overview of the two proposed loop antenna designs.	4
2.1	A loop antenna that can operate from 0.8 to 10 MHz by tuning C_r and C_m values (antenna material: copper, $w = 1m$, $a = 2cm$, $l = 4cm$, $d = 2cm$, $t = 25.4\mu m$). Not-true-to-scale illustrative view of the geometry, (a) top view, (b) side view. (c) Fabricated prototype of the proposed electrically small loop antenna.	6
2.2	Methodology road map of arriving at the single-turn loop antenna design.	7
2.3	CST full-wave electromagnetic simulation generated and analytical input impedance of a square 1m by 1m electrically small loop antenna (a) resistance, (b) reactance, and (c) impedance as plotted on the smith chart.	10
2.4	The circuit model of the small loop antenna including the radiation and ohmic loss resistance (R_r , R_L), the loop and internal inductance (L_A , L_i). The inductor L_r , and capacitors C_r , C_m form a T matching network.	11
2.5	The measured inductance and equivalent series resistance (ESR) of a 1000nH and a 380nH inductors in series. The measured inductance in the range of 1317.9nH to 1473.9nH and the measured ESR is in the range of 1.4Ω to 4.1Ω	12
2.6	The required C_r and C_m values from 0.8 to 10 MHz fitted by 5th order polynomial functions. Sampled frequency points at 1 — 10 MHz are achieved through CST simulation. It is noted that at 0.8 MHz and 1 MHz C_m is shorted, so they are not shown in the figure. The positioning of the C_r , C_m and L_r along the loop is shown.	14
2.7	Coordinate system of a square loop aligned along the xy plane and perpendicular to the z axis [1].	15

2.8	Six-meter deep near-field electric and magnetic fields of the single-turn loop antenna in free space at 1MHz. The black and white hollow squares in the figure show the position of the loop antenna relative to the observation window along an xy-plane. Electric field: (a) analytical solution, (b) CST simulation. Magnetic field: (c) analytical solution, (d) CST simulation.	18
2.9	Current non-uniformity along the feed lines of the proposed loop antenna and modified analytic model.	19
2.10	Six-meter deep near-field electric and magnetic fields of the single-turn loop antenna in free space at 1MHz using modified analytic model. The black hollow square in the figure shows the position of the loop antenna relative to the observation window along an xy-plane. (a) electric field (b) magnetic field.	20
2.11	Three-meter deep near-field electric and magnetic fields of the single-turn loop antenna in free space at 1MHz using modified analytic model compared with using CST simulation. The black and white hollow squares in the figure show the position of the loop antenna relative to the observation window along an xy-plane. Electric field: (a) modified analytical solution, (b) CST simulation. Magnetic field: (c) modified analytical solution, (d) CST simulation.	21
2.12	S11 and S21 performance of two single-turn loop antennas in vacuum. The top view of the two loops' positions and port 1 and port 2 positions are illustrated in pictures. Two loops separated by 20 cm: (a) S11 comparison between the two loops case and the one loop case, and (b) S11 and 21 of the two loops case. Two loops overlapped by 12 cm, (a) S11 comparison between the two loops case and the one loop case, and (b) S11 and 21 of the two loops case.	23
2.13	S12 of the two loop antennas separated by 20 cm with loading of (b) a sand box or (c) a gypsum box.	25
2.14	S12 of the two loop antennas overlapped with loading of (b) a sand box or (c) a gypsum box.	26

2.15	Design overview of three frequency tuning schemes that help reduce the required tuning capacitance range of T-type impedance matching network for a electrically small single-turn loop antenna.	27
2.16	Operation details of how to use a MEMS switch to switch between varactor banks, which have a collective variable capacitance range that encompasses the tuning capacitance range required for design #3.	30
2.17	(a) New geometry of the single-turn loop antenna with a copper tube as the conducting material. (b) a closed-up view of the cross section of the copper tube. (c) the curvature characterization of the bending along the corners of the original square loop.	32
2.18	Pictorial illustrations of the modelling of the loop antenna in the CST simulation and the construction of the loop antenna at the lumped element positions. . . .	33
3.1	State of the art highlights of electrically small loop antennas with linear frequency response and their respective problems with respect to this work’s application. [8, 9, 10]	36
3.2	UCLA prototype photo and pictorial overview of the proposed reconfigurable multi-turn loop antenna design with a novel continuous electrical frequency tuning capability	37
3.3	Single-turn and three-turn loop antennas design with the approximated inductance and loop perimeters equivalent to the wavelength at 1, 5 and 10MHz	38
3.4	Series capacitance needed to resonate the three-turn and the single-turn loop antennas to the corresponding resonance frequency. The maximum-to-minimum capacitance ratio is shown on the figure.	39
3.5	RF MEMS switch ADGM1004 from Analog Device, Inc. Inc, (a) picture of the MEMS switch and on resistance and off capacitance reported in the data sheet, and (c) The measured off capacitance using Agilent 4294A impedance analyzer by UCLA.	42

3.6	The operation of the MEMS switch. The top and the bottom cases show the switch turned off, while the middle state shows the switch turned on[13]	43
3.7	A wideband frequency reconfigurable electrically small multi-turn loop antenna (a) fabricated prototype lying on a simplified PVC Mars rover, (b) dual-mode configurations and zoom-in view of how MEMS switch controls the current flow, and (c) MEMS switch generalized circuit model.	45
3.8	Series capacitance C_m required to resonate the proposed electrically small multi-turn loop antenna design in the multi-turn mode operating through 0.8 — 3MHz, single-turn mode operating through 3 — 10MHz, and a simple single-turn 1m by 1m loop antenna through the entire bandwidth.	46
3.9	Schematic of the proposed impedance matching network.	47
3.10	Transmission-Line transformer, (a) basic building block of transmission-line transformer, (b) 7-turn bifilar 1:4 transmission-line impedance transformer, and (c) 14-turn 1:1 transmission-line transformer or current RF Balun	48
3.11	1:4 transmission-line impedance transformer voltage and current analysis using the basic building block in Figure 3.10(a). The circuit model is derived from [15].	50
3.12	Design curves for choosing the wire’s diameter and number of twists per inch. (a) Characteristic impedance of bifilar wire based on MLW583 wire dimensions, and (b) bifilar transmission-line twist per inch in terms of the pitch angle [19]	52
3.13	Schematic of the proposed impedance matching network incorporating electrically tuned varactors and specialized low-insertion-loss biasing structure.	53
3.14	Advanced Design System (ADS) simulation of the proposed impedance matching network incorporating varactors and biasing structure, considering only ideal transformers. (a) schematic, and (b) S11 simulation results with different multi-turn and single-turn mode antenna’s impedance.	54

3.15	Simplified schematic of the proposed use of varactors and design of a varactor biasing structure. L_loop and R_loop comprise the input impedance of the loop antenna. The nodal voltages and current values are labeled as tag and arrows.	56
3.16	Observation window illustrations of the near-field electric and magnetic fields at 1MHz. The proposed reconfigurable multi-turn electrically small loop antennas with electrical frequency tuning capability is observed in air (a) perspective view, and (b) side view and with the presence of sand (a) perspective view, and (b) side view.	60
3.17	Simulated near-field electric and magnetic fields at 1MHz with observation windows shown in Figure 3.16. The white hollow square in the figure shows the position of the loop antenna relative to the observation window along an xy-plane. (a) electric field of the antenna in air, (b) magnetic field of the antenna in air, (c) electric field of the antenna with the presence of sand, and (d) magnetic field of the antenna with the presence of sand.	61
4.1	Fabricated prototype. (a) PVC Mars rover model fabricated by UCLA. (b) Closed-up view of the loop antenna construction and surface mount inductor positioning.	63
4.2	CST simulated and measured S11 comparison of the proposed single-turn loop antenna at 1MHz, 5MHz and 10MHz with different Cr and Cm values.	64
4.3	Measurement setup of two loops separated by 20 cm apart. (a) Overview of the setup, and (b) closed-up view of the separation of the two loops. Flexible coax cables are used for feeding the loop antennas from VNA.	65
4.4	Measurement setup of two loops overlapped by 12 cm. (a) Top view of the setup, and (b) Side view of the setup.	66

4.5	Measurement setup of two loop antennas either separated by 20 cm or overlapped by 12 cm, with a copper hollow box in vicinity. (a) Overview of the copper box, (b) inside of the box, (c) box positioned 26 inches away from one of the loops and (d) box positioned 8.5 inches away from one of the loops.	66
4.6	Simulated and measured S11 and S12 of the case of two loop antennas separated by 20 cm. (a) S11 and (2) S12.	67
4.7	Simulated and measured S11 and S12 of the case of two loop antennas overlapped by 12 cm. (a) S11 and (2) S12.	67
4.8	Overview of the fabricated reconfigurable multi-turn loop antenna and the receiver PCB board using fixed capacitors as the tuning element.	68
4.9	Closed-up view of the MEMS switch, the controller unit, the impedance matching network, and the tuning capacitors. The name of the components are labeled. "TLT" in the figure stands of transmission-line transformers. The implementation corresponds to the schematic shown in Figure 3.9.	69
4.10	(a) Measured S11 of the vertically stacked multi-turn loop antenna in mode 1 and mode 2 with 6 representative C_m values. (b) Illustrations of the current flow along the loop antenna under mode 1 and mode 2.	70
4.11	Schematic of varactors and the biasing network implementation. The load is consisted of three air-core $1\mu H$ inductors in series mimicking the impedance of the antenna in the HF mode. T1 and T2 in the figure are the conventional transformers for DC isolation. Eight Skyworks Solutions, Inc. SMV1801-079LF varactors are used at each one of the two tuning points.	73
4.12	Measured S11 of the setup shown in Figure 4.11. The resonant frequency is electrically tuned through a wide range of frequencies with different bias voltage levels from 0V to 12V.	74

A.1	Winding details of the 1:4 transmission-line transformer. (a) Illustration of the two pairs of 7-turn # 30 AWG bifilar windings on a ferrite core, and (b) corresponding schematic.	77
A.2	Winding details of the RF balun. (a) Illustration of the 14-turn # 30 AWG bifilar winding on a ferrite core, and (b) corresponding schematic.	78
A.3	Sequential steps of fabricating a transformer with an winding optimal layout, using #30 AWG wires and a ferrite core.	79
B.1	Illustration of image theory [1].	81
B.2	Analytical models of an electrically small loop antenna in (a) free space, (b) 30 cm above an infinite PEC plane, and (c) 30 cm above an infinite PMC plane.	81
B.3	CST simulation setups of 6-meter deep 7m-by-7m observation plane. The infinite PEC or PMC plane is implemented in CST by setting electric (tangential $E = 0$) or magnetic (tangential $H = 0$) boundary conditions.	82
B.4	Simulated S11 of an electrically small loop antenna in (a) free space, (b) 30 cm above an infinite PEC plane, and (c) 30 cm above an infinite PMC plane.	82
B.5	Simulated 6-meter deep electric and magnetic fields of an electrically small loop antenna placed 30 cm above an infinite PEC plane.	83
B.6	Simulated 6-meter deep electric and magnetic fields of an electrically small loop antenna placed 30 cm above an infinite PMC plane.	83
B.7	Same-scale comparison of simulated 6-meter deep electric and magnetic fields of an electrically small loop antenna placed in (a) free space, (b) 30 cm above an infinite PEC plane, and (c) 30 cm above an infinite PMC plane.	84
B.8	Pictorial demonstration of the observation planes of electric and magnetic fields in Table B.1	85
B.9	E Field at $Z = +6, +2, -6, -2$ m	87
B.10	H Field at $Z = +6, +2, -6, -2$ m	87

B.11 E Field of the Loop in Air at $Z=+0.3\text{m}$	88
B.12 E Field of the Loop with an Infinite PEC at $Z=+0.3\text{m}$	88
B.13 H Field of the Loop in Air at $Z=+0.3\text{m}$	89
B.14 H Field of the Loop with an Infinite PEC at $Z=+0.3\text{m}$	89
B.15 E Field of the Loop in Air at $Z=+0.15\text{m}$	90
B.16 E Field of the loop with an Infinite PEC at $Z=+0.15\text{m}$	90
B.17 H Field of the Loop in Air at $Z=+0.15\text{m}$	91
B.18 H Field of the loop with an Infinite PEC PEC at $Z=+0.15\text{m}$	91
B.19 CST full-wave electromagnetic simulation setup of a copper tube single-turn loop antenna resonating at 5MHz in the presence of a PEC ground plate. The dimensions of the copper tube are tabulated. The capacitance and inductance used for resonant frequency tuning are also shown.	92
B.20 Simulated fields at 5MHz, zero-phase, with a 21.2m by 21.2m planar observation window. Top window is 6m away from the PEC plate and the bottom window is 6m away from the loop. (a) near-field electric field, and (b) near-field magnetic field.	93
B.21 Simulation setup of a copper tube single-turn loop antenna resonating at 5MHz in the presence of a PEC plate with 18-degree slots. The dimensions of the copper tube are tabulated. The capacitance and inductance used for resonant frequency tuning are also shown.	94
B.22 Simulated S11 comparison of the loop antenna with and without the presence of a PEC plate with slots. Simulation setup is shown in Figure B.21.	95
B.23 Simulated fields at 5MHz with a 21.2m by 21.2m planar observation window. Top window is 6m away from the PEC plate and the bottom window is 6m away from the loop. (a) near-field electric field, and (b) near-field magnetic field.	95

B.24	Simulation setup of a copper tube single-turn loop antenna resonating at 5MHz in the presence of a PEC bottom-open box with 18-degree slots. The dimensions of the copper tube are tabulated. The capacitance and inductance used for resonant frequency tuning are also shown.	96
B.25	Simulated S11 comparison of the loop antenna with and without the presence of a PEC bottom-open box with 18-degree slots. Simulation setup is shown in Figure B.24.	96
B.26	Simulated fields at 5MHz with a 21.2m by 21.2m planar observation window. Top window is 6m away from the PEC box and the bottom window is 6m away from the loop. (a) near-field electric field, and (b) near-field magnetic field.	97
B.27	Simulation setup of a copper tube single-turn loop antenna resonating at 5MHz in the presence of a PEC bottom-open box with 9-degree slots. The dimensions of the copper tube are tabulated. The capacitance and inductance used for resonant frequency tuning are also shown.	98
B.28	Simulated S11 comparison of the loop antenna with and without the presence of a PEC bottom-open box with 9-degree slots. Simulation setup is shown in Figure B.27.	99
B.29	Simulated fields at 5MHz with a 21.2m by 21.2m planar observation window. Top window is 6m away from the PEC box and the bottom window is 6m away from the loop. (a) near-field electric field, and (b) near-field magnetic field.	99

LIST OF TABLES

2.1	Implementation Comparison of Designs to Reduce Tuning Capacitance	28
2.2	Varactor Banks Designed to Cover the Tuning Capacitance of Design #3	29
2.3	Design #3 Detailed Required Tuning Capacitance for 0.8 to 3MHz	29
2.4	Design #3 Detailed Required Tuning Capacitance for 3 to 10MHz	30
2.5	Copper Tube Loop antenna with 1380nH at Lr for 0.8 — 5MHz Operation	34
2.6	Copper Tube Loop antenna with 1380nH at Lr for 6 — 10MHz Operation	34
2.7	Copper Tube Loop antenna with 4*1380nH at Lr for 0.8 — 5MHz Operation	34
2.8	Copper Tube Loop antenna with 4*1380nH at Lr for 6 — 10MHz Operation	34
3.1	Comparison among three major electrical RF switching technologies	41
4.1	Component Usage and S11 Performance of the Measurement	64
4.2	Capacitance vs. Bias Voltage Levels of the Varactors	72
B.1	Electric and Magnetic Fields Comparison	86

ACKNOWLEDGMENTS

Foremost, I would like to express my sincere gratitude to my advisor Prof. Yahya Rahmat-Samii for the continuous support of my M.S. study and research, for his patience, motivation, passion, and profound knowledge. His guidance helped me in all the time of research and writing of this thesis. I could not have imagined having a better advisor and mentor for my M.S. study.

Besides my advisor, I would like to thank the rest of my thesis committee: Professor Yuanxun Ethan Wang, and Professor Jonathan Chau-Yan Kao, for their encouragement, and insightful comments.

I would like to acknowledge fruitful discussions with colleagues at the Jet Propulsion Laboratory (JPL), especially Dr. Soon Sam Kim. This work was supported in part by a grant through the JPL, under a contract with the National Aeronautics and Space Administration (NASA).

I thank my colleagues in the UCLA Antenna Research, Analysis, and Measurement (ARAM) Laboratory: Jordan Budhu, Vignesh Manohar, Lingnan Song, Dustin Brown, Anastasios Papathanasopoulos, and Junbo Wang for the inspiring discussions, for the sleepless nights we were working together before deadlines, and for all the fun we have had in the last three years.

Last but not the least, I would like to thank my family and my girlfriend, for their unconditional love and support.

CHAPTER 1

Introduction

1.1 Background

As one of the most fundamental, and versatile antennas, loop antennas have been widely employed in communication links at a wide range of frequencies below 1GHz since the early time of radio. Loop antennas are conventionally classified as electrically large if the circumference is about a free-space wavelength ($C \approx \lambda$) and electrically small if the overall circumference is less than about one-fifth of a wavelength ($C < \lambda/5$) [1]. Electrically small single-turn loop antennas have a small radiation resistance that is smaller than its ohmic resistance. Thus, they are usually treated as poor radiators with a low radiation efficiency. However, clever impedance matching can ensure full transmission from the feed to the loop antenna and increasing the circumference and the number of turns can increase the radiation resistance. Also, small loops have narrow bandwidth of operation, typical less than 1%, so frequency tuning is required to operate loop antennas throughout a wide bandwidth.

Electrically small loop antennas are commonly used for electromagnetic field probing in the microwave frequency range and amateur radios in the HF (3 - 30 MHz) and the VHF (30 - 300 MHz) bands [1]. A distinguishing feature of electrically small loops is that they are coupled to the magnetic field of the radio wave in the near-field region, as opposed to the electric field that dipoles are coupled to. According to the Faraday's law of induction, the oscillating magnetic field of the incoming radio wave induces a current around the receiving loop antenna. This feature, along with their compactness, are the primary reasons why small loops are desirable for measuring the dielectric properties of a medium [3]. For example, in a 3-Tesla magnetic resonance imaging system, electrically small RF-coils are used to generate

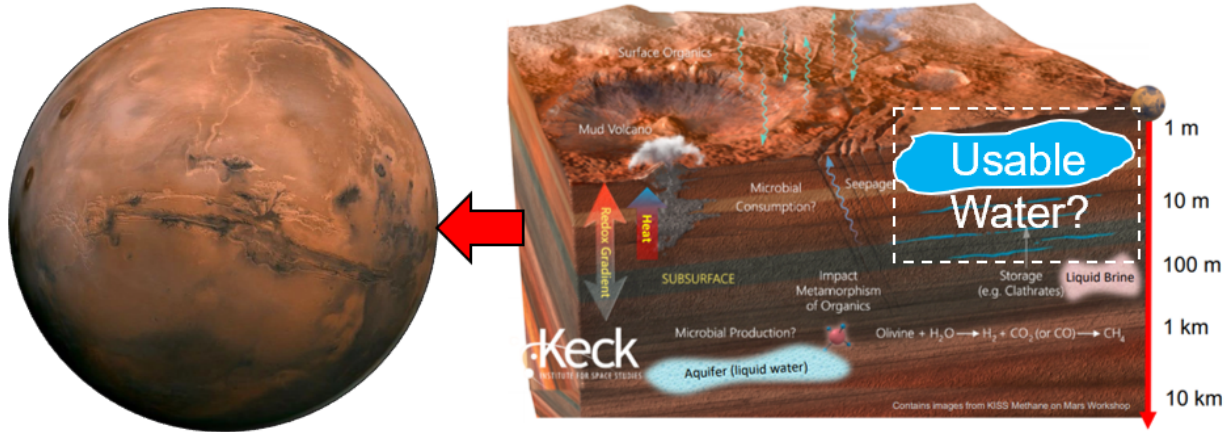


Figure 1.1: Images of Mars and Martian mantle decomposition[6]

an oscillating and rotating magnetic field to excite the water molecules within a human body, and to receive the reflected magnetic resonance (MR) signals. Similarly, electrically small loop antennas are also the winning candidates for the transmitting and receiving antennas on the dielectric spectrometer used for underground water detection [4]; in particular for the interest of this work, water in the Martian subsurface.

Today's desert-like Martian surface is believed to likely hide the presence of water below ground. Researchers post processed pictures taken by the NASA's Mars Reconnaissance Orbiter and found that at eight locations, there are noticeable bluish features that signify the existence of flowing water [2]. The potential water bodies are located as shallow as 1 meter and as deep as 80 meters underneath the ground demonstrated in Fig. 1.1. In addition, scientists at the Jet Propulsion Laboratory discovered that water has a local resonance in its permittivity around 1MHz. It is anticipated that through a broadband dielectric spectrometer, by sweeping the frequencies of the transmitting electromagnetic wave from 0.8—10MHz, the presence of water or hydrated minerals can leave some signature in the reflected EM waves.

In this work, two electrically small loop antenna designs are proposed for the 0.8—10MHz broadband dielectric spectrometer that will potentially equip the next-generation Mars rover. It is critical to stress that the wavelength is in the range of 30 meters to 300 meters, whereas

the potential water bodies are approximately 1 to 80 meters away from the antennas.

1.2 Design Overview and Challenges

1.2.1 Research Goals and Requirements

The research goal is to design a transmitting loop antenna and a receiving loop antenna that can achieve wide-band operation through 0.8—10MHz. The horizontal footprint of the two loop antennas combined must be within 1 meter by 2.4 meters. For prototyping purposes, 25.4 μ m-thick copper sheets are considered for the loop antenna design, simulation and construction (details on fabrication and measurement are available in Chapter 4).

Due to the narrow-band nature of electrically small loop antennas, a frequency tuning capability is required to operate the antenna through a large bandwidth. A fast continuous frequency sweeping through 0.8 to 10MHz is also preferred and should take less than 20 microseconds, because the sweeping speed is related to how much time the data collection cycle would take at each site.

Theoretically, according to duality theorem, the far-field radiation pattern of an electrically small loop is equivalent to that of an electrically infinitesimal magnetic dipole whose axis is orthogonal to the plane of the loop. That is, the fields radiated by an electrically small square loop are of the same mathematical form as those radiated by an infinitesimal magnetic dipole [1]. The maximum of the far-field pattern is along the plane of the loop, opposite to electrically large loops whose maximum is along the direction perpendicular to the plane. In this study, however, we are only interested in the near-field patterns of one transmitting loop antenna in free space at 1MHz. The derivation of the full solutions of the radiated electric and magnetic fields of a small loop is shown in Section 2.4. The six-meter deep observation plane in the near-field region is of primary interests.

Additionally, coupling between the transmitting and receiving loop antennas should be minimized. If there was too high of a coupled power between the two antennas, the received signals would remain high peak-to-peak values at all times and the potential signature of

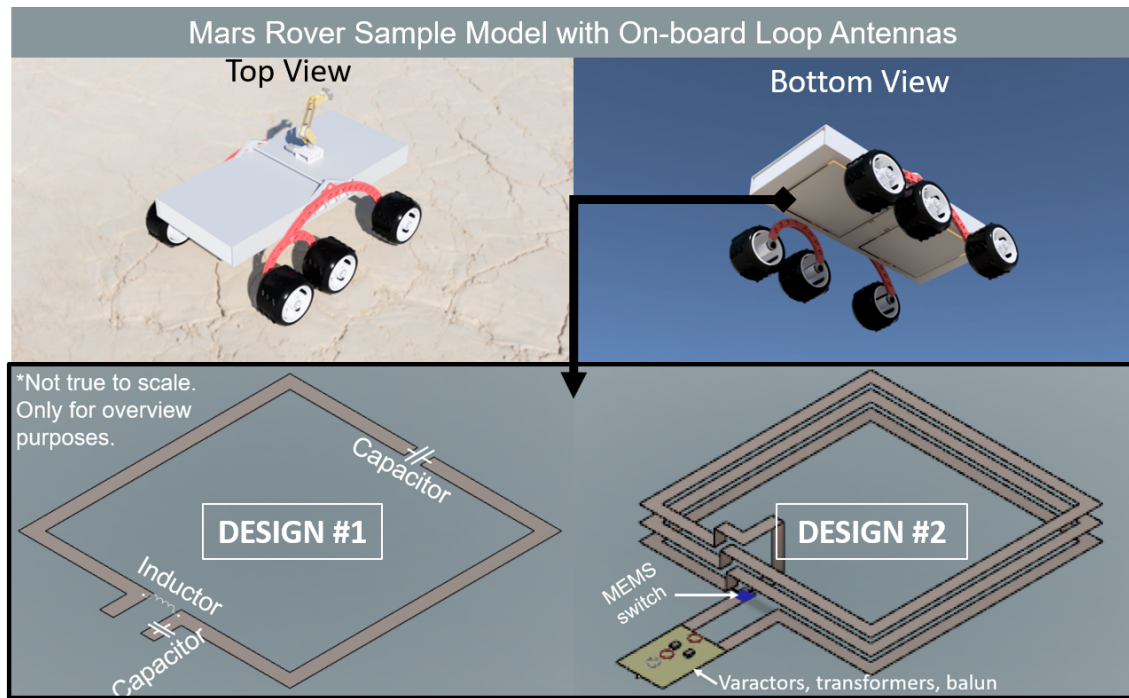


Figure 1.2: Demonstration of where the loop antennas are mounted on the Mars rover and an overview of the two proposed loop antenna designs.

hydration in Martian subsurface would most likely be misplaced.

1.2.2 Proposed Designs

Shown in Figure 1.2 is a pictorial overview of the two proposed designs.

In the first part of the thesis, an electrically small single-turn loop antenna is presented. The two capacitors and one inductor connected with the loop are part of a T-type impedance matching network to maximize the radiation efficiency of the transmitting loop antenna. The determination of the lumped element values is a result of an equivalent circuit model that is derived in Section 2.3.2. Continuous frequency tuning of the single-turn loop antenna can be achieved through an interpolation of the capacitors' values (Section 2.3.3). The near-field electric and magnetic fields of the single-turn loop antenna design are investigated. Section 2.4 includes a thorough investigation of how the current is distributed along the loop and how the current distribution affects the near-field radiation of the loop antenna.

In the second part of the thesis, a wide-band frequency reconfigurable multi-turn loop antenna is presented. A revolutionary low-insertion-loss RF-MEMS switch from Analog Device Inc. is used to reconfigure a three-turn electrically small loop antenna to single-turn from 3-10MHz. The impedance matching network of the loop antenna, composed of varactors, transformers and RF balun, is positioned between the feed and the loop. The methodology and design of transmission-line transformers are available in Chapter 3. Off-the-shelf varactors are used to achieve continuous frequency tuning and specialized biasing structures is incorporated with the multi-turn loop antenna design.

Last but not least, fabrication and measurements details are presented in Chapter 4. Network analyzers are primarily used for the measurement of the S-parameter performance of the loop antennas.

CHAPTER 2

Single-Turn Electrically Small Loop Antennas with Mechanical Frequency Tuning Capability

2.1 Overview

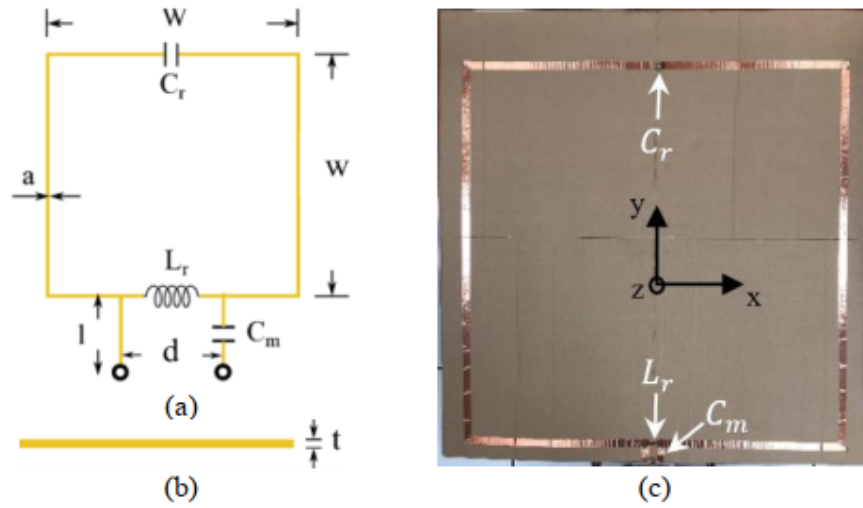


Figure 2.1: A loop antenna that can operate from 0.8 to 10 MHz by tuning C_r and C_m values (antenna material: copper, $w = 1m$, $a = 2cm$, $l = 4cm$, $d = 2cm$, $t = 25.4\mu m$). Not-true-to-scale illustrative view of the geometry, (a) top view, (b) side view. (c) Fabricated prototype of the proposed electrically small loop antenna.

The configurations and geometry of an electrically small loop antenna are shown in Figure 2.1. The proposed structure is a $1m \times 1m$ square loop antenna, which has a series tuning capacitor C_r , a parallel inductor L_r , and another series capacitor C_m that connects to one end of the input terminal. The three lumped elements essentially constitute a Tee impedance matching network for the loop antenna. The small radiation resistance of an

electrically small antenna leads to its high Q-factor. Thus, matching a small loop antenna's input impedance to the $50 - \Omega$ port impedance with a single set of C_r , C_m and L_r is only possible within a narrow bandwidth.

2.2 Design Specifications

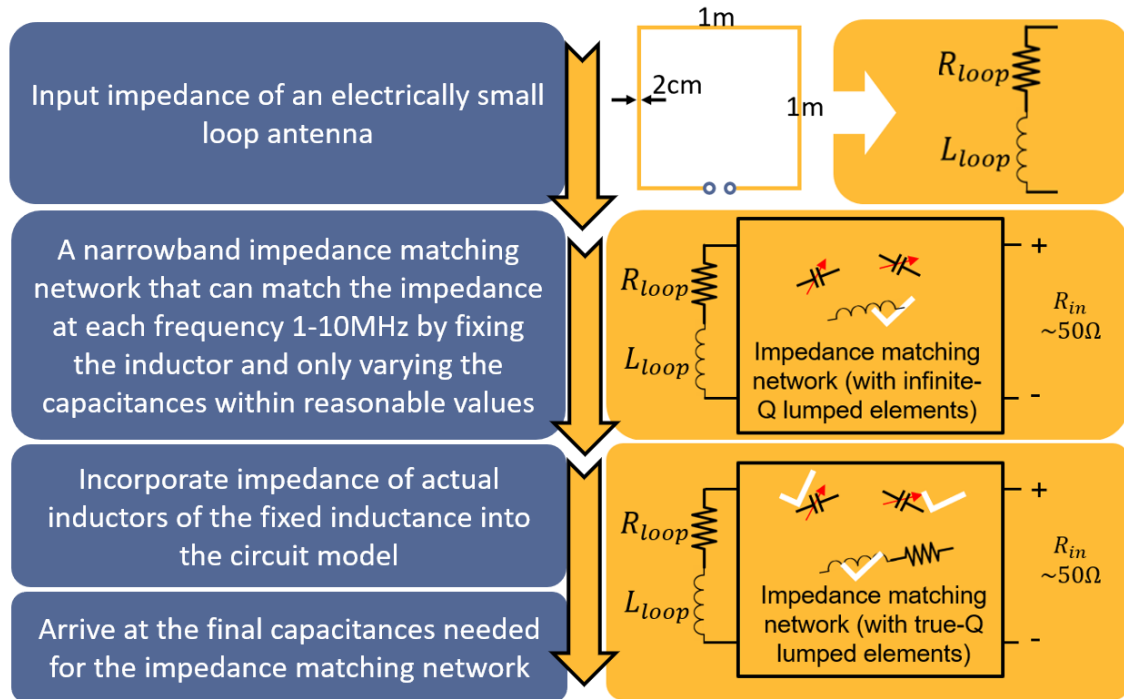


Figure 2.2: Methodology road map of arriving at the single-turn loop antenna design.

Shown in Figure 2.2 are the steps that are taken to arrive at an optimal design. The input impedance of a 1m by 1m electrically small loop antenna can be approximated as an inductor and a resistor in series. Then a narrow band impedance matching network is arrived at that can match the impedance at each frequency from 1 to 10MHz by fixing the inductor and only varying the capacitance within reasonable values. The reasons for this criterion are that electrically tuned inductors are rarely seen off-the-shelf, while electrically tuned capacitors also known as varactors are very common. Also, practical inductor components have a finite quality factor, meaning they always have a series resistance that changes with respect to the frequency and to specific components. This would significantly complicate the design

process, so it is preferred to get the inductor fixed and only varying the capacitance in the network. Once a good candidate of an impedance matching network topology is obtained, the measured impedance of actual inductor components is incorporate into the circuit model. Finally, optimization algorithm is run to arrive at the optimal capacitance values for every frequency. Since the series resistance is not vary large, the final capacitance values do not deviate a lot from the ones calculated from the ideal model.

2.2.1 Radiation Characteristics of Single-Turn Small Loops

The perimeter of the proposed 1m by 1m single-turn loop is 4 m and electrically is one-seventy-fifth of the wavelength at 1MHz, and two-fifteenths of the wavelength at 10MHz. It is considered as an electrically small loop antenna as the perimeter is less than one fifth of the wavelength through out the frequencies of operation. 25.4- μm -thick copper sheet is used for the conducting material of the loop antenna. Copper has a conductivity σ of $5.8e7$ S/m and skin depth of 65.2 μm at 1MHz, 29.2 μm at 5 MHz and 20.6 μm at 10MHz. The skin depth over most of the frequencies is larger than the thickness of the copper sheet, meaning the loss resistance would not be dominantly due to the skin depth loss. The input impedance of an electrically small transmitting square loop Z_{in} can be approximated to be [1],

$$Z_{in} = R_{in} + jX_{in} = (R_r + R_L) + j(X_A + X_i)$$

where

R_r [Radiation resistance]:

$$R_r = \eta \frac{8}{3} \pi^3 \left(\frac{A}{\lambda^2} \right)^2 \quad (2.1)$$

where η is the impedance of the free space — 120π , A is the area of the square loop — 1m^2 , and λ is the wavelength.

R_L [Loss/ohmic resistance]:

$$R_{ohmic} = \frac{a}{b} R_s \left(\frac{R_p}{R_0} + 1 \right) \quad (2.2)$$

where a is the width of the square loop, b is the wire radius,

$$R_s[\text{surface impedance of conductor}] = \sqrt{\frac{\omega\mu_0}{2\sigma}}$$

R_p [ohmic resistance per unit length due to proximity effect]

R_p is initially set to be 0.02Ω for preliminary analysis and later optimized by fitting the analytical input impedance by Computer Simulation Technology(CST) full-wave electromagnetic EM simulation results.

$$R_0[\text{ohmic skin effect resistance per unit length}] = \frac{R_s}{2\pi b}$$

X_A [external inductive reactance of loop antenna] = ωL_A :

$$L_A = 2\mu_0 \frac{a}{\pi} \left[\ln\left(\frac{a}{b}\right) - 0.774 \right] \quad (2.3)$$

X_i [internal high-frequency reactance of loop conductor] = ωL_i :

$$L_i = \frac{1}{\omega P} \sqrt{\frac{\omega\mu_0}{2\sigma}} = \frac{2a}{\omega\pi b} \sqrt{\frac{\omega\mu_0}{2\sigma}} \quad (2.4)$$

where l is the length and P is the perimeter of the cross section of the wire of the square loop. The internal reactance of the loop conductor, usually wires, is usually negligible.

Finally, the approximated input impedance Z_{in} is calculated to be a fixed $4.04\mu H$ inductance in series with a frequency dependent resistance. Mathematically,

$$R_r \approx (6.24 \cdot 10^{-6})f^4, R_L \approx 0.026f^{0.5}\Omega \quad (2.5)$$

$$X_A + X_i = j\omega(L_A + L_i) \approx j\omega \cdot 4.04\mu H = 25.38f \quad (2.6)$$

$$Z_{in} \approx (6.24 \cdot 10^{-6})f^4 + 0.026f^{0.5} + 25.38f\Omega \quad (2.7)$$

where f is frequency in MHz. The ohmic resistance is much larger than the radiation resistance, which is in general true for an electrically small single-turn loop. The radiation efficiency is defined as $e_r = \frac{R_r}{R_L + R_r}$, so the corresponding radiation efficiency is very low. Also, the reactance is more dominant than the resistance in the impedance, which is consistent with the expectation that electrically small loop antenna is inherently inductive.

2.2.2 Equivalent Circuit Model

The equivalent circuit for the input impedance of a square loop while used as a transmitting antenna is shown in step one of the road map in Figure 2.2. Computer Simulation Technology(CST) full-wave electromagnetic simulation is done to compare the simulated impedance

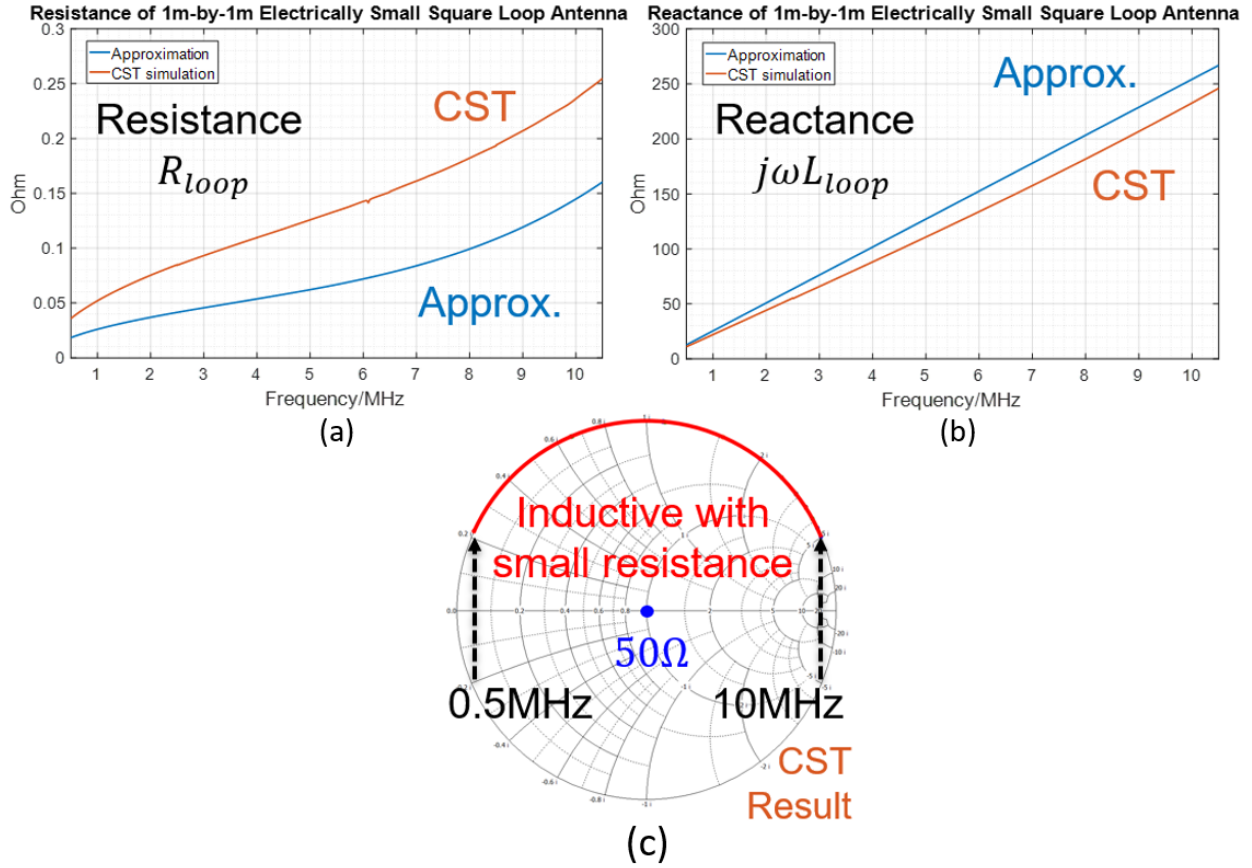


Figure 2.3: CST full-wave electromagnetic simulation generated and analytical input impedance of a square 1m by 1m electrically small loop antenna (a) resistance, (b) reactance, and (c) impedance as plotted on the smith chart.

with the analytical solution. The resistance and the reactance results are plotted separately in the Figure 2.3(a) and (b).

The CST simulated reactance and the approximated reactance from the Equation 2.7 agree well. Even though the resistance is visually different for the two curves, the values are in fact on the same order of magnitude. The CST simulation gives more realistic impedance values than the approximated impedance, because the assumption of the approximation is that it has to be an electrically small loop, while the proposed loop design is near the verge of conventionally defined “electrically small”, especially at the high end of the bandwidth. Also, the approximation fails to characterize the current nonuniformity and mutual coupling effect between the edges of the loop. Given that the impedance is “far away” from the

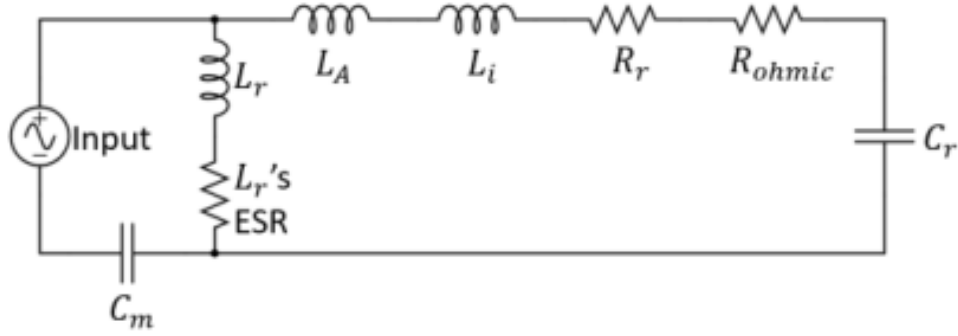


Figure 2.4: The circuit model of the small loop antenna including the radiation and ohmic loss resistance (R_r , R_L), the loop and internal inductance (L_A , L_i). The inductor L_r , and capacitors C_r , C_m form a T matching network.

50- Ω port impedance on the smith chart, as shown in Figure 2.3(c), an impedance matching network is necessary to arrive at maximum transmission from the feed to the antenna.

2.3 Narrow-band Impedance Matching Network Design

Impedance matching is necessary to provide maximum delivery to the load of the RF power available from the source [7]. A narrow-band impedance matching network with lumped elements can match the impedance of the load to 50 Ω perfectly at a single resonant frequency and marginally within a narrow bandwidth.

2.3.1 T-type Impedance Matching Network

The most fundamental matching circuit with lumped elements is in a form called L-type. Essentially, L-type match is to use one inductor or capacitor in series and another inductor or capacitor in parallel to match the impedance to 50 Ω . Nevertheless, the lumped element values can be impractical, if the frequency is too low and the required impedance matching bandwidth is large. For matching the dominantly inductive impedance of the 1m by 1m loop to 50 Ω through 0.8 to 10MHz is found to be extremely difficult, and impossible with L-type network. Thus, a T-type impedance matching network, essentially a back-to-back

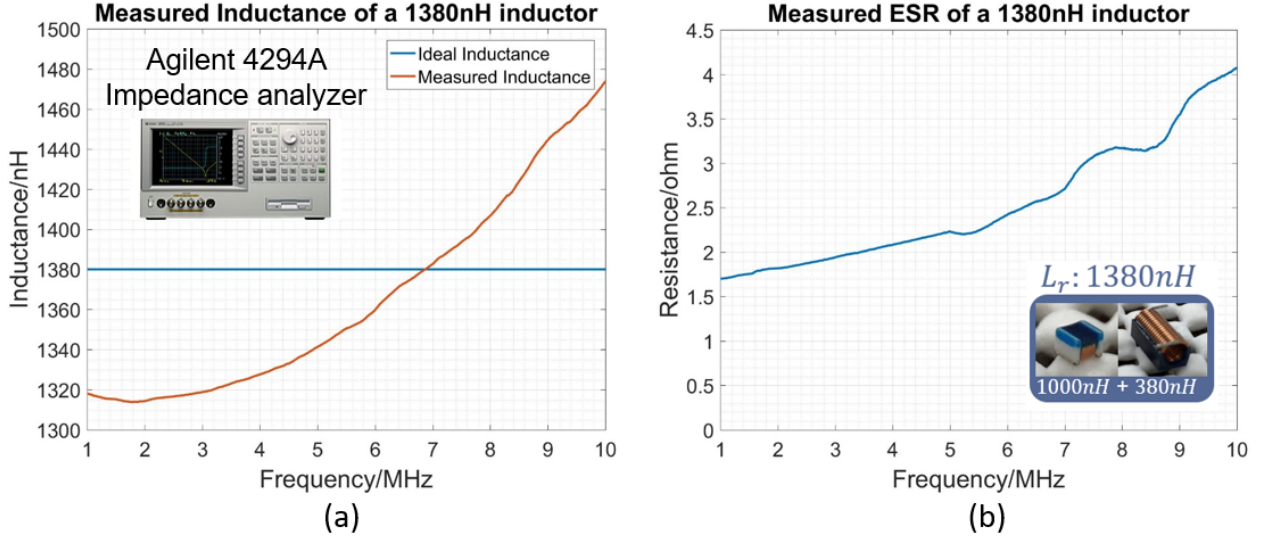


Figure 2.5: The measured inductance and equivalent series resistance (ESR) of a 1000nH and a 380nH inductors in series. The measured inductance in the range of 1317.9nH to 1473.9nH and the measured ESR is in the range of 1.4 Ω to 4.1 Ω .

cascade of two L-type networks, offers more degrees of freedom for tunability. Mathematical equations to solve for the lumped element values in a T-type network can be found in [7]. A T-type network with two-series capacitors and a parallel 1380-nH inductor can match the impedance of the loop to 50 Ω through the full bandwidth by tuning the capacitors.

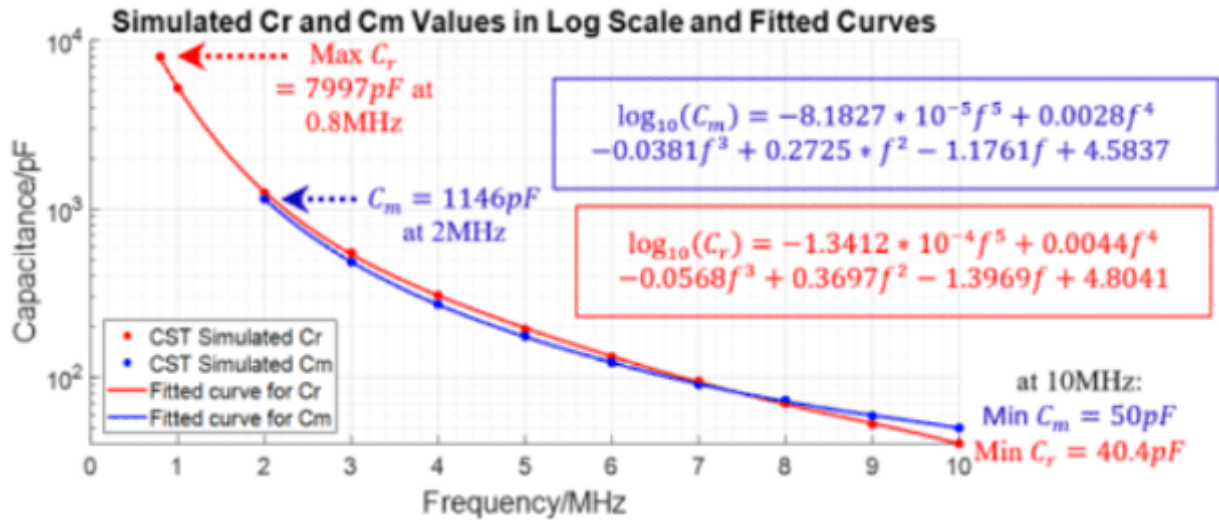
2.3.2 Equivalent Circuit Model of Matched Electrically Small Loop

A circuit model of the proposed electrically small loop antenna, incorporating analytical input impedance of the main loop, is shown in Figure 2.4. Intuitively, the series capacitor C_r shifts the resonance of the loop, the parallel inductor L_r transforms the small resistance of the loop to around 50 Ω , and the series capacitor C_m cancels out the residual reactance before the feed. It is critical that the equivalent series resistance (ESR) of the used inductor is included in the circuit model because the input impedance is very sensitive to the inductor ESR in the structure and as a result have a large impact on the C_r and C_m in impedance matching. Large ESR may increase the loss of the loop antenna and decrease system sensitivity, so a criteria for the inductors is to have less than 10 Ω ESR. Inductors with non-magnetic cores is selected

to guarantee low ESR from 0.8 to 10 MHz. $1\mu H$ inductors and 380nH inductors with air core were measured using Agilent 4294A impedance analyzer. The measured impedance is shown in Figure 2.5. Both the inductance and the resistance increase as the frequency increases. It is crucial that the frequency-dependent impedance L_r of the inductor components is incorporated in both the circuit model and the Computer Simulation Technology (CST) full wave electromagnetic simulation.

2.3.3 Continuous Frequency Tuning

The circuit model shown in Figure 2.4, with the calculated loop antenna's parameters and measured inductance and capacitance, is used as the starting point for the impedance matching and frequency tuning at sampled frequency points from 1 MHz to 10 MHz. 5th order polynomial curve fitting functions in Figure 2.6 of the C_r and C_m are used to extrapolate their required values throughout the frequencies. Continuous tuning of the resonant frequencies can be done by following the polynomial curve fittings. The circuit model using CST simulated input impedance of the small loop antenna predicts the results more accurately than the model using approximated impedance does, which is expected as CST gives a more realistic impedance value.



(a)

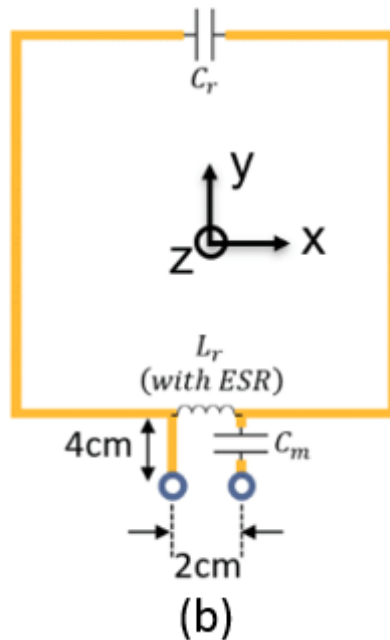


Figure 2.6: The required C_r and C_m values from 0.8 to 10 MHz fitted by 5th order polynomial functions. Sampled frequency points at 1 — 10 MHz are achieved through CST simulation. It is noted that at 0.8 MHz and 1 MHz C_m is shorted, so they are not shown in the figure. The positioning of the C_r , C_m and L_r along the loop is shown.

2.4 Near-field Electric Field and Magnetic Field of an Electrically Small Single-turn Loop Antenna at 1MHz

This study emphasizes on the six-meter away electric and magnetic fields of the single-turn loop antenna in free space at 1MHz. For an electrically small radiator, the outer boundary of the reactive near-field region is commonly a distance of $\lambda/2\pi$ from the antenna surface [1]. At 1MHz, the distance is calculated to be 47.7 meters, which is much larger than 6 meters. Thus, the observation plane is in the near-field region. From the simulation results shown in Figure 2.4, required C_m at 1MHz is infinite, therefore equivalent to a short-circuit.

2.4.1 Analytic Solution

Small loop antenna duality states that an electrically small loop of electric current I and of area A creates an electromagnetic field equivalent to that of an infinitesimal magnetic dipole (magnetic current element) with current equaling to $I_m \Delta l$ such that $j\omega\mu IA = I_m \Delta l$. The implicit assumption of the duality theory is that the current along the loop has to be uniform, which is in general true for far-field observation of electrically small loop antennas.

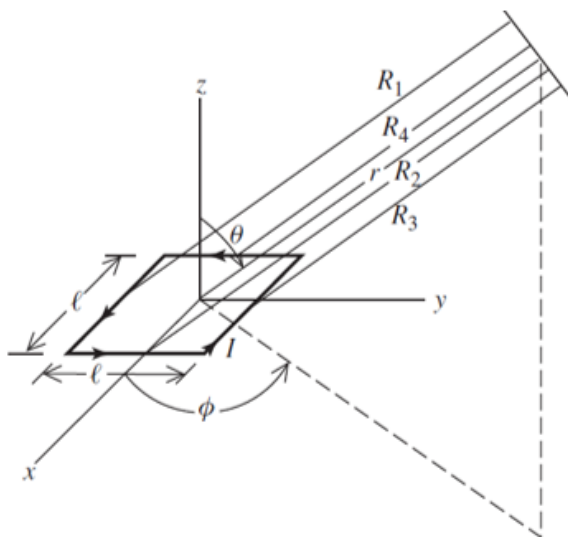


Figure 2.7: Coordinate system of a square loop aligned along the xy plane and perpendicular to the z axis [1].

The analytic solution of the electric and magnetic fields in a coordinate system defined in Figure 2.7 can be readily calculated for the electrically small loop to be [1],

$$\vec{A}(x, y, z) = \frac{\mu}{4\pi} \int_C I_e(x', y', z') \frac{e^{-jkR}}{R} dl' \quad (2.8)$$

$$\vec{H} = \frac{1}{\mu} \nabla \times \vec{A} \quad (2.9)$$

$$\vec{E} = -j\omega\vec{A} - j \frac{\nabla(\nabla \cdot \vec{A})}{\omega\mu\epsilon} \quad (2.10)$$

$$E_r = E_\theta = 0 \quad (2.11)$$

$$E_\phi = -\eta\beta^2 \frac{IA \cdot \sin\theta}{4\pi r} \left(1 + \frac{1}{j\beta r}\right) e^{-j\beta r} \quad (2.12)$$

$$H_r = j\beta \frac{IA \cdot \cos\theta}{2\pi r^2} \left(1 + \frac{1}{j\beta r}\right) e^{-j\beta r} \quad (2.13)$$

$$H_\theta = -\beta^2 \frac{IA \cdot \sin\theta}{4\pi r} \left(1 + \frac{1}{j\beta r} - \frac{1}{\beta^2 r^2}\right) e^{-j\beta r} \quad (2.14)$$

$$H_\phi = 0 \quad (2.15)$$

where I is the current along the loop 0.64 Ampere derived from CST full-wave electromagnetic simulation, r is the distance from the origin of the coordinate system to the the observation point, and A is the area of the loop $1m^2$. From the inspection of the equations 2.8 - 2.15, the magnitude of the electric field has a null at $\theta = 0^\circ$ and the magnitude of the near-field magnetic field has a peak at $\theta = 0^\circ$.

CST simulation is done to compare the near-field patterns calculated from analytic solution and those generated from full-wave electromagnetic simulation. The results are shown in Figure 2.8. The magnetic fields agree well between the analytic solution and the CST result both in pattern and magnitude. Nevertheless, the electric fields are very different not only in the pattern but also in the maximum and minimum. This is because the assumption is not valid in this application. The 7m by 7m observation window is six meters away from the loop, which translated to one-fiftieth of the wavelength at 1MHz. Since the observation is in the near-field region, a slight non-uniformity in the current along the loop can result in a non-symmetry in the near-field electric field pattern. The current distribution through the proposed single-turn loop antenna is not uniform and non-symmetrical with respect to the

center of the loop. It has peaks around the feed located roughly at $(x = 0m, y = -0.54m)$, which primarily leads to the non-symmetrical near-field electric field.

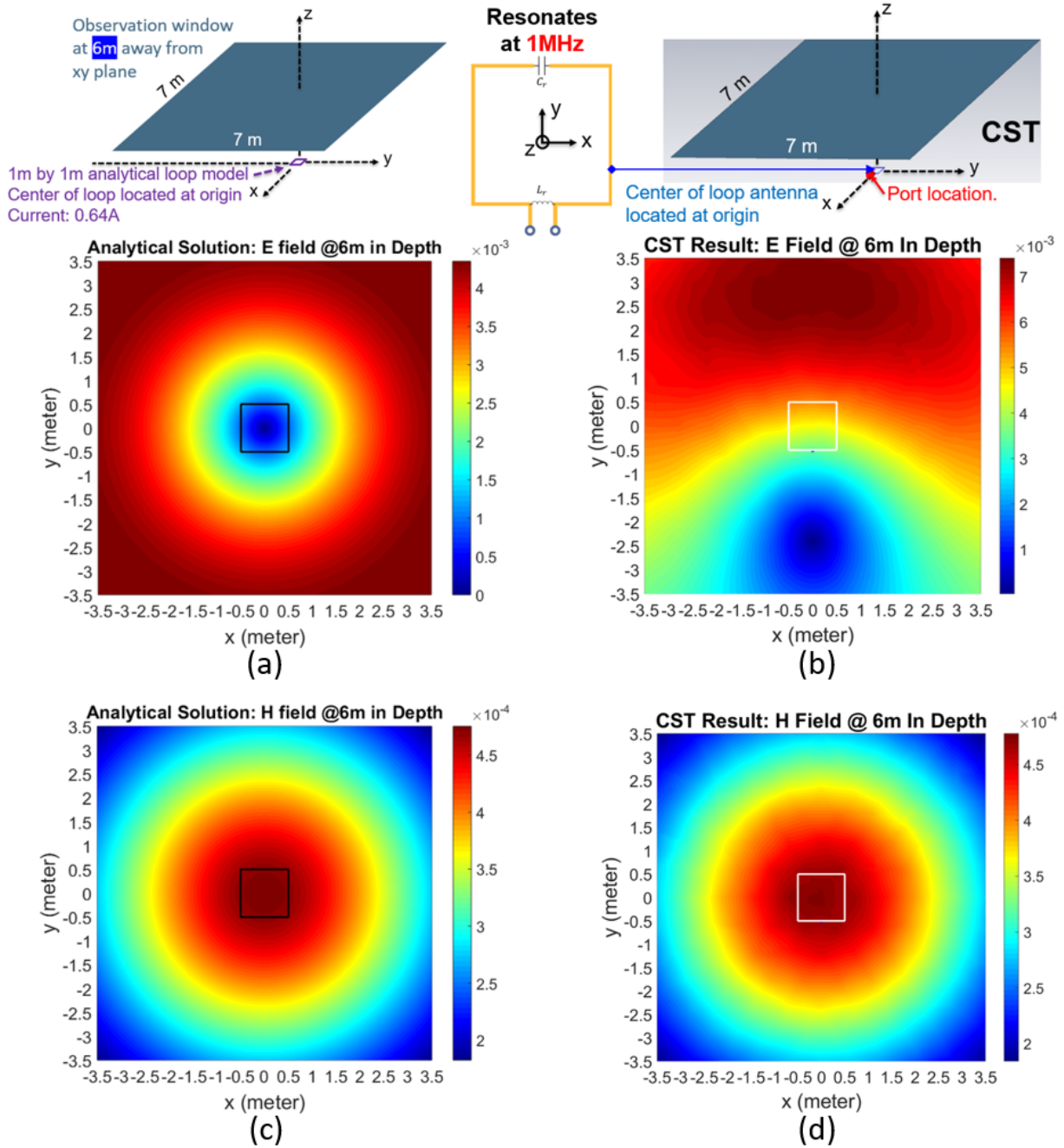


Figure 2.8: Six-meter deep near-field electric and magnetic fields of the single-turn loop antenna in free space at 1MHz. The black and white hollow squares in the figure show the position of the loop antenna relative to the observation window along an xy-plane. Electric field: (a) analytical solution, (b) CST simulation. Magnetic field: (c) analytical solution, (d) CST simulation.

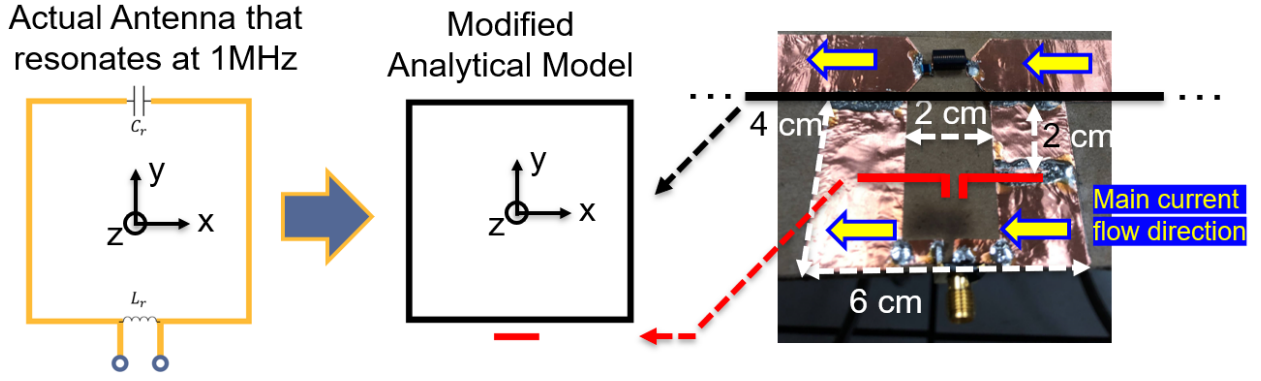


Figure 2.9: Current non-uniformity along the feed lines of the proposed loop antenna and modified analytic model.

2.4.2 Modification of Analytical Solution

Since the current flow along the two feed lines are in phase, we can model it equivalently as an infinitesimal 4-cm long electric dipole in a way shown in Figure 2.9. Analytical solution of the electric and magnetic fields of the dipole can be derived similarly from the vector potential as,

$$E_r = \eta I_e l \sin \theta \cos \phi \left[1 + \frac{1}{j\beta r} \right] \frac{e^{-j\beta r}}{2\pi r^2} \quad (2.16)$$

$$E_\phi = -j\eta\beta I_e l \cos \theta \cos \phi \left[1 + \frac{1}{j\beta r} - \frac{1}{\beta^2 r^2} \right] \frac{e^{-j\beta r}}{4\pi r} \quad (2.17)$$

$$E_\theta = j\eta\beta I_e l \sin \phi \left[1 + \frac{1}{j\beta r} - \frac{1}{\beta^2 r^2} \right] \frac{e^{-j\beta r}}{4\pi r} \quad (2.18)$$

$$H_r = 0 \quad (2.19)$$

$$H_\theta = -I_e l \sin \phi \left[j\beta + \frac{1}{r} \right] \frac{e^{-j\beta r}}{4\pi r} \quad (2.20)$$

$$H_\phi = -I_e l \cos \theta \cos \phi \left[j\beta + \frac{1}{r} \right] \frac{e^{-j\beta r}}{4\pi r} \quad (2.21)$$

where l is the length of the dipole 4cm, I is the equivalent current along the dipole that is found to be 0.019 A, and r is the distance from the origin of the coordinate system to the observation point. Equation 2.16 - 2.21 are added to the original analytic solution of small loops and the results are shown in Figure 2.10. The patterns generated from the modified

model are very similar to the CST simulation generated results shown in Figure 2.8(b) and (d). Additionally, although the six-meter observation window is of primary interest in this work, the electric and magnetic fields at a three-meter depth are also investigated. From the comparison of the results shown in Figure 2.11, the similarity between the simulation and modified analytical solution remains the same.

In conclusion, this part of the work proves that the current distribution along an electrically small loop antenna plays a paramount role on the the electric and magnetic field patterns observed in the near-field region.

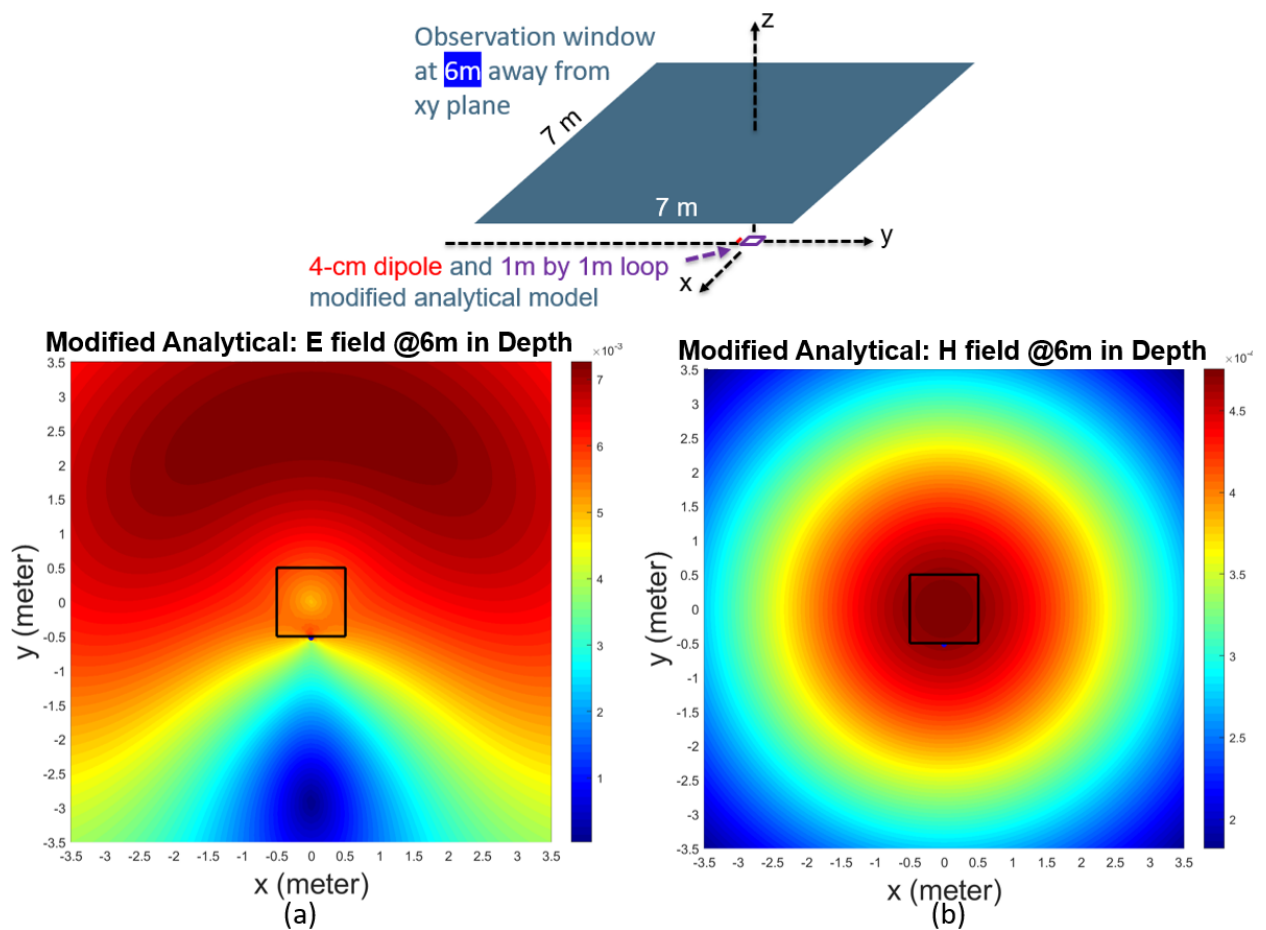


Figure 2.10: Six-meter deep near-field electric and magnetic fields of the single-turn loop antenna in free space at 1MHz using modified analytic model. The black hollow square in the figure shows the position of the loop antenna relative to the observation window along an xy-plane. (a) electric field (b) magnetic field.

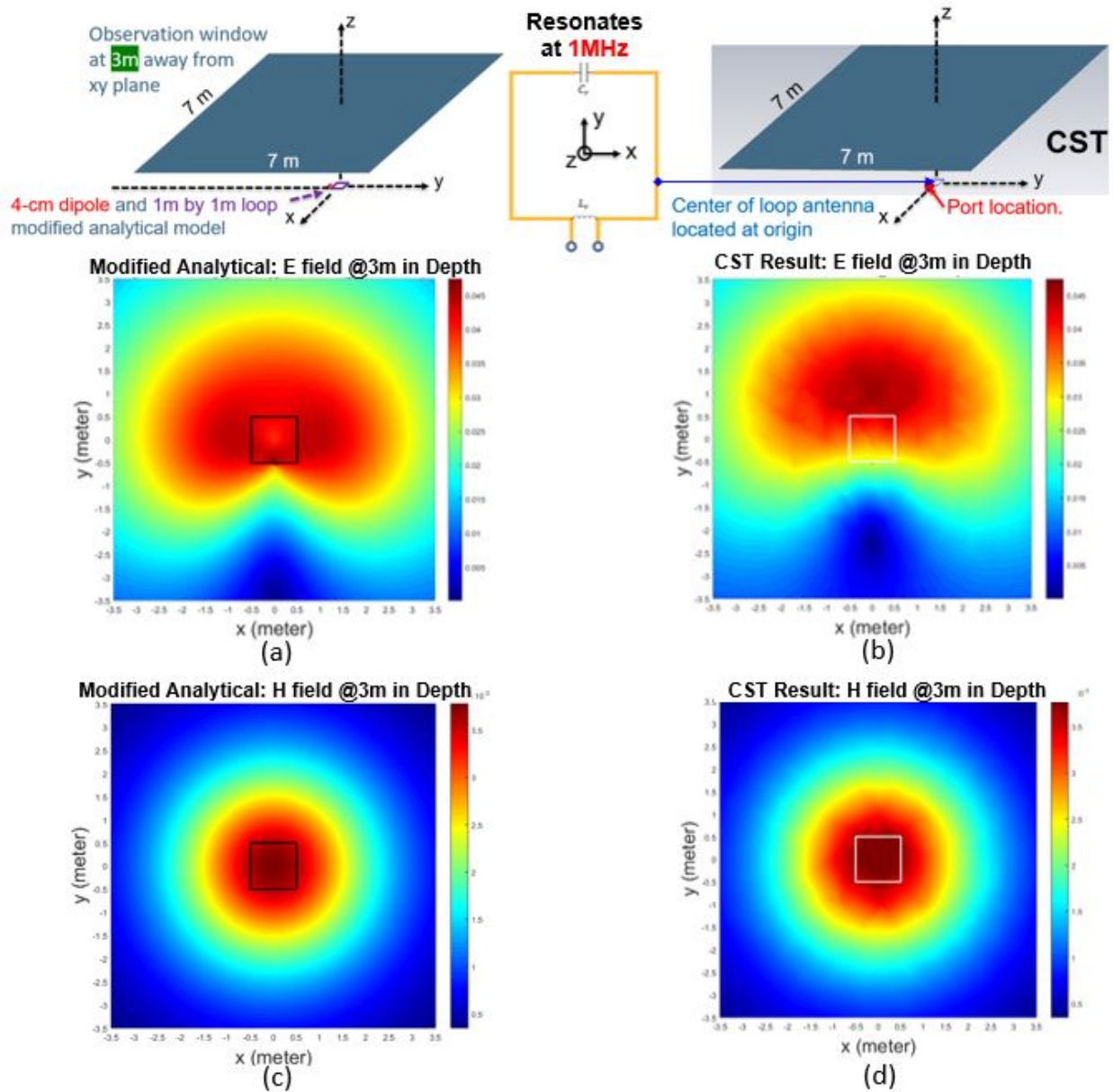


Figure 2.11: Three-meter deep near-field electric and magnetic fields of the single-turn loop antenna in free space at 1MHz using modified analytic model compared with using CST simulation. The black and white hollow squares in the figure show the position of the loop antenna relative to the observation window along an xy-plane. Electric field: (a) modified analytical solution, (b) CST simulation. Magnetic field: (c) modified analytical solution, (d) CST simulation.

2.5 Two Single-turn Loop Antennas

Ultimately, the dielectric spectroscopy measurement's antenna setup is composed of a transmitting loop antenna and a receiving loop antenna, both mounted at most 20 centimeters apart on the bottom of the Mars rover chassis. This section focuses on the performance study of the case of two single-turn loop antennas. The technique used to decouple the two loops is discussed in Section 2.5.1. The S21 performance of two single-turn loop antennas, with or without the loading of different targets in the near-field region, is investigated through CST full-wave electromagnetic simulation in Section 2.5.2 and 2.5.3.

2.5.1 Decoupling Technique

Given that the dimensions of the two loops and the distance between them are minimal compared to the wavelength, the coupling between them needs to be reduced so that the coupling power between the transmitter and the receiver is not too high to completely cover the power of the reflected electromagnetic wave from the targets. A rule of thumb is to have the S21 between the transmitter and the receiver to have a magnitude of less than -15dB at the resonant frequency. Shown in Figure 2.12 (a) and (b), the S21 of the two loop antennas placed 20 cm apart is slightly above -15dB at the resonant frequency. Thus, the coupling between the two loops needs to be minimized.

Theoretically, if two resonators operating at the same frequency f_0 are positioned in close proximity, then the resonances will be separated apart: one resonates at a frequency above and the other below the original resonant frequency f_0 . The coupling between two electrically small single-turn loop antennas can often be approximated as [5]

$$k = \frac{L_{12}}{L_1 L_1} \quad (2.22)$$

where k is defined as the coupling coefficient that characterizes the coupling between the two resonators, L_1, L_2 are the inductance of the respective loop and the mutual inductance between the two loops L_{12} can be calculated as

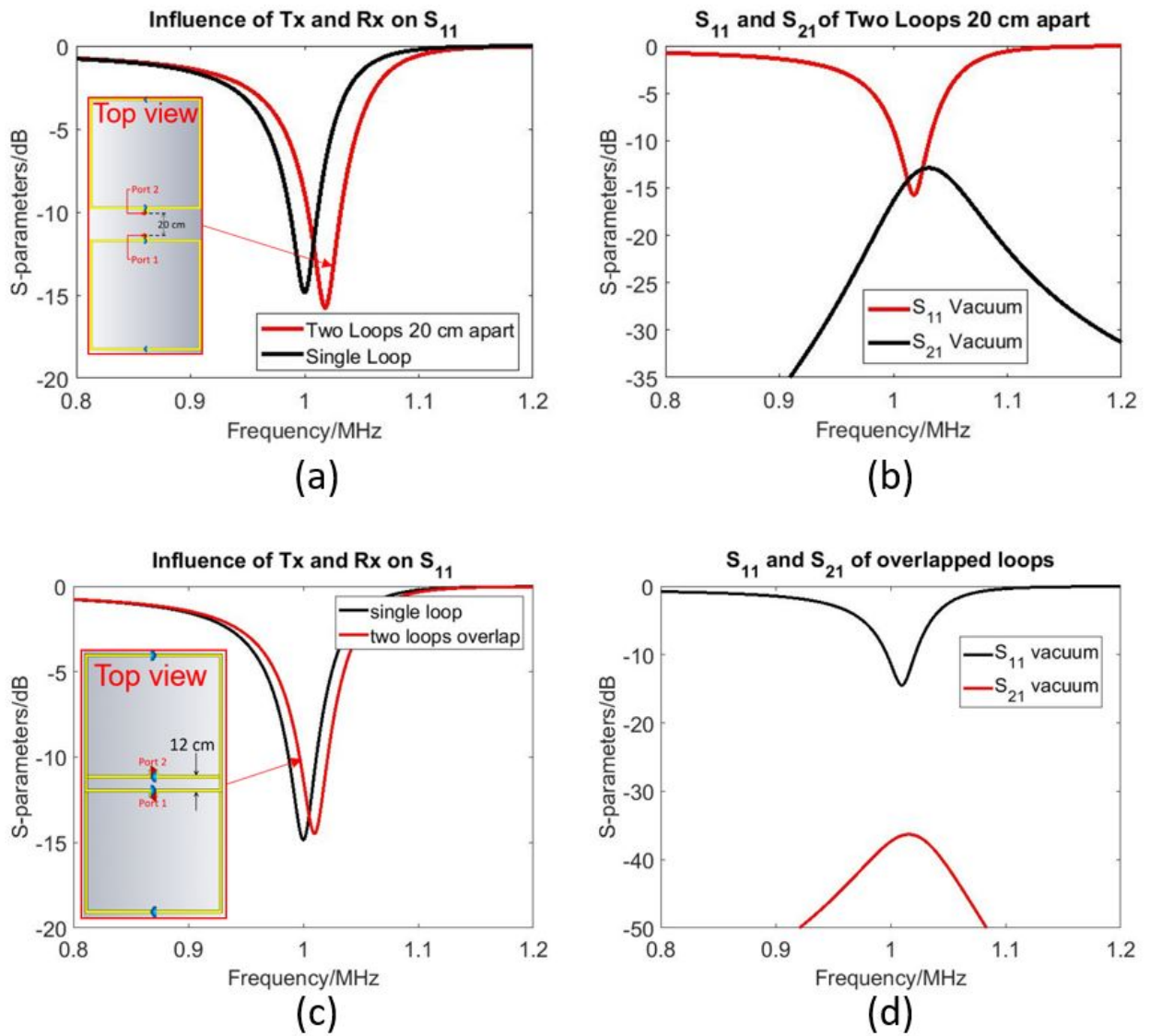


Figure 2.12: S_{11} and S_{21} performance of two single-turn loop antennas in vacuum. The top view of the two loops' positions and port 1 and port 2 positions are illustrated in pictures. Two loops separated by 20 cm: (a) S_{11} comparison between the two loops case and the one loop case, and (b) S_{11} and S_{21} of the two loops case. Two loops overlapped by 12 cm, (a) S_{11} comparison between the two loops case and the one loop case, and (b) S_{11} and S_{21} of the two loops case.

$$L_{21} = \frac{1}{\mu} \int B_{1,loop1} \cdot B_{2,loop2} dV \quad (2.23)$$

To first order, the two shifted frequencies can then be found to be

$$\begin{aligned} f_1 &= f_0 \cdot (1 + k), \\ f_2 &= f_0 \cdot (1 - k) \end{aligned} \quad (2.24)$$

Since neither of the two loop antennas now resonates at f_0 , the combined antenna has very low total efficiency. Additionally, coupled noise between the two would become substantial. There are a variety of methods to minimize the coupling. Since the coupling is predominantly due to the mutual inductance between the loop antennas, it can be reduced by optimizing the overlap between the two loops. For two square loops, the distance should roughly be 0.86 times the linear dimension in which the loops are overlapped. In principle, by Lenz's law the optimal decoupling state is achieved when the magnetic flux induced by one loop onto the other is perfectly canceled by its self-generated magnetic flux. Shown in Figure 2.12, the S21 level is significantly reduced by approximately 20dB through the method of critically overlapping the two loop antennas.

Further decoupling can be accomplished with the use of decoupling capacitors between the loops or other approaches, but for the preliminary investigation of the coupling between the loop antennas in this work, only the method of critical overlap is studied to minimize coupling.

2.5.2 S-12 Performance with loading

In this study, the S12 performance of the two electrically small loop antennas with a loading of a sandbox or a gypsum box is investigated. The purpose of such study is to evaluate the sensitivity of the proposed single-turn loop antennas to reflected signals from targeting substances.

A good indicator of loop antenna's sensitivity is the ratio of the unloaded quality factor (Q-factor) to the loaded quality factor (Q-factor). What has been considered in the prior

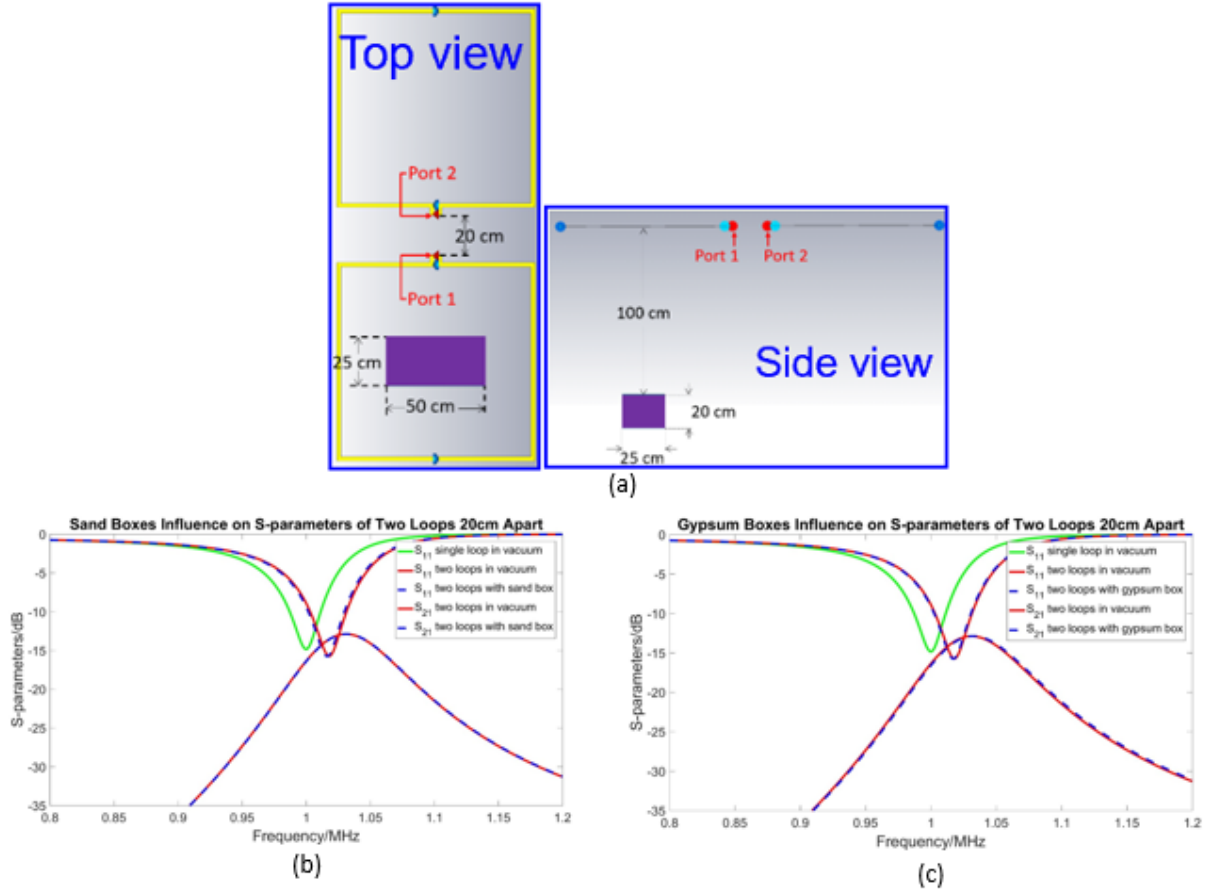


Figure 2.13: S_{12} of the two loop antennas separated by 20 cm with loading of (b) a sand box or (c) a gypsum box.

sections is only unloaded Q-factor, meaning antennas are positioned in vacuum. A higher unloaded Q-factor leads to a better sensitivity to the signals. Hereafter, $\frac{Q[\text{unloaded}]}{Q[\text{loaded}]}$ is denoted as "Q-ratio". First and foremost, in simulation the loaded Q-factor can be computed from the S_{12} data, if the dielectric properties of the targeted hydrated minerals is provided and the location of the mineral relative to the loops.

A $50\text{cm} \times 25\text{cm} \times 20\text{cm}$ box, material of which is either sand or gypsum, is positioned underneath one of the two loops for the simulation of S_{12} . Gypsum is a hydrated mineral of interest for Mars subsurface exploration. It conventionally has a relative permittivity of 12 and a conductivity of 0.025 S/m. As seen in Figure 2.13 and 2.14, with classic definitions of sand's or gypsum's dielectric properties, it seems that the loop antenna's S-parameter

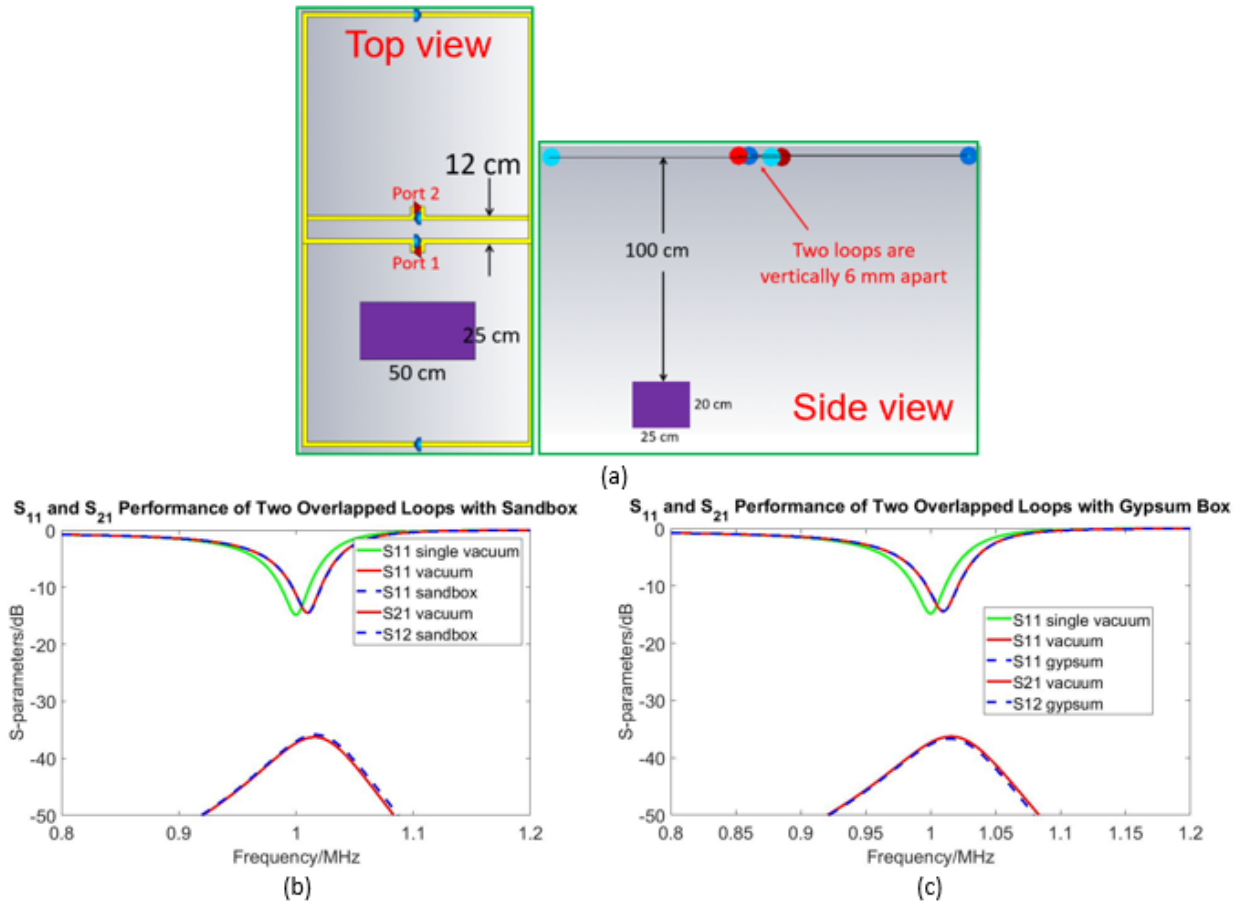


Figure 2.14: S₁₂ of the two loop antennas overlapped with loading of (b) a sand box or (c) a gypsum box.

and thus Q-factor does not change much. It means that the Q-ratio is close to one, and therefore the antenna is insensitive to the presence of such small box of substances. Future work includes simulating the two loop antennas with a bigger size of box or a new substance with a different dielectric properties.

In measurement, it is more difficult to get the precise Q-ratio number, because technically any metallic objects within the near-field region act as a load to the loops. So it would be expected to see the unloaded Q to be closer to the loaded Q in measurement, therefore a smaller Q-ratio, than it would be seen in the simulation. A rule of thumb for loop antenna's sensitivity is to have Q-ratio to be at least two. Different applications may require different levels of Q-ratio.

2.6 Required Tuning Capacitance Reduction

As seen in Section 2.3.1, continuously tuning the resonant frequency of an electrically small single-turn loop antenna through 0.8 — 10MHz by a variable T-type impedance network is possible theoretically. However, the range of the required capacitance is extremely large: The required C_m value is infinity at 0.8MHz, which leads to an infinite maximum-to-minimum ratio of the required tuning capacitance for 0.8 — 10MHz operation. This leads to difficulty in implementing the tuning network in practice, because off-the-shelf electrically variable capacitors (also known as varactors) only have at most such a maximum-to-minimum capacitance ratio of 29.

In this study, methods to reduce the required tuning capacitance (section 2.5.1) and attempts to implement such a large capacitance tuning range through switchable varactor banks (section 2.5.2) are presented.

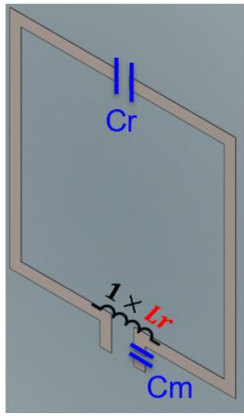
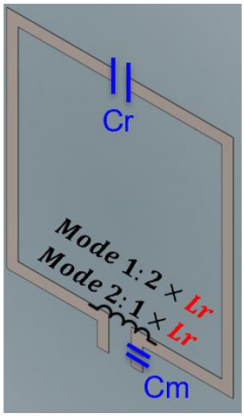
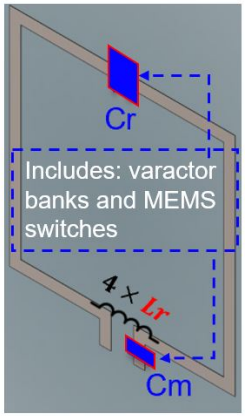
Designs	#1 With 1 Inductor	#2 With up to 2 Inductors	#3 With 4 Inductors
Inductor Values	1380nH (Lr)	Mode 1 (0.8-2MHz): 2*1380nH (Lr) Mode 2 (2-10MHz): 1*1380nH (Lr)	4*1380nH (Lr)
Cr/Cm	Cr: 8270pF – 32.3pF Cm: Short – 50 pF	Cr: 6000 pF – 36.3 pF Cm: 3000 pF – 50 pF	Cr: 3450 pF – 5 pF Cm: 2600 pF – 22.9 pF
Cap max-to-min Ratio	Cr ratio: 256, Cm ratio: inf	Cr ratio: 165, Cm ratio: 60	Cr ratio: 690, Cm ratio: 114
Structure			

Figure 2.15: Design overview of three frequency tuning schemes that help reduce the required tuning capacitance range of T-type impedance matching network for a electrically small single-turn loop antenna.

2.6.1 Methodology

The solution to reduce the required tuning capacitance range in a T-type impedance matching network for 0.8 — 10MHz operation of an electrically small single-turn loop antenna can be categorized into two methodologies: 1) increase the inductance L_r , and 2) use a switch to switch between different L_r values at different frequencies. Fundamentally, the capacitance of C_r and C_m can be altered by changing the value of the linear component L_r or making L_r have a non-linear impedance through the bandwidth by introducing a switch.

Shown in Figure 2.15, design #1 is the design that was proposed and studied in the previous sections. Design #2 has a switch that switches between two L_r values at 0.8 — 2MHz and 2 — 10MHz respectively. Design #3 changes the value of L_r in the original design. Since all the components used through the three designs are still linear, the optimal choice of L_r value and the tuning capacitance range can be readily solved through optimization technique such as convex optimization in MATLAB. The cost function of the optimization runs needs to be deliberately designed a priori: it is the difference between the maximum-over-minimum ratio of all the tuning components, C_r and C_m , and the desired ratio of 29, while the capacitance values still have to be positive and practical. Mathematically, working with ratios dramatically simplifies the optimization procedure (the derivations can be found in Section 3.2.2). Examples of the results of the optimization are listed in the Figure 2.15. It can be see that both design #2 and #3 have managed to eliminate the problem of infinite C_m maximum-to-minimum ratio in design #1. Nevertheless, the ratios are still much more than the goal of 29. Table 2.1 gives a comparison of the implementation aspect of the three designs. Although design #2 has the least maximum-over-minimum capacitance ratio, tuning three elements significantly increases the complexity.

Table 2.1: Implementation Comparison of Designs to Reduce Tuning Capacitance

	Maximum Cap.	Tuned Elements	Network Complexity
Design #1	Inf (short)	C_r and C_m	High
Design #2	6000pF	C_r , C_m and L_r	High
Design #3	3450pF	C_r and C_m	Moderate

Through a comprehensive search in the solution space through MATLAB, it is numerically proven that since the required bandwidth of operation is too large, end-to-end ratio of 10 (10MHz/ 1MHz), no variable narrow-band impedance matching schemes can successfully tune the resonant frequency of an electrically small 1m by 1m single-turn loop antenna through 0.8 — 10MHz, with a practical tuning capacitance range and an acceptable implementation complexity. This result motivates the pursue of the reconfigurable multi-turn loop antenna design that will be proposed and presented in details in chapter 3.

2.6.2 Switchable Varactor Banks Methodology

As seen in the previous section, considering the implementation complexity, design #3 using a larger Lr value is the most practical solution in reducing the tuning capacitance range. The attempt to arrive at a strategy and analysis of the challenges are illustrated in this study.

Table 2.2: Varactor Banks Designed to Cover the Tuning Capacitance of Design #3

	Min Cap	Max Cap	Max/min ratio	Covered frequency
Bank #1	4 pF	120 pF	30	4 — 10 MHz
Bank #2	115.2 pF	3455 pF	30	0.8 — 4 MHz

Table 2.3: Design #3 Detailed Required Tuning Capacitance for 0.8 to 3MHz

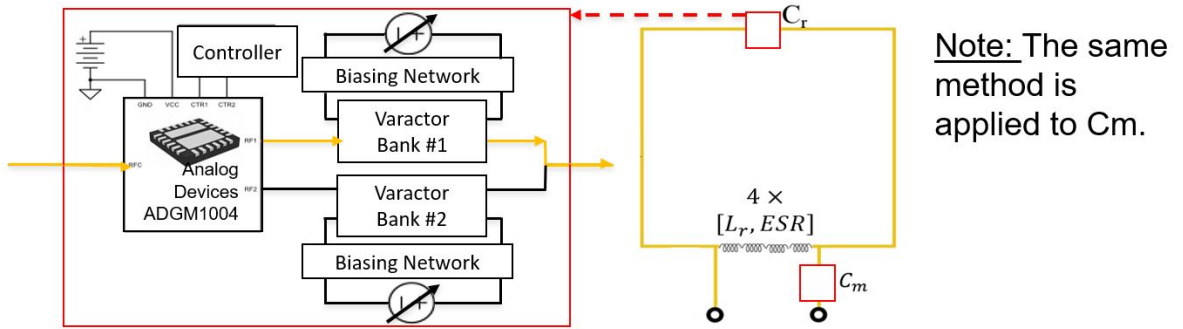
	Varactor Bank #2				
MHz	0.8	1	2	3	4
Cr /pF	3450	2282	537	226.3	118.4
Cm /pF	2600	2076.3	480.1	219.7	129.3
Freq /MHz	0.835	1.000	1.999	3.001	3.999
S11 /dB	-15.9	-35.1	-42.0	-44.6	-44.8
Lr [4*1380nH] /nH	5162	5147.6	5130	5139.6	5170.4
ESR /Ohm	6.8	6.8	7.2	8	8.8

Figure 2.16 demonstrates an oversimplified and naive method to switch between varactor banks using a MEMS switch. MEMS switch is chosen here as a representative switching

Table 2.4: Design #3 Detailed Required Tuning Capacitance for 3 to 10MHz

MHz	Varactor Bank #1						
	4	5	6	7	8	9	10
C_r /pF	118.4	71.3	43.6	28	16.3	9.2	5
C_m /pF	129.3	82.7	60.2	44.2	36	29.4	22.9
Freq /MHz	3.999	5	5.999	6.998	7.998	8.998	9.948
S11 /dB	-44.8	-60.2	-32.9	-42.5	-31.3	-28.2	-27.0
L_r [4*1380nH] /nH	5170.4	5217.6	5284	5371.2	5483.6	5606	5755.2
ESR /Ohm	8.8	9.2	10	10.8	12.4	13.6	15.6

State 1: Select varactor bank #1 by using the control signal (covering 4 – 10 MHz)



State 2: Select varactor bank #2 by using the control signal (covering 0.8 – 4 MHz)

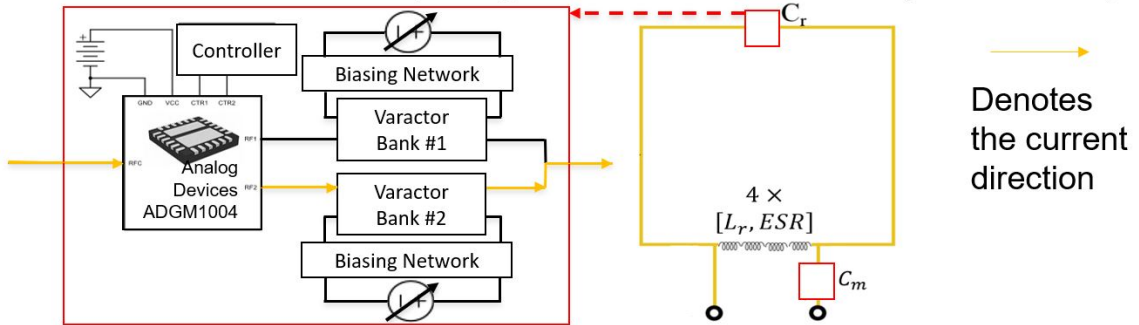


Figure 2.16: Operation details of how to use a MEMS switch to switch between varactor banks, which have a collective variable capacitance range that encompasses the tuning capacitance range required for design #3.

mechanism. A varactor bank is basically varactors put in parallel to achieve certain capacitance, values of which are designed and listed in table 2.2. Each bank has a maximum-over-

minimum capacitance ratio of 30, a marginally practical ratio to achieve using off-the-shelf varactors. Also, comparing Table 2.3 and 2.4 with Table 2.2, it can be observed that the deliberate arrangement of the varactor banks lead to a collective tuning capacitance range that can reasonably cover the entire operation bandwidth of 0.8 — 10MHz, required for design #3.

From a mathematical standpoint, the strategy of switching between varactors banks is demonstrated to be plausible. Nevertheless, implementation of the entire system is not practical and the performance of it is also substandard. This is because first there are two tuning positions, C_r and C_m . Placing two such switching varactor tuning circuitry along the loop is very cumbersome and power hungry. Secondly, The biasing network is extremely demanding for this setup, because the lower cutoff frequency 0.8MHz is very low for achieving a decent attenuation for DC power along the main signal path with conventional RF chokes or filters, while attenuation here is crucial to avoid damaging the MEMS switch. Last but not least, available in the last rows of Table 2.3 and 2.4, the equivalent series resistance (ESR) of the inductance at L_r is significantly large, well above 10 Ohm at higher frequencies. This leads to large loss and noise in the impedance matching network.

Thus, continuous mechanical frequency tuning for an electrically small single-turn 1m by 1m loop antenna through a variable T-type impedance matching network is shown to be successful; whereas an electrical frequency tunability remains challenging for the setup discussed in this chapter.

2.7 Copper Tube Single-Turn Loop Antenna

In this study, a variation of the geometry of the loop antenna is investigated. Instead of copper sheet, copper tube is considered for a more sturdy construction of the loop. Although the material is the same, the geometry of the conducting material of the loop antenna is different resulting in a different antenna's input impedance. And thus, the impedance matching network needs to be adjusted accordingly. The goal is to demonstrate that the proposed impedance matching scheme can be adapted for any electrically small loop antennas.

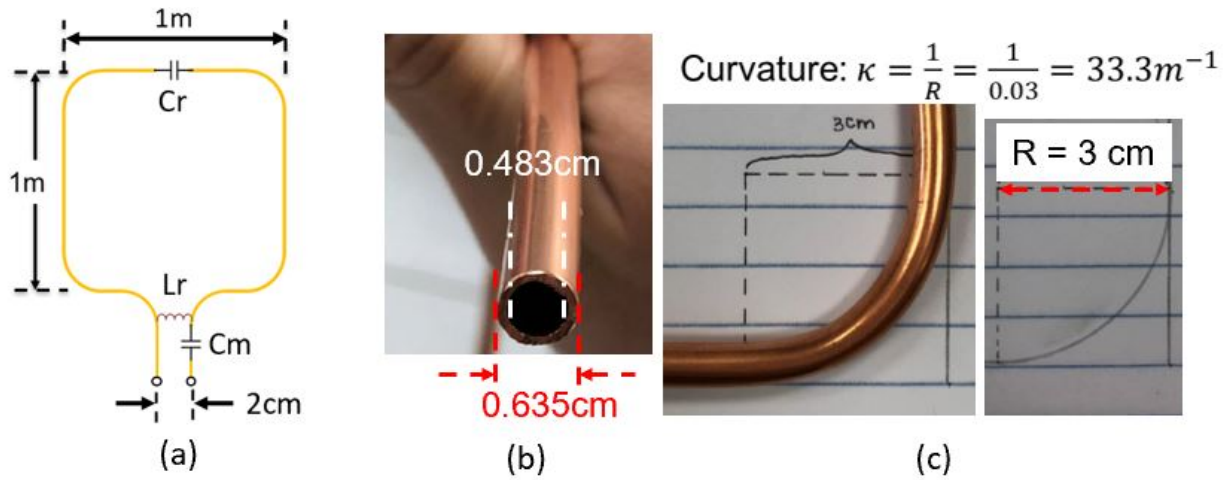


Figure 2.17: (a) New geometry of the single-turn loop antenna with a copper tube as the conducting material. (b) a closed-up view of the cross section of the copper tube. (c) the curvature characterization of the bending along the corners of the original square loop.

From Figure 2.17, due to the usage of copper tubes, there is a curvature at the bending of every corner along the original square single-turn loop. To model the realistic implementation as much as possible, the loop antenna is fully modeled in CST full-wave electromagnetic simulation, along with components other than the capacitors and inductors in the impedance matching network such as zip ties, poster supporting board, and PCB board. The impedance matching and frequency tuning strategies are consistent as the ones discussed in Section 2.3. In essence, first finding the input impedance of the single-turn loop antenna through 0.8 — 10MHz. Since the perimeter of the loop is similar to the one investigated in the prior sections, the impedance does not vary much. The next step is to find an optimal narrow-band impedance matching network that has an acceptable tuning range. The results are shown in Table 2.5, 2.6, 2.7, and 2.8. The tuning capacitance range is very similar to that of the original square single-turn copper sheet loop antenna.

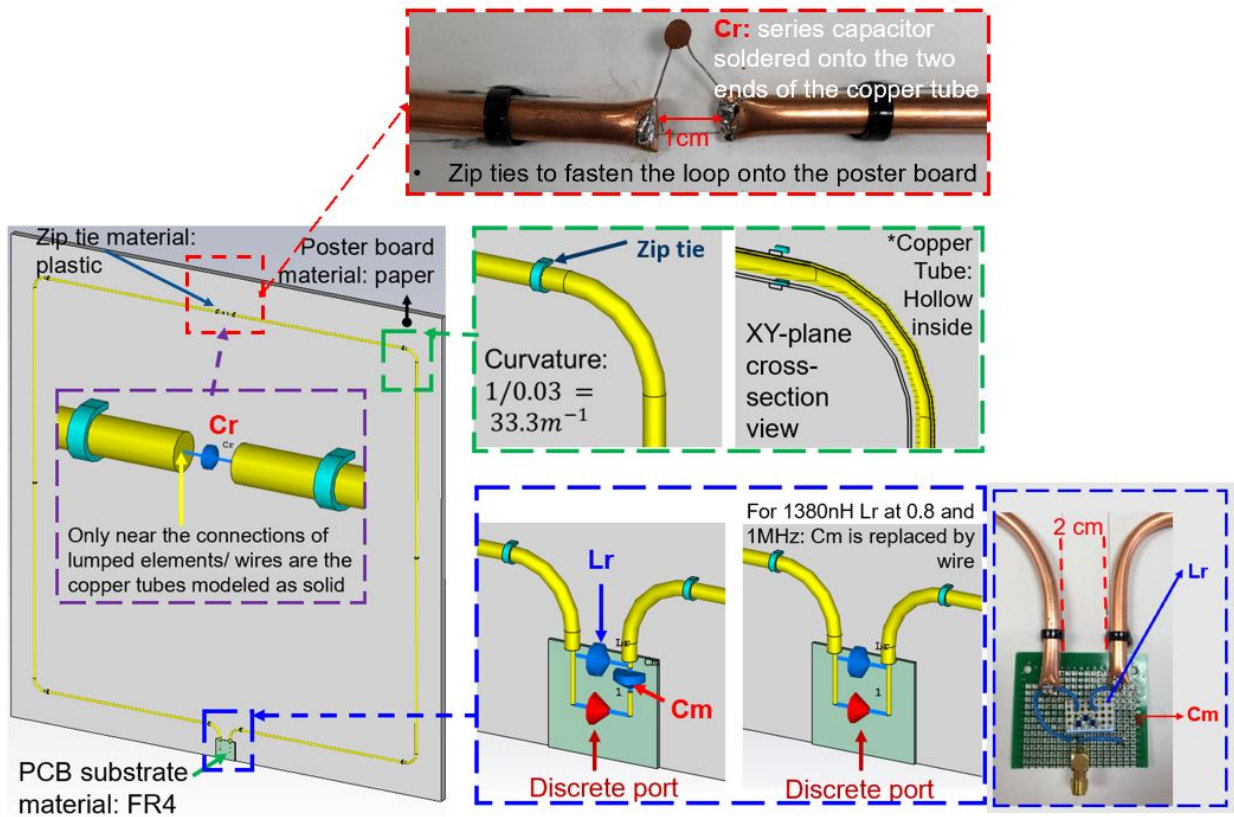


Figure 2.18: Pictorial illustrations of the modelling of the loop antenna in the CST simulation and the construction of the loop antenna at the lumped element positions.

For the impedance matching network design with 1380nH inductance at Lr , at 0.8 and 1MHz the Cm needs to be replaced by copper wires, as shown in Table 2.5. This is the same feature as observed previously in Section 2.3. It significantly complicates the the implementation process, as also discussed in Section 2.6 for the single-turn copper sheet loop antenna. On contrary, the $4 \times 1380nH$ inductance at Lr option is recommended, because throughout the whole bandwidth, Cr and Cm are always capacitors as indicated in Table 2.7 and 2.8. Fabrication and measurement have also been performed to validated the simulated results.

In conclusion, this study shows that the proposed impedance matching and frequency tuning scheme is agile to be adapted for any electrically small loop antennas with any geometry and frequencies of targets.

Table 2.5: Copper Tube Loop antenna with 1380nH at Lr for 0.8 — 5MHz Operation

Freq/MHz	0.8	1	2	3	4	5
Cr/pF	7300	4737	1125.5	497.7	274.6	172
Cm/pF	Short	Short	1125	437.7	248	161.5
Res Freq/MHz	0.80	1.00	2.01	3.00	4.00	5.00
S11/dB	-10.5	-19.8	-36.6	-26	-26	-30.6

Table 2.6: Copper Tube Loop antenna with 1380nH at Lr for 6 — 10MHz Operation

Freq/MHz	6	7	8	9	10
Cr/pF	117	83.1	61.5	47	35.4
Cm/pF	111.5	84	65.5	50	45
Res Freq/MHz	6.00	7.00	8.00	8.99	10.01
S11/dB	-25	-27.5	-22.8	-17.7	-24.5

Table 2.7: Copper Tube Loop antenna with 4*1380nH at Lr for 0.8 — 5MHz Operation

Freq/MHz	0.8	1	2	3	4	5
Cr/pF	3135	2141	530	225	118	70.5
Cm/pF	3964	2068	435.4	199.6	116.8	75.5
Res Freq/MHz	0.82	1.00	2.00	3.00	4.00	5.01
S11/dB	-22	-35	-20.1	-19.9	-20.7	-21

Table 2.8: Copper Tube Loop antenna with 4*1380nH at Lr for 6 — 10MHz Operation

Freq/MHz	6	7	8	9	10
Cr/pF	44.8	28.7	17.5	10.3	5
Cm/pF	53.0	40.0	32.7	26.6	22.2
Res Freq/MHz	6.00	7.01	8.00	9.00	10.00
S11/dB	-19.5	-20.2	-22.1	-22.7	-21.7

CHAPTER 3

Reconfigurable Multi-Turn Electrically Small Loop Antennas with Electrical Frequency Tuning Capability

3.1 Motivations

Chapter 2 has shown that with a conventional impedance matching network (e.g., T-type network), using linear lumped elements, the resonant frequency of a single-turn loop antenna can be mechanically tuned through 0.8 — 10MHz. The capacitance range of the lumped capacitors to tune the resonant frequency through the entire bandwidth has a maximum-to-minimum ratio of at least 256. It is much larger than the limited electrically variable capacitance range of off-the-shelf varactors, which has a maximum-to-minimum capacitance ratio of at most 29. Thus, to implement the conventional linear impedance matching network through 0.8 — 10MHz with an electrical frequency tunability is tremendously difficult. Shown in Figure 3.1, no prior literature has conquered the research goals of this work. Receiving coils for magnetic resonance imaging (MRI) only operate at single frequency [11]; antenna tuners developed for radio hobbyist have achieved wide-band but mechanical frequency tunability [9]; and magnetic field probes rely on the merits of impedance mismatch, which is the opposite to what is pursued in this project [10].

In this chapter, a reconfigurable multi-turn loop antenna design with an electrical frequency tunability is proposed and investigated. The use of Microelectromechanical systems (MEMS) switches and transformers enable the reconfigurability and wide-band impedance matching of the proposed loop antenna.


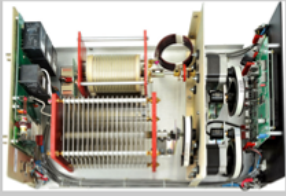

Electrically Small Loop Antenna with Linear Frequency Response – State of the Art Highlights			
Pictures			
Application	Magnetic Resonance Imaging (MRI)	Antenna tuner for loop antennas	Magnetic Field Probe
Frequency	127 MHz or 298MHz	1.8 MHz – 54 MHz	100 kHz – 50 MHz
Problems	single-frequency operation	mechanically tuned lumped elements	impedance mismatched

Figure 3.1: State of the art highlights of electrically small loop antennas with linear frequency response and their respective problems with respect to this work’s application. [8, 9, 10]

3.2 Design Specifications

The proposed design in Figure 3.2 is originated from a classic multi-turn loop antenna design (Section 3.2.1). Further, a revolutionary low-insertion-loss RF-MEMS switch from Analog Device, Inc is integrated to reconfigure a three-turn electrically small loop antenna between a three-turn mode through 0.8 – 3MHz and a single-turn mode through 3 – 10MHz (Section 3.3); also, the concept of broadband transmission-line impedance transformers is revisited and a specialized low-loss impedance matching network and a low-insertion-loss biasing structure for varactors are designed to efficiently tune the resonant frequency of the loop antenna over the 0.8 – 10MHz bandwidth (Section 3.4).

3.2.1 Loop Antenna Design

Shown in Figure 3.3, the perimeter of a 1m by 1m single-turn loop is 4m, consistently less than one-fifth of wavelength through 0.8 – 10MHz. Thus, such a single-turn loop is electrically small [1]. A three-turn loop with each turn 1m by 1m has a perimeter of less than one-fifth of wavelength only from 0.8 to 5MHz, so technically it should be considered electrically small

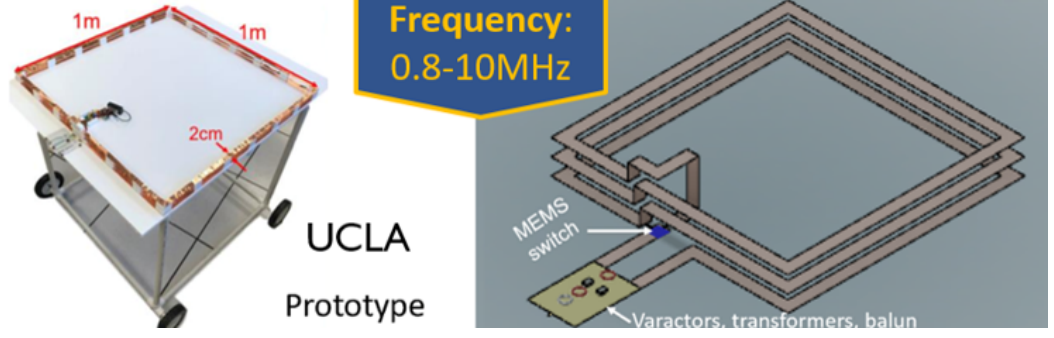


Figure 3.2: UCLA prototype photo and pictorial overview of the proposed reconfigurable multi-turn loop antenna design with a novel continuous electrical frequency tuning capability only at this bandwidth of operation. The adjacent turns are 2cm apart from each other. $25.4\text{-}\mu\text{m}$ -thick copper sheet is used for the conducting material of the loop antenna. Copper has a conductivity σ of $5.8e7\text{S/m}$ and skin depth of $65.2\mu\text{m}$ at 1MHz , $29.2\mu\text{m}$ at 5MHz and $20.6\mu\text{m}$ at 10MHz . The skin depth over most of the frequencies is larger than the thickness of the copper sheet, meaning the loss resistance would not be dominantly due to the skin depth loss. The input impedance of an electrically small transmitting square loop Z_{in} can be approximated to be [1],

$$Z_{in} = R_{in} + jX_{in} = (R_r + R_L) + j(X_A + X_i)$$

where

R_r [Radiation resistance]:

$$R_r = \eta \frac{8}{3} \pi^3 \left(N \frac{A}{\lambda^2} \right)^2 \quad (3.1)$$

where N is the number of turns, η is the impedance of the free space – 120π , A is the area of the square loop – 1m^2 , and λ is the wavelength.

R_L [Loss/ohmic resistance]:

$$R_{ohmic} = \frac{Na}{b} R_s \left(\frac{R_p}{R_0} + 1 \right) \quad (3.2)$$

where a is the loop radius, b is the wire radius,

$$R_s[\text{surface impedance of conductor}] = \sqrt{\frac{\omega\mu_0}{2\sigma}}$$

R_p [ohmic resistance per unit length due to proximity effect]

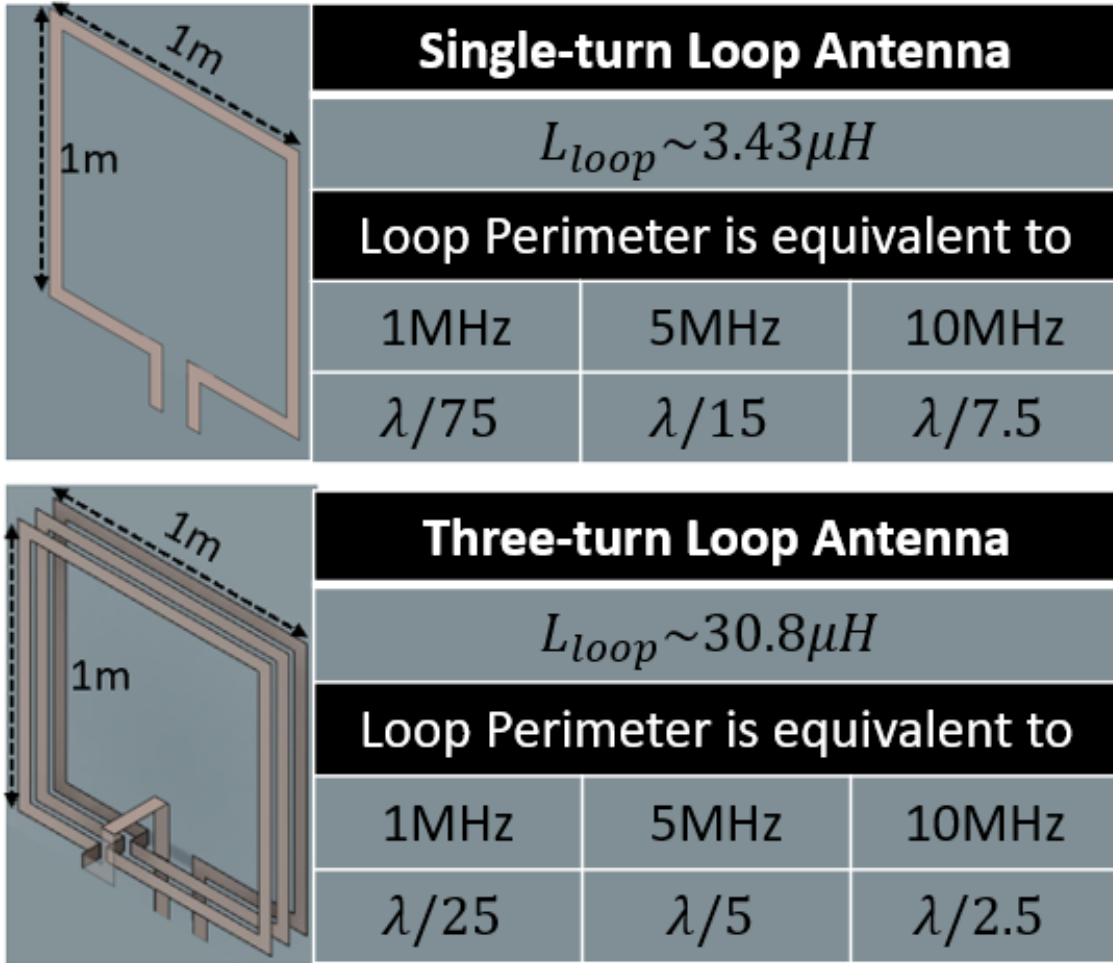


Figure 3.3: Single-turn and three-turn loop antennas design with the approximated inductance and loop perimeters equivalent to the wavelength at 1, 5 and 10MHz

The ratio R_p/R_o is proportional to c/b , where c is half of the separation between adjacent turns.

$$R_0[\text{ohmic skin effect resistance per unit length}] = \frac{NR_s}{2\pi b}$$

From equation 3.1 - 3.2, with the additional two turns, the three-turn loop has 3^2 times the radiation resistance of the single-turn loop and 3 times the ohmic loss resistance of the single-turn loop.

For the single-turn loop antenna, X_A [external inductive reactance of loop antenna] = ωL_A : [1]

$$L_A = 2\mu_0 \frac{a}{\pi} \left[\ln\left(\frac{a}{b}\right) - 0.774 \right] \quad (3.3)$$

X_i [internal high-frequency reactance of loop conductor] = ωL_i :

$$L_i = \frac{1}{\omega P} \sqrt{\frac{\omega \mu_0}{2\sigma}} = \frac{2a}{\omega \pi b} \sqrt{\frac{\omega \mu_0}{2\sigma}} \quad (3.4)$$

where l is the length and P is the perimeter of the cross section of the wire of the square loop. The internal reactance of the loop conductor, typically wires, is usually negligible. Intuitively the inductance of a multi-turn loop antenna is approximately calculated from that of a single-turn loop multiplied by N^2 , where N is the number of turns. Thus the inductance of the three-turn loop is 9 times that of the single turn. The final approximated inductance of the two loops is shown in Figure 3.3.

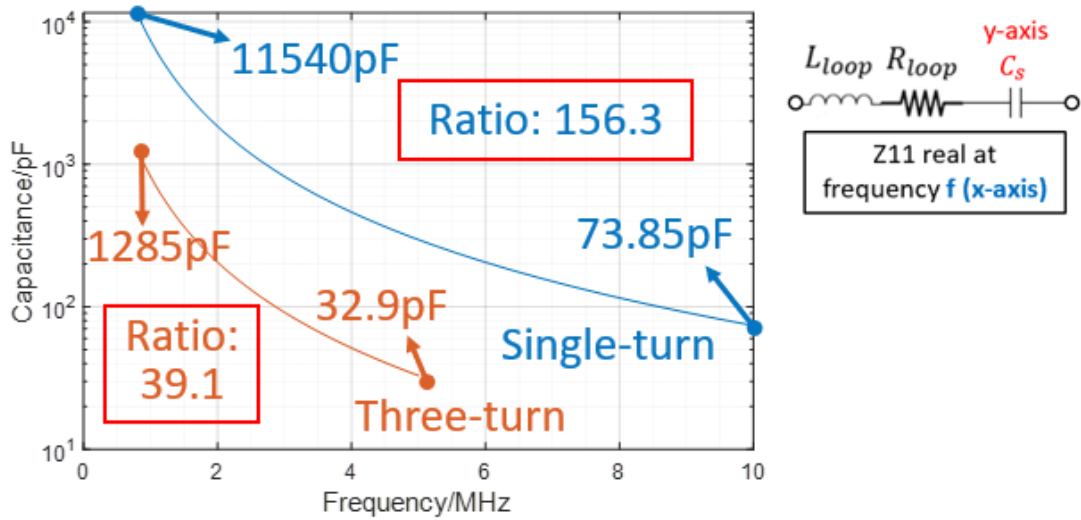


Figure 3.4: Series capacitance needed to resonate the three-turn and the single-turn loop antennas to the corresponding resonance frequency. The maximum-to-minimum capacitance ratio is shown on the figure.

3.2.2 Resonant Frequency Tuning

To resonant a loop antenna requires a capacitance either in parallel or in series to cancel out the inductive reactance of the loop. Shown in Figure 3.4, the series capacitance, C_s , required to resonate the loop antennas to a certain frequency, f_0 , has a relationship with the frequency in

$$C_s = \frac{1}{4\pi^2 f_0^2 L} \quad (3.5)$$

where L is the inductance of the loop. Three-turn loop with a larger inductance would need larger series capacitance to resonate than a single-turn loop does for the same frequency. Further, the maximum over minimum ratio of the required C_s (referred to as series capacitance ratio) for $f_0 \in [f_1, f_2]$ can be calculated to be,

$$\text{ratio}_{C_s} = \frac{\frac{1}{4\pi^2 f_1^2}}{\frac{1}{4\pi^2 f_2^2}} = \frac{f_2^2}{f_1^2} \quad (3.6)$$

Note here that the ratio is not dependent on the the impedance of the loop antenna, but only the resonant frequency.

Off-the-shelf varactors with the largest maximum-to-minimum capacitance ratio is the hyper-abrupt junction tuning varactor SMV1801-079LF from Skywalks having maximum and minimum capacitance of: 87pF when 0-Volt biased and 3pF when 3-Volts biased, with a factor of 29 in the ratio. The max-to-min ratio required for the proposed single-turn and three-turn loops, available in Figure 3.4, are significantly larger than that of varactor SMV1801-079LF. The capacitance ratio is more important of a design parameter than the absolute value, because the capacitance can be increased or decreased by having more or less capacitors in parallel, but the ratio is the parameter that remains unchanged. Shown in Section 2.5.2, although it is conceptually possible to to increase the ratio by switching between varactor banks, in practice due to the desired ultra-wide-band operation over 0.8 — 10MHz, it would be merely impossible to implement. Through convex optimization technique through MATLAB program with the approximated loop antenna impedance as the input, it has proven that there is no solution of a linear impedance matching network composed of lumped elements that can transforms the input impedance to around 50 ohm through the entire desired bandwidth. The T-type impedance matching network design illustrated in Chapter 2 is one example of a linear impedance network. Fundamentally the problem stems from the substantially large series capacitance ratio. Thus, a non-linear component such as an RF switch is necessary to be introduced into the system to break the f_0^{-2} trajectory in the equation 3.3 so that the ratio can be significantly reduced to accommodate the limitation of

off-the-shelf varactors.

Table 3.1: Comparison among three major electrical RF switching technologies

Parameters	Pin Diode	FET	MEMS Switch
Frequency range	From 100MHz	From DC	From DC
Intersection loss	Medium	High	Low
Isolation	Good at high frequencies	Good at low frequencies	Good across a broad frequency range

3.3 Switching Technologies

Reconfigurable electromagnetic devices, in particular RF switches, have the ability to route the electric current path through the antenna structure. The switching mechanisms can be categorized into four main classes: electrical, mechanical, optical, and material changes [12]. Given the requirements of reliability and energy efficiency for Mars rover missions, electrical RF switches are the most preferable among the four classes.

3.3.1 Overview

During operation, electrical switches have different electrical properties, such as capacitance and resistance, when being biased by different voltage levels. Table 3.1 summarizes the key parameters of the three major electrical RF switching technologies: 1) pin diode, 2) field effect transistor (FET) switches and 3) microelectromechanical systems (MEMS) switch. All modern electrical switching technologies have their respective trade-offs and disadvantages. For the application of this work the desired frequency of operation is 0.8 — 10 MHz, so PIN diode operating only at frequencies higher than 100MHz is not suitable. FET switches have another drawback with a high intersection loss at the low frequencies. Thus, RF MEMS switch is the optimal option for this work, among all the major classes electrical RF switches.

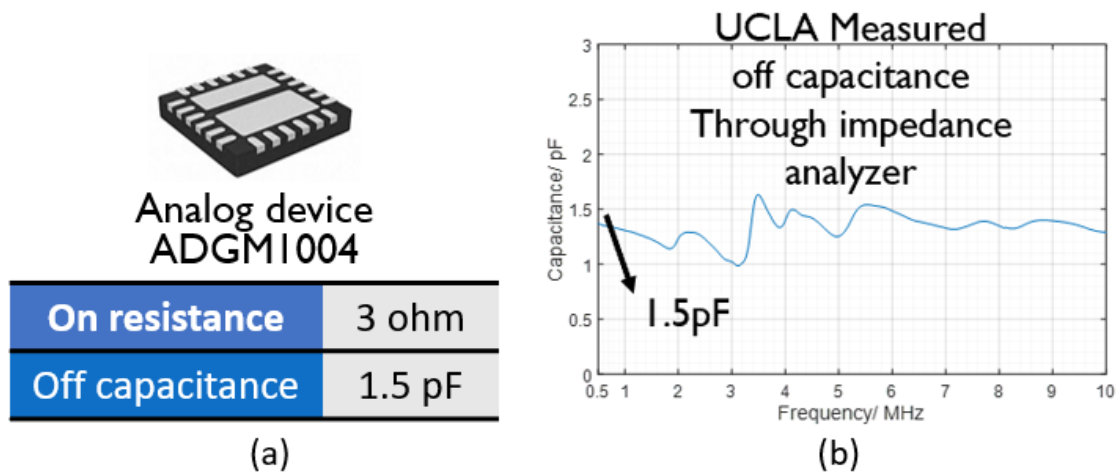


Figure 3.5: RF MEMS switch ADGM1004 from Analog Device, Inc. Inc, (a) picture of the MEMS switch and on resistance and off capacitance reported in the data sheet, and (c) The measured off capacitance using Agilent 4294A impedance analyzer by UCLA.

3.3.2 MEMS Switch

Over the past three decades, microelectromechanical systems (MEMS) switches have been recognized in many applications as a superior substitute for conventional electromagnetic relays, such as PIN diodes and FET relays. The advantages of MEMS switch technology are operation simplicity, small form factor, low loss and ultra-wide frequency bandwidth.

The most critical challenge that many engineers have faced in developing MEMS switch technology is the reliability in mass production. The world's first electromechanical switch was invented by the Foxboro Company in 1984 [13]. Nevertheless, it was not until 2018, when Analog Device, Inc. provided a high-performance, reliable and energy-efficient MEMS switch that a precise and robust production method became feasible.

MEMS switch has an electrostatically actuated, micro-machined cantilever that can be physically lifted up or down, creating an electrical open or close. Essentially, it can be thought of as a micrometer scale relay that behaves as a small capacitance when open, and a small resistance when close. One of the most fundamental criteria to evaluate switching technologies is the on resistance (R_{on}) and off capacitance (C_{off}), both of which need to be as

small as possible. Shown in Figure 3.5(a), the reported ON resistance and OFF capacitance of the ADGM1004 MEMS switch are significantly small. C_{off} for controlling the current path along a loop antenna is a more important factor than R_{on} , because if the C_{off} is too large, a significant fraction of the current would still "leak" through even when the cantilever is supposed to be open. Validated by UCLA through impedance measurement, the C_{off} is in practice around 1.5pF as reported in the datasheet, results of which is shown in Figure 3.5(b).

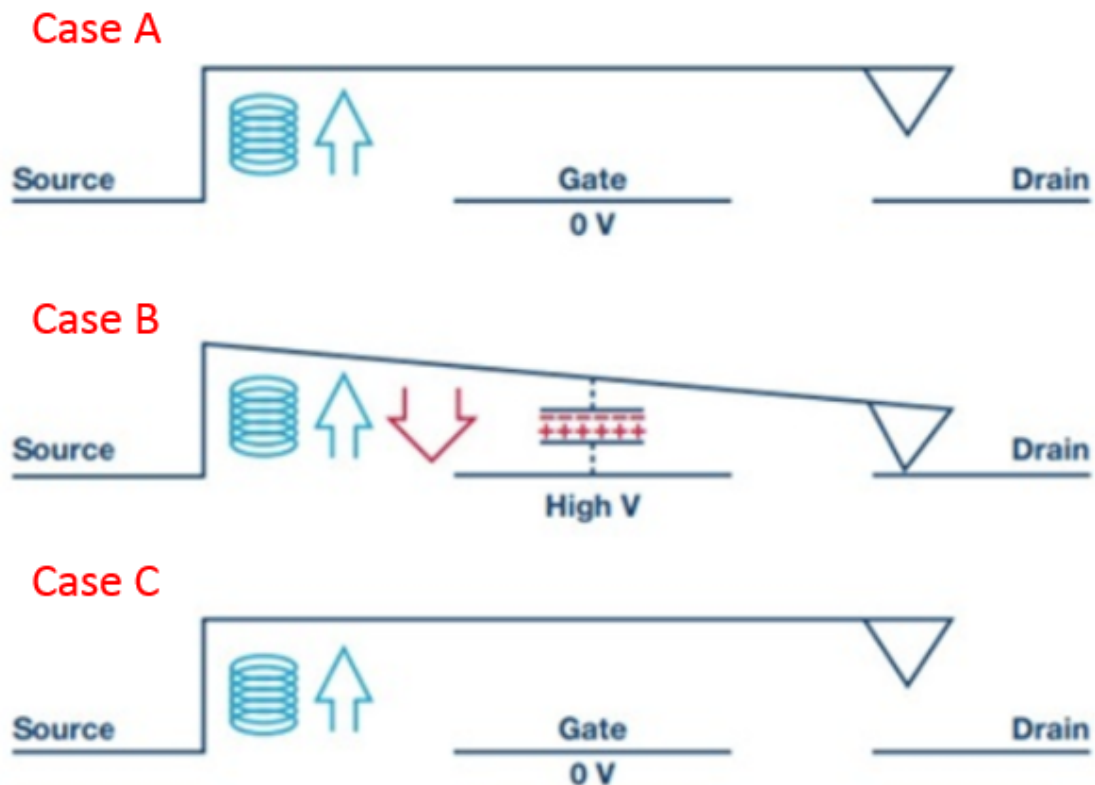


Figure 3.6: The operation of the MEMS switch. The top and the bottom cases show the switch turned off, while the middle state shows the switch turned on[13]

The MEMS switch has three terminals, which can be seen approximately as source, gate and drain [13]. Figure 3.6 shows a visual demonstration of how the switch functions: in case A the switch is off. After a voltage is applied to the gate, an electrostatic force is generated to pull down on the switch beam. The electrostatic force is the same as the force generated in the case of a parallel plate capacitor, when opposite charges accumulated on the top and the bottom plates attracting each other. When the gate voltage increases to a certain level, the

attraction force is accumulated enough so that the resistive spring force of the switch beam is overruled. Then, the beam starts to move down until it touches the drain terminal, as shown in Figure 3.6 case B. Consequently, the source and the drain is connected, and the switch is now on. Reversely, if the gate voltage is absent, the electrostatic attraction disappears, and the switch beam opens up the connection, analogous to a spring with sufficient restoration force. Then, the switch is back to the off state, shown as case C in Figure 3.6.

3.3.3 MEMS Switch Integration

Reconfigurability of the electrically small loop antennas is achieved by using an ADGM1004 MEMS switch, which has three inputs and one output. The two different modes of the antenna are demonstrated figuratively in Figure 3.7(b). At mode 1, the current flows through the full structure and radiates as a three-turn loop antenna from 0.8 to 3MHz. At mode 2, the current is mostly accumulated along the bottommost turn of the loop. Despite mutual coupling effects due to the presence of the two other turns, it radiates similarly as a single-turn loop antenna does from 3 to 10MHz.

The MEMS switch circuit model is devised, and a generalized schematic view is shown in Figure 3.7(c). The vendor provides that the switch has a 3Ω on-resistance and a $1.5pF$ off-capacitance. Each of the impedance Z_1 , Z_2 and Z_3 is adjusted according to the ON or OFF state of the corresponding input. The switch models under the two modes along with the loop antenna structure are simulated in CST full-wave electromagnetic simulation. The impedance of electrically small loop antennas is inherently and primarily inductive: the simulated reactance is in the range of 119.6Ω to 577.4Ω from 0.8 to 3MHz and 32.7Ω to 140.6Ω from 3 to 10MHz. The required capacitance C_m to cancel out such reactance χ at each angular frequency ω can be calculated as, $C_m = (\omega\chi)^{-1}$. The theoretical maximum over minimum ratio of C_m is 28.3, which is below the maximum ratio achievable with off-the-shelf varactors (e.g., Skywalks SMV1801-079LF tuning Varactor). Plotted in Figure 3.8, comparison between the with and the without integration of the MEMS switch cases illustrates that by introducing the switch into the antenna structure the inverse 2^{nd} order parabolic relation

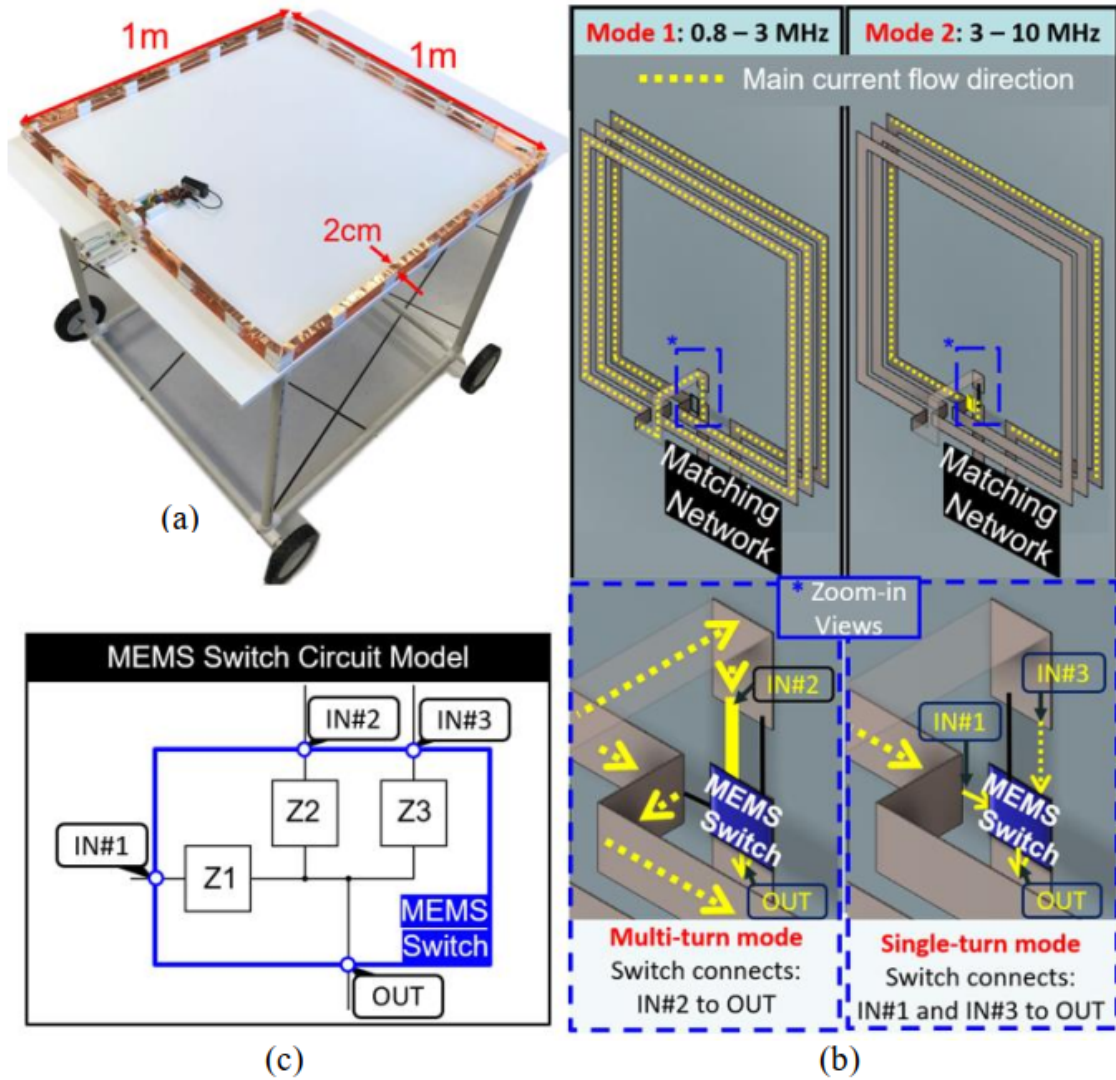


Figure 3.7: A wideband frequency reconfigurable electrically small multi-turn loop antenna (a) fabricated prototype lying on a simplified PVC Mars rover, (b) dual-mode configurations and zoom-in view of how MEMS switch controls the current flow, and (c) MEMS switch generalized circuit model.

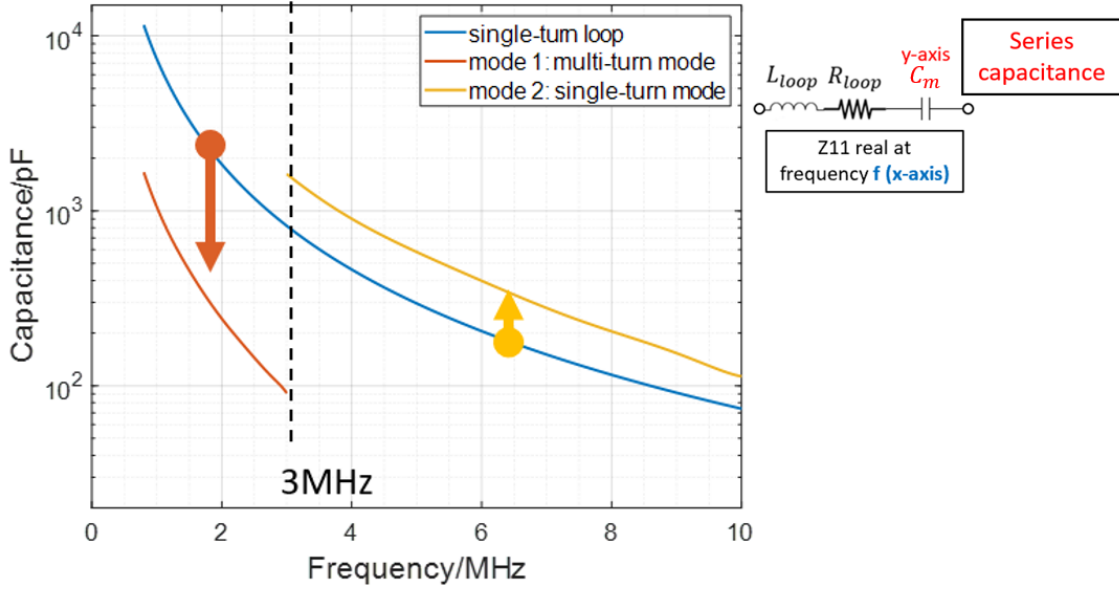


Figure 3.8: Series capacitance C_m required to resonate the proposed electrically small multi-turn loop antenna design in the multi-turn mode operating through 0.8 — 3MHz, single-turn mode operating through 3 — 10MHz, and a simple single-turn 1m by 1m loop antenna through the entire bandwidth.

between the series and frequency is broken apart and the two "halves" are brought closer to each other in magnitude. This is exactly the goal that the integration of a non-linear switch component is aimed to achieve by manipulating the current path for different frequencies of operation.

In addition, the simulated resistance is in the range of 7Ω to 10Ω , which can be transformed to around 50-Ohm port impedance to maximize radiation efficiency using a 1:4 impedance transformation network.

3.4 Impedance Matching network Design

Impedance matching is required to deliver the highest amount of RF energy accessible from the source to the load. It is essential to set the circumstances under which a electrical signal can be fully transmitted through the antenna propagation chain without any reflection back to the input port.

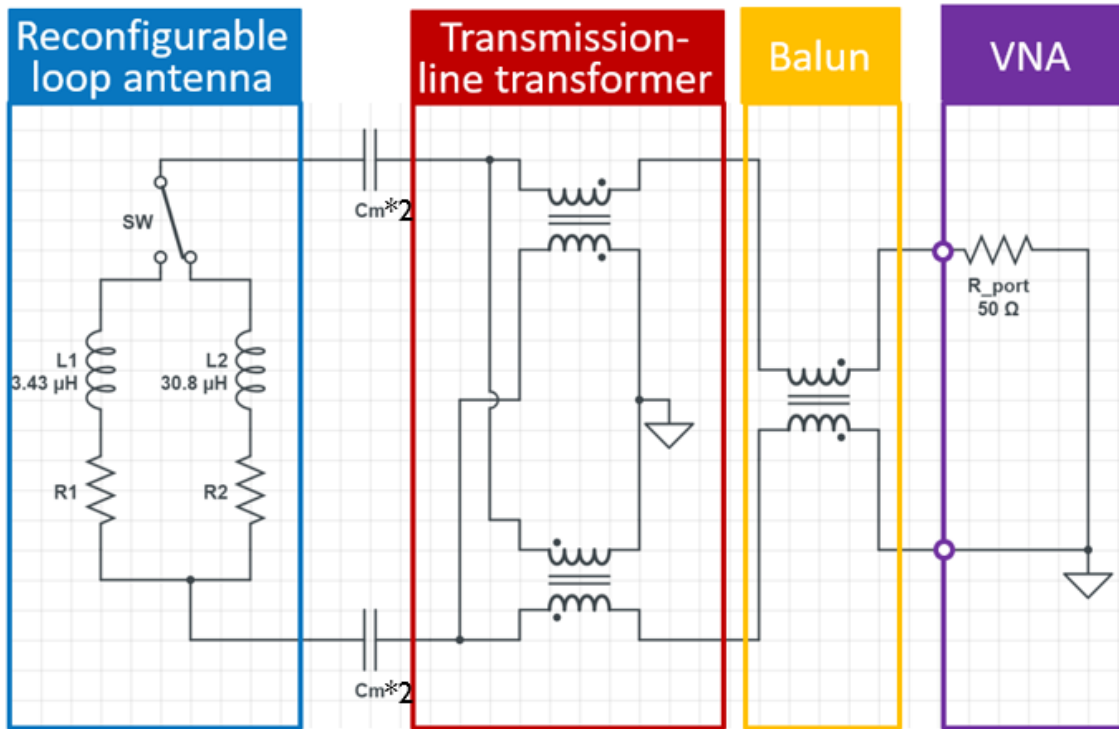


Figure 3.9: Schematic of the proposed impedance matching network.

In Section 2.3, a narrow-band impedance matching network using lumped elements for electrically small single-turn loop antenna is thoroughly studied and designed. This chapter focuses on a new paradigm of impedance-matching electrically small loop antennas, especially for High Frequency band (HF, 3-30 MHz) and Very High Frequency band (VHF, 30-300 MHz). Figure 3.9 shows the schematic of the proposed impedance matching network design. From left to right, at the resonant frequency the two capacitors in series, each having a capacitance of $C_m * 2$, are used to cancel out the reactance of the loop antenna; 1:4 Guanella Transmission-line transformer amplifies the resistance to around 50Ω ; and the current balun, in essence a 1:1 transmission-line transformer, is present to maintain balanced RF signals around the loop antenna, which leads to a more uniform current distribution and radiated electric and magnetic fields. Concepts and methods of employing transmission-line transformer in the design of the impedance matching network is available in Section 3.4.1. Integration of electrically tunable varactors and design of a specialized biasing structure for varactors are discussed in Section 3.4.2.

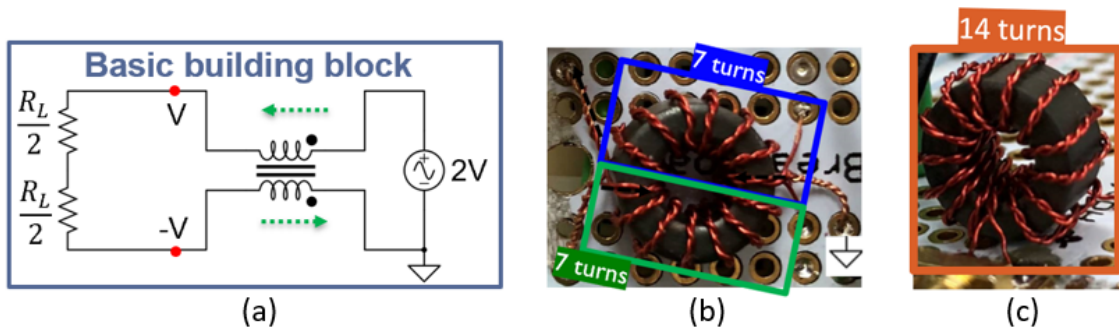


Figure 3.10: Transmission-Line transformer, (a) basic building block of transmission-line transformer, (b) 7-turn bifilar 1:4 transmission-line impedance transformer, and (c) 14-turn 1:1 transmission-line transformer or current RF Balun

3.4.1 Transmission-Line Transformers

There are two basic methods for constructing broadband, impedance-matching transformers. One employs the conventional transformer that transmits the energy to the output circuit by flux linkages; the other uses the transmission line transformer to transmit the energy by a transverse transmission line mode. With techniques exploiting high magnetic efficiency, conventional transformers have been constructed to perform over wide bandwidths. Losses on the order of one decibel can exist over a range from a few kilohertz to over 200 MHz. Throughout a considerable portion of this band, the losses are only 0.2 dB.

On the other hand, transmission line transformers exhibit far wider bandwidths and much greater efficiencies. The stray inductances and interwinding capacitances are generally absorbed into the characteristic impedance of the transmission line. As such, they form no resonances that could seriously limit the high-frequency response. Here the response is limited by the deviation of the characteristic impedance from the optimum value; the parasitics not absorbed into the characteristic impedance of the transmission line; and, in some transformer configurations, the length of the transmission line.

With transmission lines, the flux is effectively canceled out in the core and extremely high efficiencies are possible over large portions of the passband-losses of only 0.02 to 0.04 dB with certain core materials. Therefore, the power ratings of transmission line transformers are

determined more by the ability of the transmission lines to handle the voltages and currents than by the size and conventional properties of the core.

The earliest presentation on transmission line transformers was by Guanella in 1944 [14]. Even though they do not have a planar profile, as pursued by most modern technologies, transmission line transformers are ideal for the application of this work because high performance and wide bandwidth are more desired features than a minimal antenna profile.

The single bifilar winding, shown in Figure 3.10(a), is the basic building block for the understanding and design of all transmission line transformers. The circuit of Figure 3.10(a) can perform as a balun, the operation of which can be explained by fundamental transmission line theory. When current is flowing along one winding of the transformer, current is enforced to flow in the anti-parallel direction in the other winding. The choking reactance of the transmission lines, which isolates the input from the output, is obtained by coiling the transmission line around a ferrite core or by threading the line through ferrite beads. The most important objective is to have the choking reactance of the transmission line much greater than the load impedance, R_L , so that no common-mode current would go through the back end of the receiver chain. Given that only odd-mode current would flow through the two windings of the transformer, shown as green arrows in Figure 3.10(a), Signals remain balanced through the signal path. The upper limit of the bandwidth usually extends to few hundreds of GHz, whereas the lower limit is directly determined by the saturation of the ferrite core and the reactance of the transmission line. Thus, the choice of the ferrite core and the number of turns contribute the most among all the factors in determining the performance of the transmission-line transformers [15, 16, 17, 18].

Shown in Figure 3.11 is the usage of the basic building block of transmission-line transformers to achieve 1:4 impedance transformation. Voltage and current derivation can be done as follows,

voltage analysis is based on the illustration in Figure 3.10(a). Assume the induced voltage across one winding of the transformer is v volts, having the positive polarity at the positive

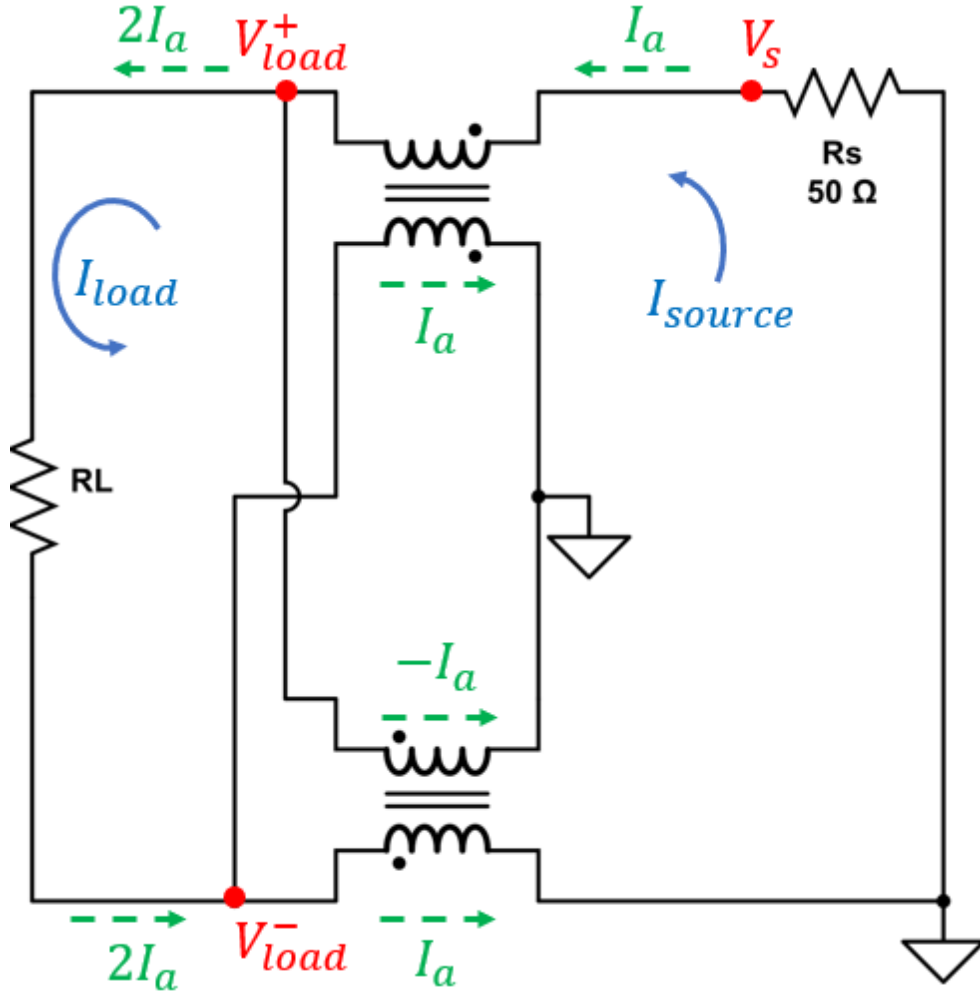


Figure 3.11: 1:4 transmission-line impedance transformer voltage and current analysis using the basic building block in Figure 3.10(a). The circuit model is derived from [15].

phase point on the winding. Then,

$$V_{load}^+ = v, \quad (3.7)$$

$$V_{load}^- = v, \quad (3.8)$$

Thus, the load voltage, the voltage across the input of the antenna can be found in terms of the source voltage as,

$$V_{load} = V_{load}^+ - V_{load}^- = 2v \quad (3.9)$$

The source voltage can be found to be,

$$V_s = (V_{load}^+ + v) - (V_{load}^- - v) = 4v \quad (3.10)$$

Thus,

$$V_s = 2 * V_{load} \quad (3.11)$$

Current at the load and the source can be calculated as,

$$I_{source} = I_a \quad (3.12)$$

$$I_{load} = 2 * I_a \quad (3.13)$$

Finally, the load impedance in terms of the source impedance can be derived to be,

$$Z_{load} = \frac{V_{load}}{I_{load}} = \frac{\frac{V_s}{2}}{2 * I_a} = 0.25 * \frac{V_s}{I_a} = \frac{1}{4} * Z_{source} \quad (3.14)$$

Equation 3.12 verifies that the antenna's impedance can be amplified by four times in magnitude at the source by cunningly placing and wiring the input and output of a pair of transmission-line transformers.

The fabricated prototypes are shown in the Figure 3.10(b) and (c). Bifilar 7-turn and 14-turn #30 AWG wire wound around Ferrite 73-2401 core Guanella transmission line transformer and current balun are used.

Ferrites have the ability to attract magnetic flux. Hence, when a cable is passed through a ferrite core, it creates a concentrated magnetic field inside the core, which is eventually converted to heat. This heat gets dissipated along with the magnetic loss of the ferrite, which prevents noise emission. That is how ferrite cores can suppress noise without grounding. However, no ferrite cores are ideal for every application. Immunity from saturation at the frequency of operation is an important factor to consider when choosing the right ferrite core. FB-73-2401 Ferrite Core is one of the only two ferrite cores available on the commercial market that are optimal for the highest quality factor, when operated at a frequency lower than 30MHz. Thus, FB-73-2401 is chosen for the 1:4 transmission-line transformers and current balun.

Although for operating the transmission-line transformers near the lower limit of the bandwidth the choice of the wire's diameter and the number of twists for the bifilar wires are not critical, the process of deciding these parameters is demonstrated here to be precise.

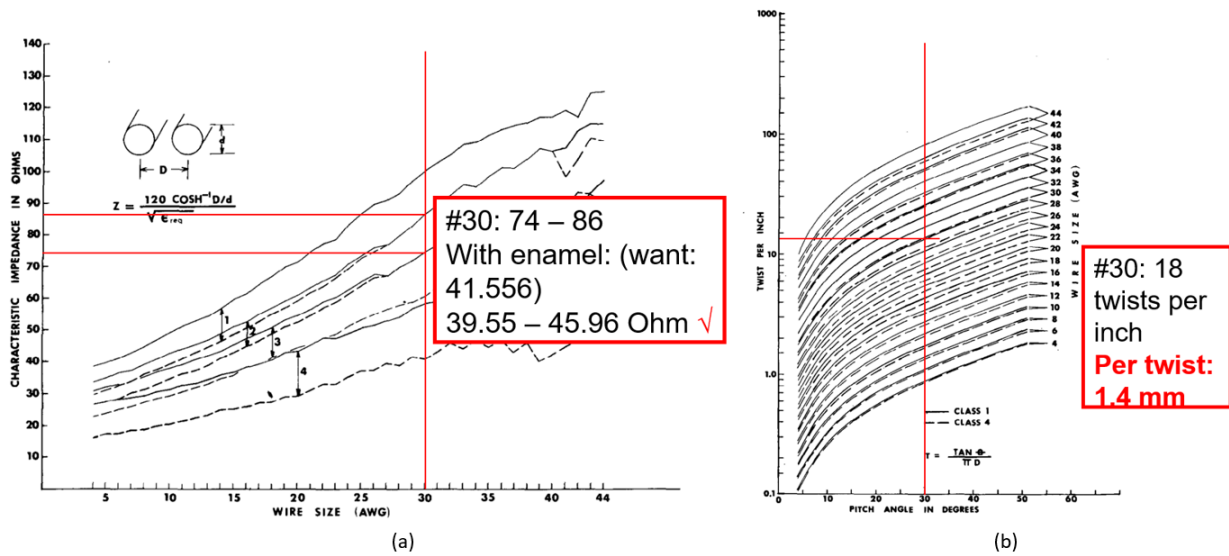


Figure 3.12: Design curves for choosing the wire’s diameter and number of twists per inch. (a) Characteristic impedance of bifilar wire based on MLW583 wire dimensions, and (b) bifilar transmission-line twist per inch in terms of the pitch angle [19]

Available in Figure 3.12 are the design curves utilized to finalize the choice of wire and the number of twists. To achieve an approximately 50-Ohm characteristic impedance, #30 wire with 1.4mm per twist on bifilar wires are chosen. The details of how the transformer are meticulously wound are available in the appendix.

3.4.2 Varactors and Biasing Structure

A varactor diode is a P-N junction diode that changes its capacitance and series resistance as the bias applied to the diode is varied. The term “varactor” comes from the phrase “variable reactor” and means a device whose reactance can be varied in a controlled manner, in this case, with dc bias voltage [20]. Unlike a mechanically variable capacitor that changes its capacitance through the relative movement of two conducting plates, varactor diode is operated through a purely electrical methodology. Hyperabrupt junction tuning varactor, among all types of varactors, has the largest capacitance range. For example, SMV1801-079LF from Skyworks Solutions, Inc. achieves a capacitance from 87.66pF to 2.65pF with a reverse bias voltage from 0V to 30V. The capacitance range of SMV1801-079LF is wide

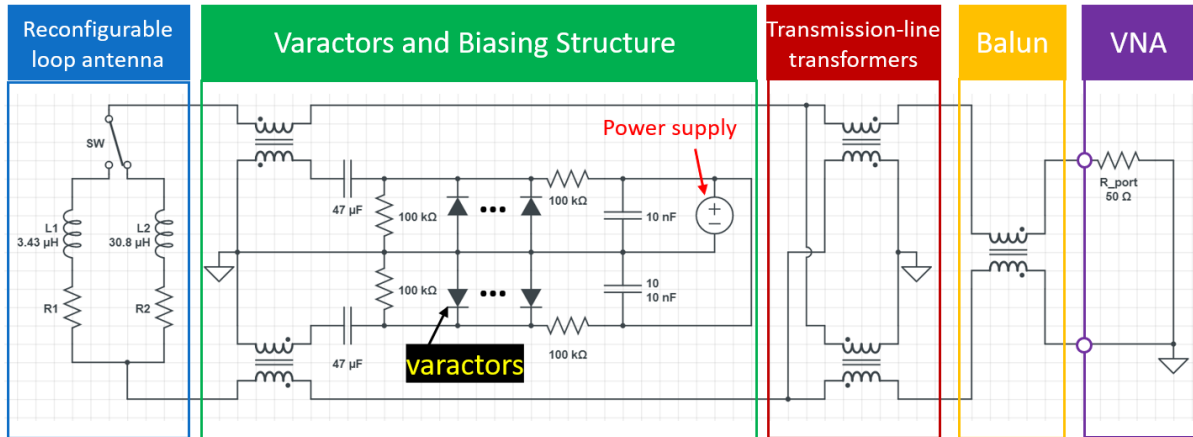
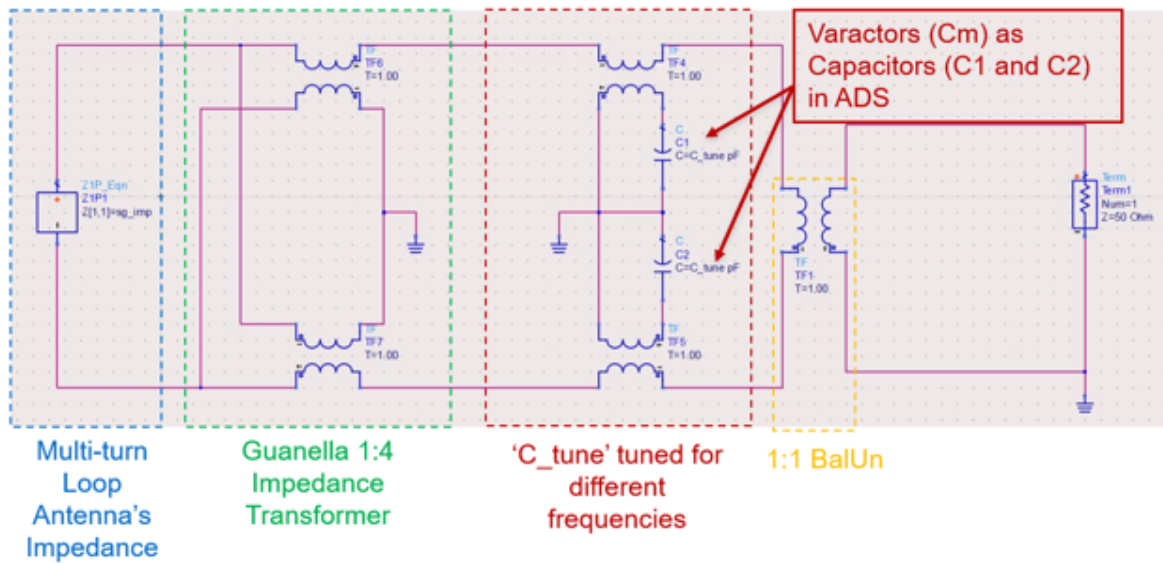


Figure 3.13: Schematic of the proposed impedance matching network incorporating electrically tuned varactors and specialized low-insertion-loss biasing structure.

enough to tune the frequency of the proposed reconfigurable loop antenna through 0.8 to 10MHz.

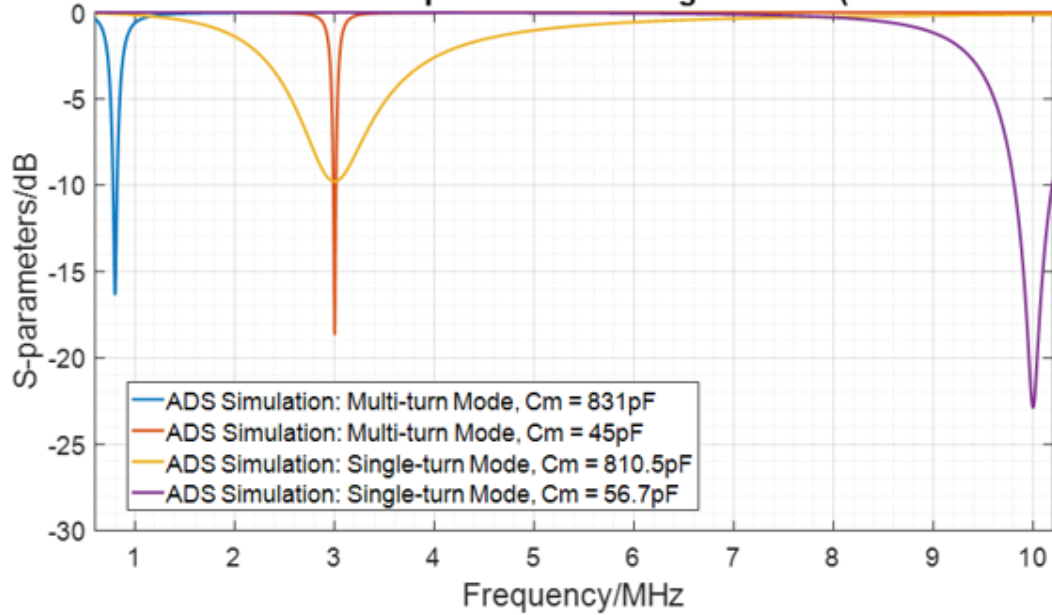
Apart from choosing the suitable varactor, another critical step is to develop an optimal biasing structure. The criteria of the structure is three-fold: 1) the RF signal needs to travel through the varactor but not into the DC power supply, 2) DC bias only goes through the varactor and not into the signal path, otherwise the vector network analyzer (VNA) or the receiving chain would be destroyed by the DC power, and 3) the bandwidth of operation needs to be wide enough to cover 0.8 — 10MHz. In prior literature, RF chokes and low-pass filters (LPF) have been popular options for accomplishing the criteria 1 and 2. However, a RF choke operates only within a narrow bandwidth and LPF requires a cutoff frequency much higher than 10MHz for an optimal signal suppression at the "stop" frequencies and relatively simple architecture (i.e., less than 5 stages). Thus, due to failure in meeting the criteria 3, RF chokes and LPF are not applicable for the application of this work.

Herein, a varactor biasing network that achieves complete DC isolation and wide-band RF choking performance is proposed. A full schematic of the network is available in Figure 3.13. Conventional transformers are used to isolate the DC power from the main signal path, while still introducing variable capacitance in series with the reconfigurable loop antennas' inductance in order to turn the resonant frequency. It can be seen that the varactors and



(a)

ADS Simulated Results of Impedance Matching Network (Ideal Transformers)



(b)

Figure 3.14: Advanced Design System (ADS) simulation of the proposed impedance matching network incorporating varactors and biasing structure, considering only ideal transformers. (a) schematic, and (b) S11 simulation results with different multi-turn and single-turn mode antenna's impedance.

biasing structure section of the schematic remains symmetrical from the center "axis" of the circuit. Consequently, the symmetry and the opposite phase directions on the two transformers lead to balanced signals throughout the antenna and the frequency tuning section. Assume that the signal path is connected to the primary winding of the transformer and the varactors are connected to the secondary winding. Protection resistors, DC blocking capacitors, and safety capacitors are added in the secondary winding to ensure safe and accurate application and of biasing levels across the varactors, while the signal path remains intact from the DC current. For proof of concept, the proposed biasing network with ideal transformers and lumped elements is modeled and simulated in the Advanced Design System (ADS) software. The results are shown in Figure 3.14. By tuning the capacitance of C_m through a max-to-min ratio less than 29, the resonant frequency of the reconfigurable loop antenna can be turned through 0.8 to 3MHz (in the multi-turn mode) and 3 to 10MHz (in the single-turn mode). From Figure 3.14(b), noticeably the bandwidth of the S-11 is much narrower in the multi-turn mode than that in the single-turn mode. Consequently, a larger quality factor is achieved during the operation in the lower frequencies than that in the higher frequencies. This phenomenon is consistent with the expectation, because the quality factor is defined as

$$Q = 2\pi \times \frac{\text{energy stored}}{\text{energy dissipated per cycle}} = \frac{\omega L}{R} = \frac{f_0}{BW|_{-10dB}} \quad (3.15)$$

where f_0 is the resonant frequency, $BW|_{-10dB}$ is the -10dB bandwidth, L is the inductance of the loop antenna, and R is the resistance of the loop antenna. As seen through the equations provided in section 3.2.1, the inductance of the three-turn loop is roughly nine times that of the single-turn loop. However, the resistance of the three-turn loop is extremely small and at the same order of magnitude as that of the single-turn loop. Thus, the quality factor of the loop antenna during the multi-turn mode is larger than that of the antenna during the single-turn mode. According to Equation 3.15, consequently the observed -10dB bandwidth is also narrower in the multi-turn mode.

Traditionally, a conventional transformer is used with parallel capacitance soldered across either the primary or the secondary winding to cancel out the excessive inductance in the

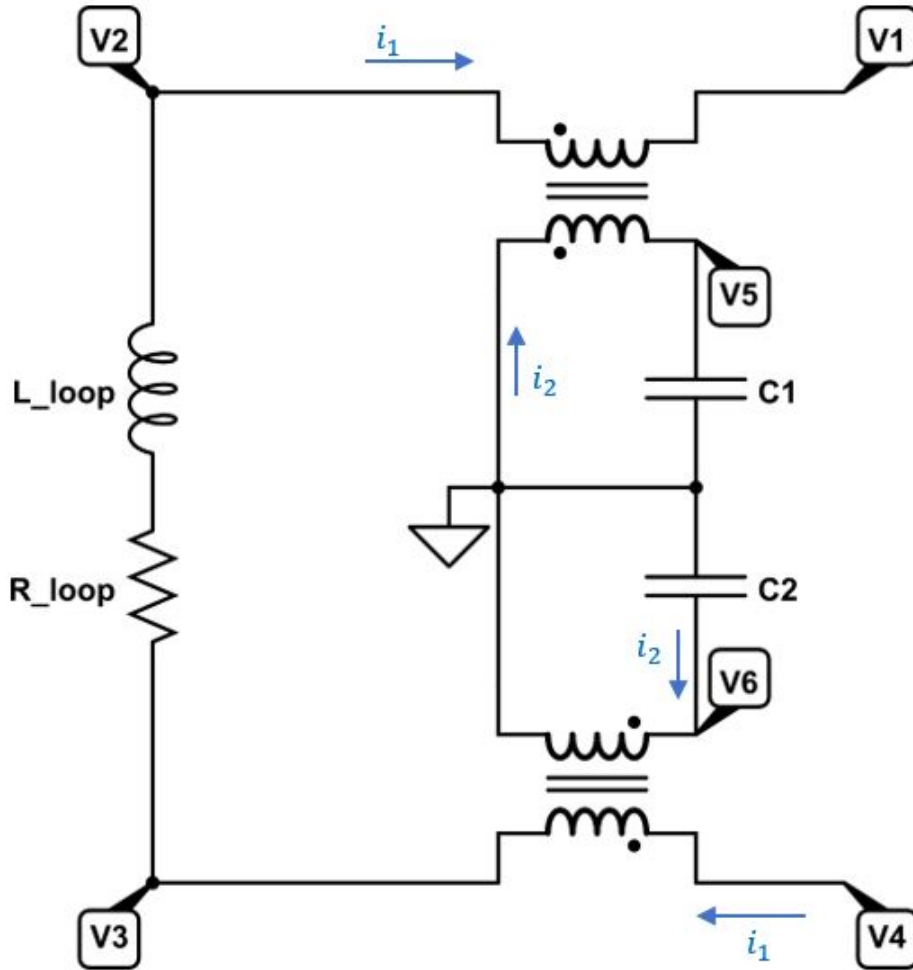


Figure 3.15: Simplified schematic of the proposed use of varactors and design of a varactor biasing structure. L_{loop} and R_{loop} comprise the input impedance of the loop antenna. The nodal voltages and current values are labeled as tag and arrows.

winding at the single frequency of operation. Nevertheless, For this work since the operation is required through an extremely wide bandwidth, instead of adding fixed capacitors, the excessive inductance of the winding in the transformer has to be considered and accommodated in the implementation. Shown in Figure 3.15 is a schematic of the loop antenna and the frequency tuning network incorporating varactors. The protection resistors and capacitors, and parasitic series inductance and resistance of varactors are neglected here for the sake of simplicity. A rigorous voltage and current can be done as following:

Assume L is the inductance of a winding in the transformer. Further, the inductance of the primary and the secondary winding are approximated to be the same. M is the mutual inductance, and can be calculated as,

$$M = k \cdot L \quad (3.16)$$

where k is the coupling coefficient, having a value of around 0.7 for strongly coupled bifilar wires wound on a ferrite magnetic core in traditional transformers. Thus,

$$V_2 - V_1 = j\omega Li_1 + j\omega Mi_2, \quad (3.17)$$

$$-V_5 = j\omega Li_2 + j\omega Mi_1 = -\frac{1}{j\omega C_1} i_2, \quad (3.18)$$

$$V_4 - V_3 = j\omega Li_1 + j\omega Mi_2, \quad (3.19)$$

For the requirement of symmetry, the capacitance of the varactors at C_1 is the same as that of the varactors at C_2 . Therefore,

$$V_6 = j\omega Li_2 + j\omega Mi_1 = -\frac{1}{j\omega C_1} i_2. \quad (3.20)$$

From Equation 3.18,

$$i_2(j\omega L + \frac{1}{j\omega C_1}) = -j\omega Mi_1, \quad (3.21)$$

Isolating i_2 to one side of the equation and simplifying the divisions, it can be found that,

$$i_2 = i_1 \left(\frac{\omega^2 M C_1}{1 - \omega^2 L C_1} \right) \quad (3.22)$$

Substituting Equation 3.22 into Equation 3.17 and 3.19, i_2 can be eliminated from the expression of the voltage as,

$$\begin{aligned} V_2 - V_1 &= j\omega i_1 \left(L + \frac{\omega^2 M^2 C_1}{1 - \omega^2 L C_1} \right) \\ &= V_4 - V_3 \end{aligned} \quad (3.23)$$

In addition, the voltage across the loop antenna can be generalized as,

$$V_3 - V_2 = i_1(j\omega L_{loop} + R_{loop}) \quad (3.24)$$

The input voltage V_{in} can be found to be,

$$\begin{aligned} V_{in} &= V_1 - V_2 + V_2 - V_3 + V_3 - V_4 \\ &= -2j\omega i_1 \left(L + \frac{\omega^2 M^2 C_1}{1 - \omega^2 L C_1} \right) - i_1 (j\omega L_{loop} + R_{loop}) \end{aligned} \quad (3.25)$$

Finally, the input impedance looking into the frequency tuning network is,

$$Z_{in}(\omega) = \frac{V_{in}}{-i_1} = j\omega \left(2L + 2k^2 \frac{\omega^2 M^2 C_1}{1 - \omega^2 L C_1} + L_{loop} \right) + R_{loop} \quad (3.26)$$

To tune the resonant frequency of the loop antenna to $\omega_i = 2\pi f_i$, the impedance at the frequency needs to be resistive. Equivalently, the imaginary part of $Z_{in}(\omega_i)$ in the Equation 3.26 needs to be zero. Thus,

$$2L + L_{loop} = 2k^2 \frac{\omega_i^2 L^2 C_1}{\omega_i^2 L C_1 - 1} \quad (3.27)$$

Let's denote $\frac{2L+L_{loop}}{2k^2}$ as L_{eff} , then for a given desired resonant frequency f_i , the required tuning capacitance C_1 can be readily calculated through

$$C_1 = \frac{1}{4\pi^2 f_i^2 L \left(1 - \frac{L}{L_{eff}} \right)} \quad (3.28)$$

In turn, for a known tuning capacitance C_1 , the resulting resonant frequency f_i can be found through

$$f_i = \frac{1}{2\pi} \sqrt{\frac{1}{C_1 L \left(1 - \frac{L}{L_{eff}} \right)}} \quad (3.29)$$

From Equation 3.29, it can be seen that the inductance of the winding in the transformer plays a role in determining the required tuning capacitance. However, the inductance is not the only factor that characterizes the performance of the transformer. Another equally important factor is the saturation of the magnetic core, which can only be characterized empirically through S-parameter measurement. In chapter 4, how to ensure non-saturated operation of magnetic cores is demonstrated.

3.5 Near-field Electric Field and Magnetic Field of an Electrically Small Multi-turn Loop Antenna at 1MHz

This study emphasizes on the six-meter away near-field electric and magnetic fields of the reconfigurable multi-turn loop antenna at 1MHz in free space. The proposed reconfigurable multi-turn electrically small loop antennas with electrical frequency tuning capability for 1-MHz operation is a 1m by 1m vertically stacked three-turn loop antenna. It is investigated and compared between two cases: 1) with and 2) without the presence of sand (pictorial illustrations are available in the Figure 3.16). For both cases, the observation window is consistently placed at a fixed position relative to the loop antenna. In the second case, the sand box is a one-tenth of the wavelength dimension cube. As discussed in chapter 1, the loop antenna is still on the bottom of the Mars rover chassis, so the antenna is 1m away from the surface of the sand box in the simulation.

From the results and derivation shown in Section 2.4, the current along an electrically small loop antenna contributes tremendously to the electric and magnetic fields of the antenna, observed in the near-field region. The goal is to have the current be evenly distributed across the loop antenna, so that the E and H fields' patterns can be analytically estimated. It is a common practice to add dummy lumped capacitors or distributed capacitance in series along an electrically small loop antenna to improve the current uniformity, especially in the field of MRI RF coil designs [5]. Thus, for the vertically stacked three-turn loop of the proposed design for 1-MHz operation, three dummy series capacitors are added across different positions of the loop. The simulation results are shown in Figure 3.17. At phase = 0° , the null of the electric field is at $\theta = 0$ and the peak of the magnetic field is at $\theta = 0$, which is consistent with the classic analytical solution of the electric and magnetic fields of an electrical small loop antenna, derived in Section 2.4. More important, by comparing Figure 3.17 (a) and (b) with Figure 3.17 (c) and (d), it can be observed that the near-field electric and magnetic fields of the loop antenna remain approximately the same whether with or without the presence of the sand box. Both the pattern and the magnitude of the fields are not degraded when observed in the dry sandy soil, a material modeled in the CST

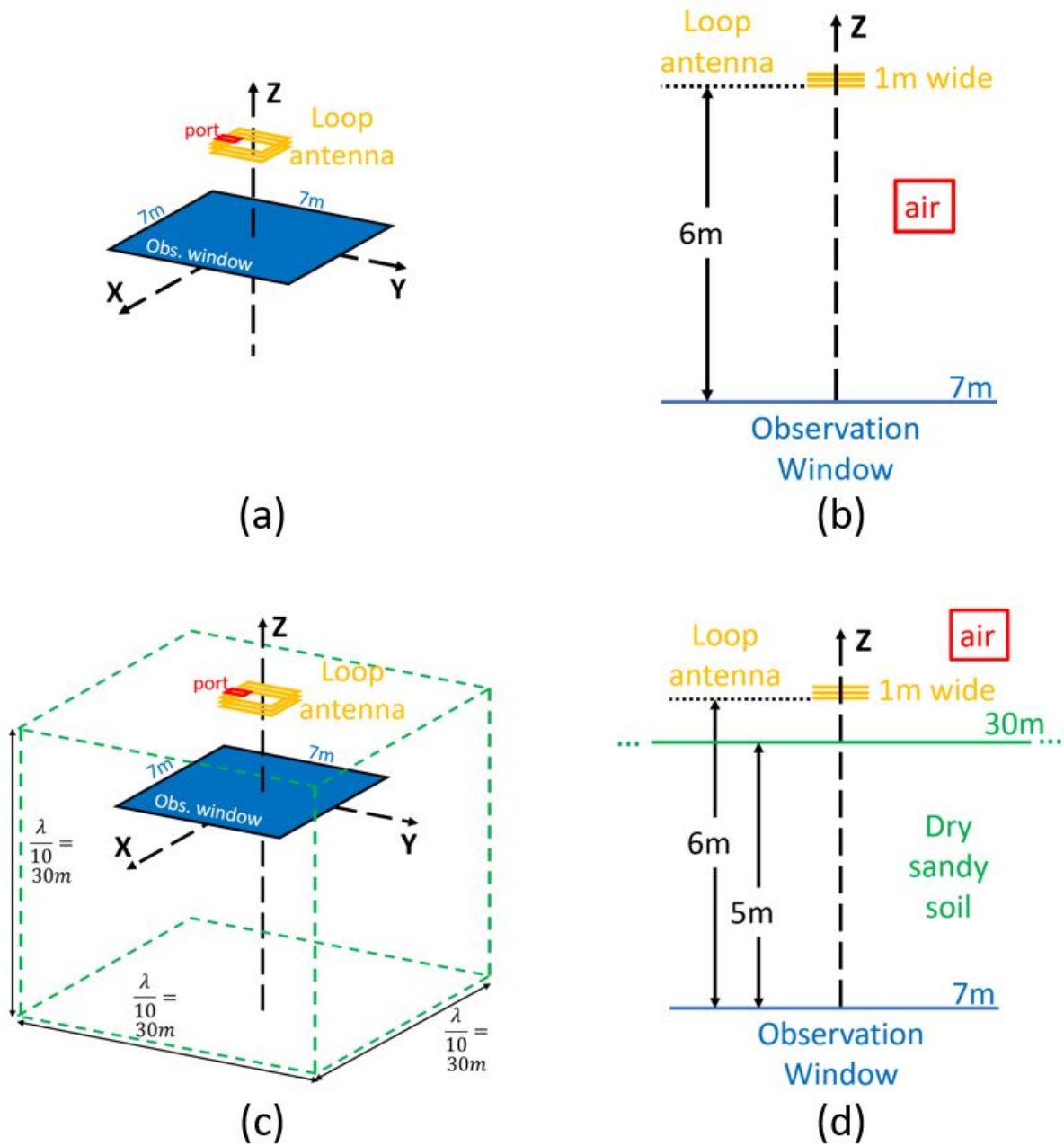


Figure 3.16: Observation window illustrations of the near-field electric and magnetic fields at 1MHz. The proposed reconfigurable multi-turn electrically small loop antennas with electrical frequency tuning capability is observed in air (a) perspective view, and (b) side view and with the presence of sand (a) perspective view, and (b) side view.

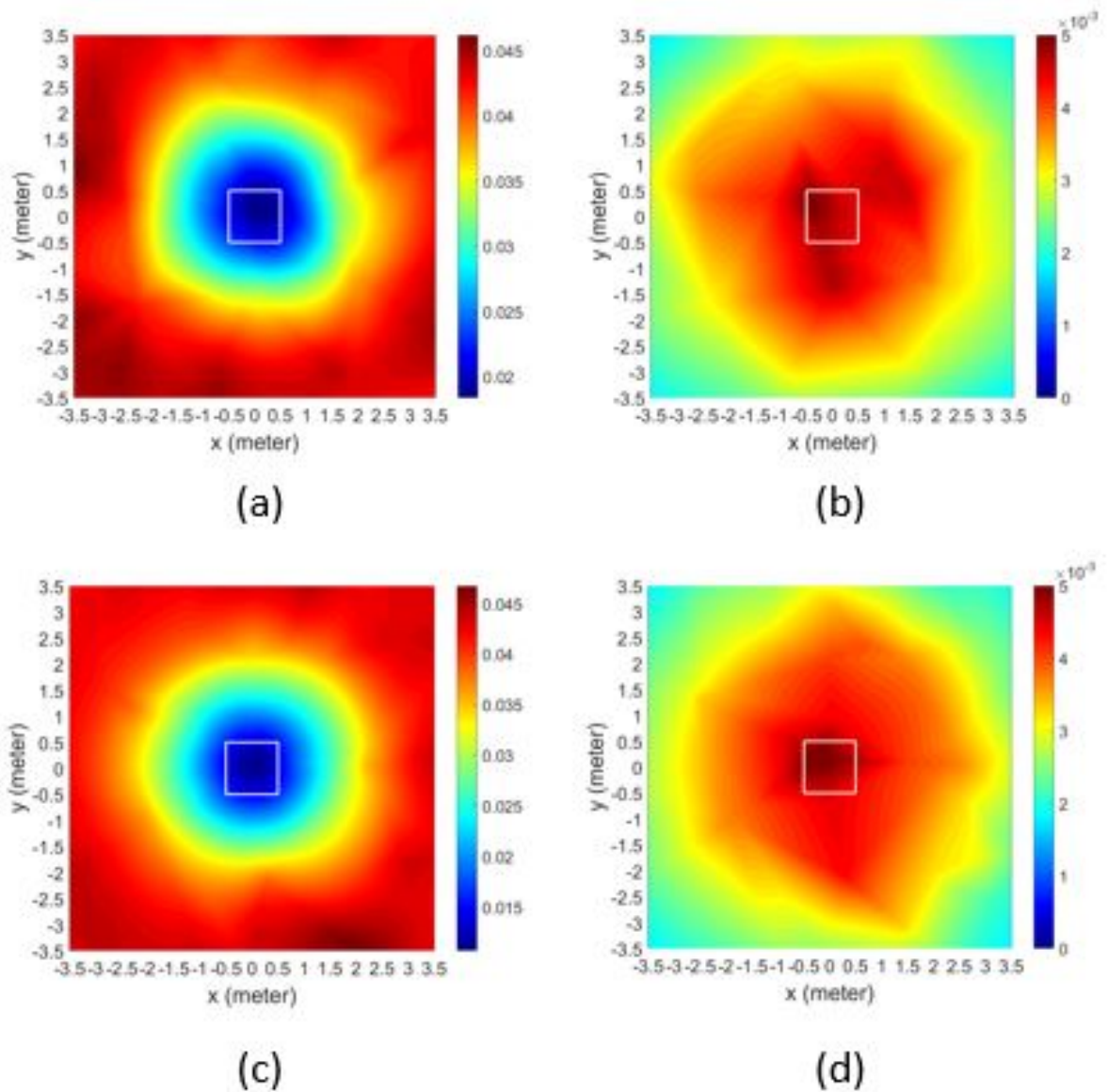


Figure 3.17: Simulated near-field electric and magnetic fields at 1MHz with observation windows shown in Figure 3.16. The white hollow square in the figure shows the position of the loop antenna relative to the observation window along an xy-plane. (a) electric field of the antenna in air, (b) magnetic field of the antenna in air, (c) electric field of the antenna with the presence of sand, and (d) magnetic field of the antenna with the presence of sand.

full-wave simulation. This exercise supports that the radiated electromagnetic wave from the proposed multi-turn loop antenna at 1MHz would not lose its power and pattern, even when being operated in the environment of a large sand box.

CHAPTER 4

Fabrication and Measurements

4.1 Single-Turn Electrically Small Loop Antennas with Mechanical Frequency Tuning Capability

4.1.1 Single Loop Antenna

A prototype was built and measured for the electrically small single-turn loop antenna proposed in Chapter 2. For construction, 2-cm-wide $30\text{-}\mu\text{m-thick}$ copper foil tapes were used for the loop antenna, and a $1.17\text{m} \times 1.12\text{m}$ cardboard was used as support.

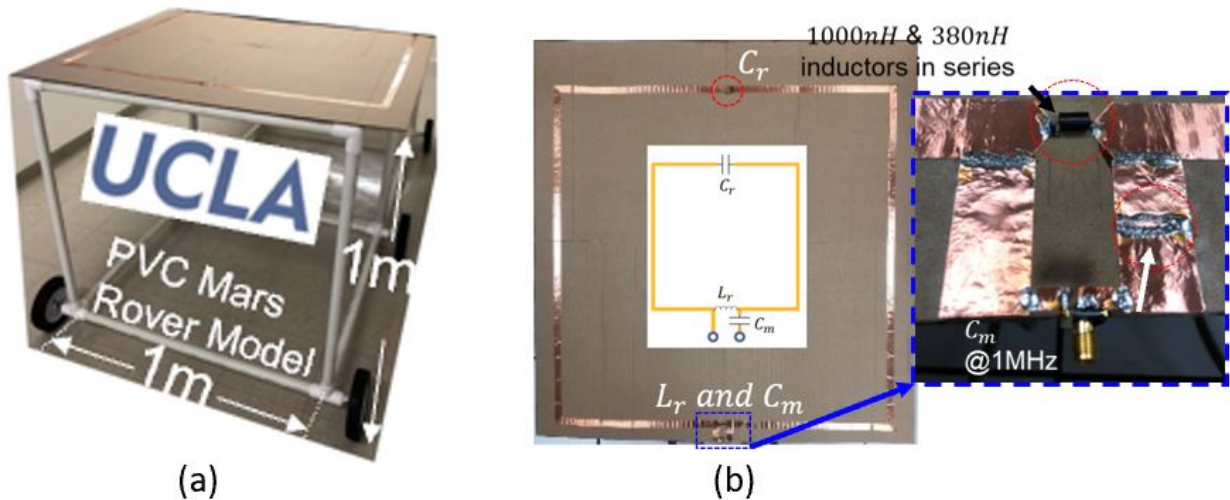


Figure 4.1: Fabricated prototype. (a) PVC Mars rover model fabricated by UCLA. (b) Closed-up view of the loop antenna construction and surface mount inductor positioning.

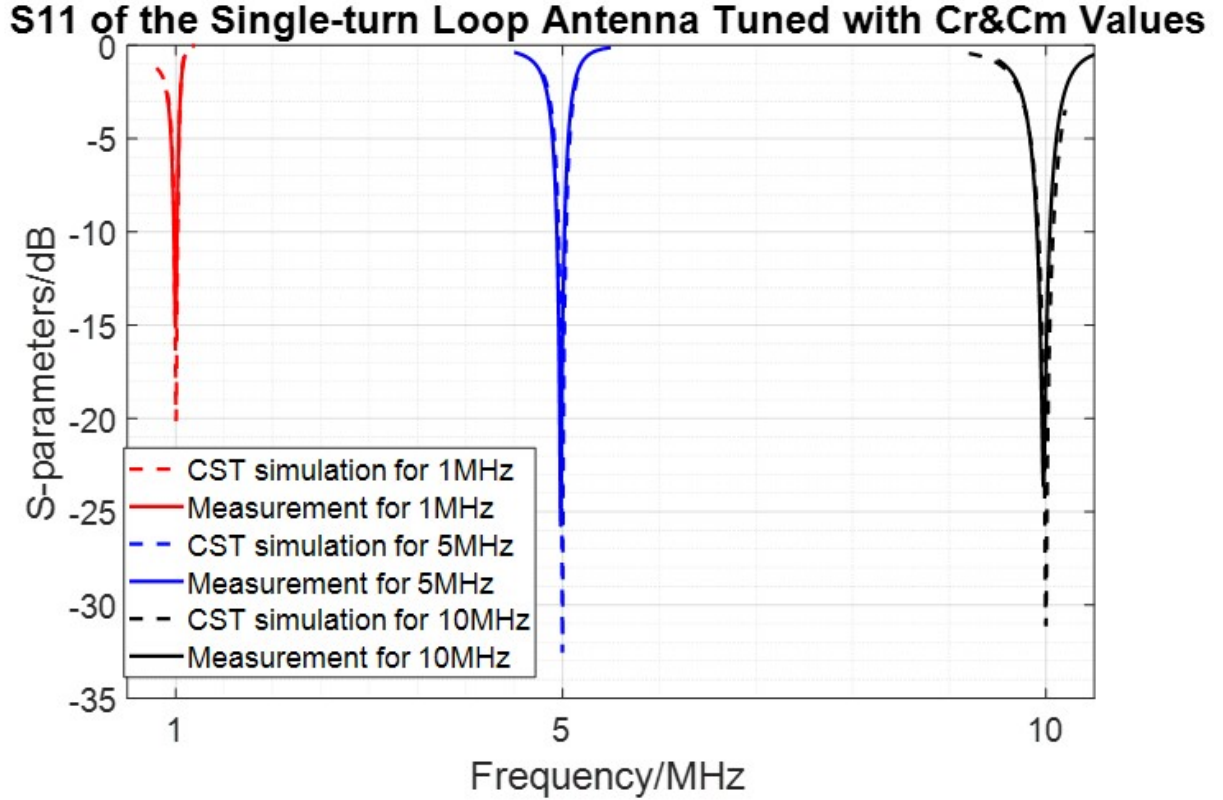


Figure 4.2: CST simulated and measured S11 comparison of the proposed single-turn loop antenna at 1MHz, 5MHz and 10MHz with different Cr and Cm values.

Table 4.1: Component Usage and S11 Performance of the Measurement

	1 MHz	5 MHz	10 MHz
Cr	5160pF	193.4pF	40.4pF
Cm	shorted	175pF	50pF
Measured Lr (ESR)	1286.9nH (1.7 Ohm)	1304.4nH (2.3 Ohm)	1438.8nH (3.9 Ohm)
Simulated S11	-20.1dB @1.00MHz	-32.6dB @5.00MHz	-31.1dB @10.00MHz
Measured S11	-15.1dB @1.00MHz	-25.7dB @4.98MHz	-23.6dB @9.98MHz

S11 measurement of the single-turn loop antenna at each discrete frequency from 1 to 10MHz has been performed using a vector network analyzer (VNA). shown in Figure 4.2 and Table 4.1 are the results of the measurement done at five representative frequencies, 1MHz, 5MHz and 10MHz. It can be observed that the simulated and measured S11 agree very well,

and the resonance frequency of the loop antenna gets effectively tuned with the designed capacitance at C_r and C_m through the entire desired bandwidth of 0.8 to 10MHz.

4.1.2 Two Loop Antennas

S_{11} and S_{12} performance of two loop antennas have been measured. Two designs have been evaluated: 1) two loops separated by 20 cm and 2) two loops overlapped by a critical distance to have the coupling be minimized. Three loading scenarios have been considered: 1) without any loading in vicinity to the bore-side of the loops, 2) with an 18 inches \times 18 inches \times 18 inches copper hollow box 8.5 inches away from one of the two loops, and 3) with an 18 inches \times 18 inches \times 18 inches copper hollow box 26 inches away from one of the two loops. Due to the large size of the loop, the port is positioned half a meter away from the ports on the VNA. Thus, a flexible coaxial is used to connect the feeding point on the loop antenna to the VNA. A port extension procedure is conducted prior to the measurement.

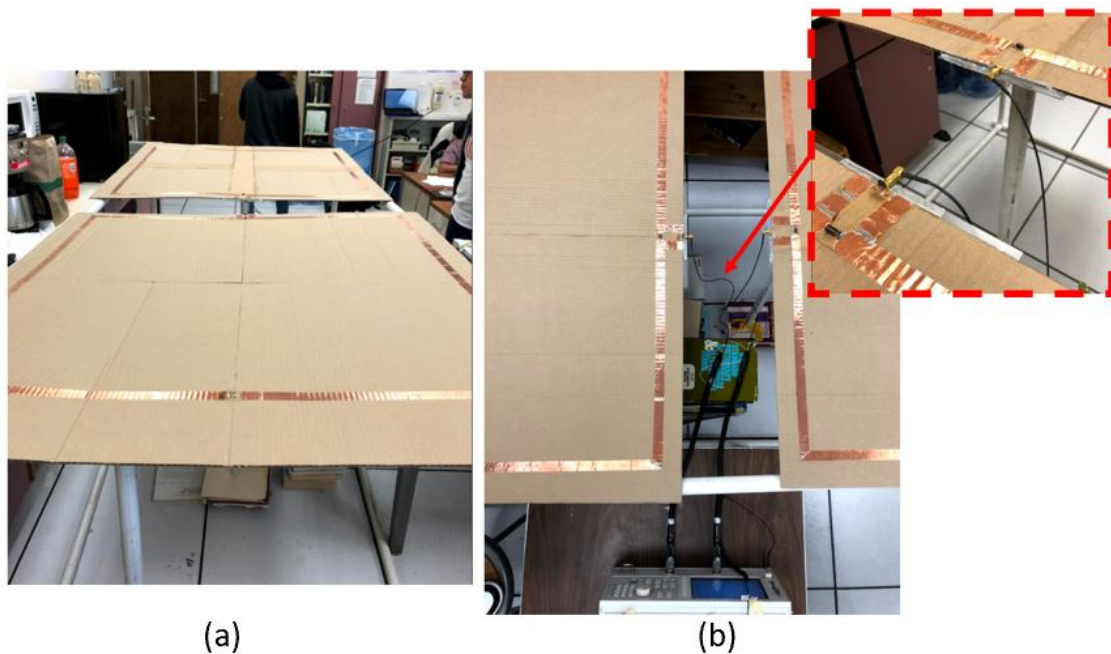


Figure 4.3: Measurement setup of two loops separated by 20 cm apart. (a) Overview of the setup, and (b) closed-up view of the separation of the two loops. Flexible coax cables are used for feeding the loop antennas from VNA.

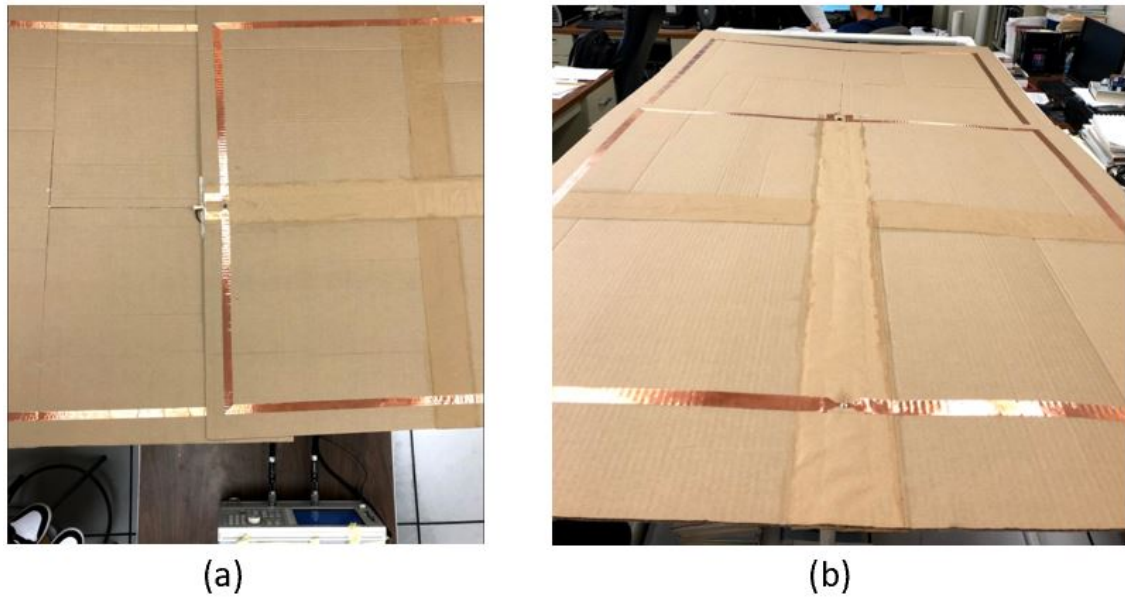


Figure 4.4: Measurement setup of two loops overlapped by 12 cm. (a) Top view of the setup, and (b) Side view of the setup.

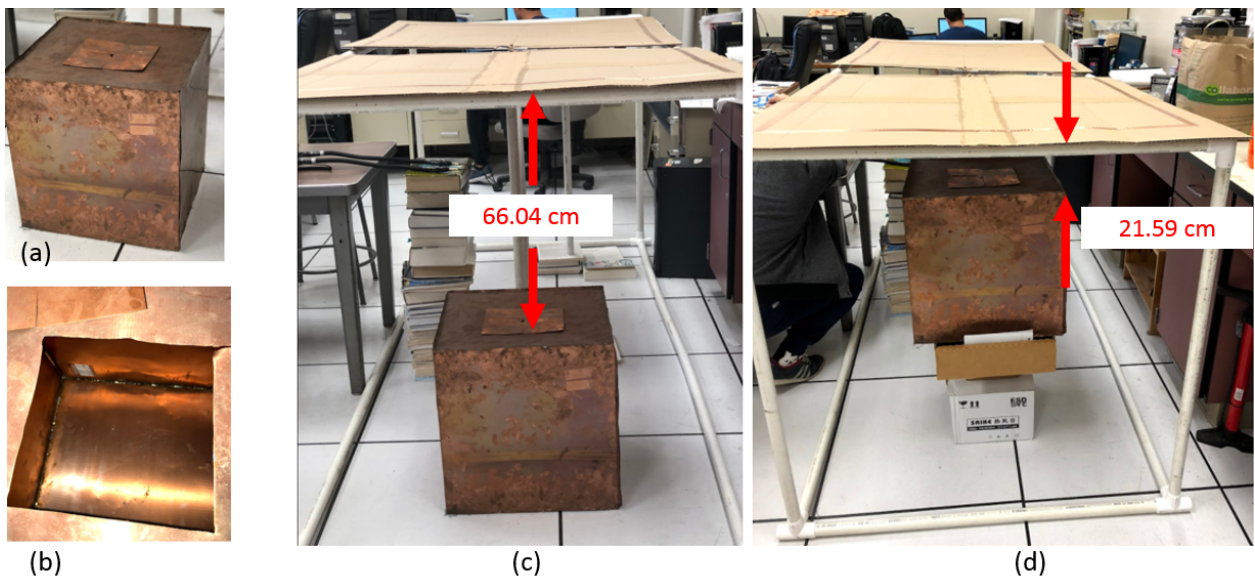


Figure 4.5: Measurement setup of two loop antennas either separated by 20 cm or overlapped by 12 cm, with a copper hollow box in vicinity. (a) Overview of the copper box, (b) inside of the box, (c) box positioned 26 inches away from one of the loops and (d) box positioned 8.5 inches away from one of the loops.

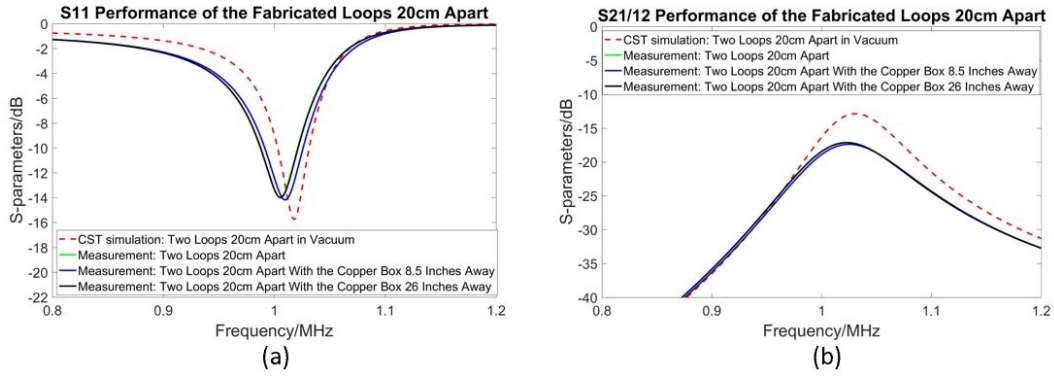


Figure 4.6: Simulated and measured S11 and S12 of the case of two loop antennas separated by 20 cm. (a) S11 and (2) S12.

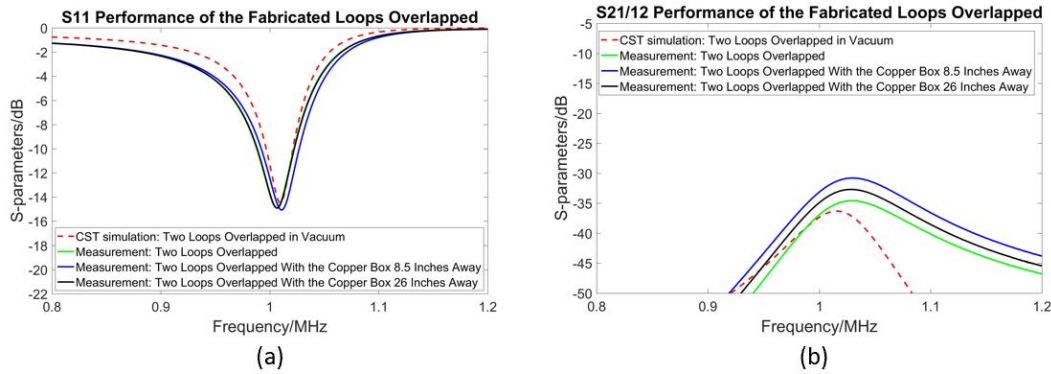


Figure 4.7: Simulated and measured S11 and S12 of the case of two loop antennas overlapped by 12 cm. (a) S11 and (2) S12.

The measurement setups are shown in Figure 4.3, 4.4, and 4.5. From the comparison of the measurement shown in Figure 4.6, it can be seen that the S12 barely changes with or without the presence of the small copper box. This is due to the strong coupling between the two loops, when separated by 20 cm apart. On contrary, from Figure 4.7 the two loops, when overlapped by a critical distance of 12 cm, are more sensitive to the presence and position of the copper box in vicinity as the S12 levels change noticeably with a change in the loading. Future work is to conduct large-scale measurements on the proposed transmitting and receiving loop antennas with a more realistic loading, i.e. similar to Mars.

4.2 Reconfigurable Multi-Turn Electrically Small Loop Antennas with Electrical Frequency Tuning Capability

In this study, a reconfigurable multi-turn electrically small loop antenna with electrical frequency tuning capability is fabricated and investigated through measurement. The design of the impedance matching network, the frequency tuning network and RF balun are presented in Chapter 3. Measurements have been thoroughly and incrementally conducted to test the performance of every section of the circuitry in the receiver chain.

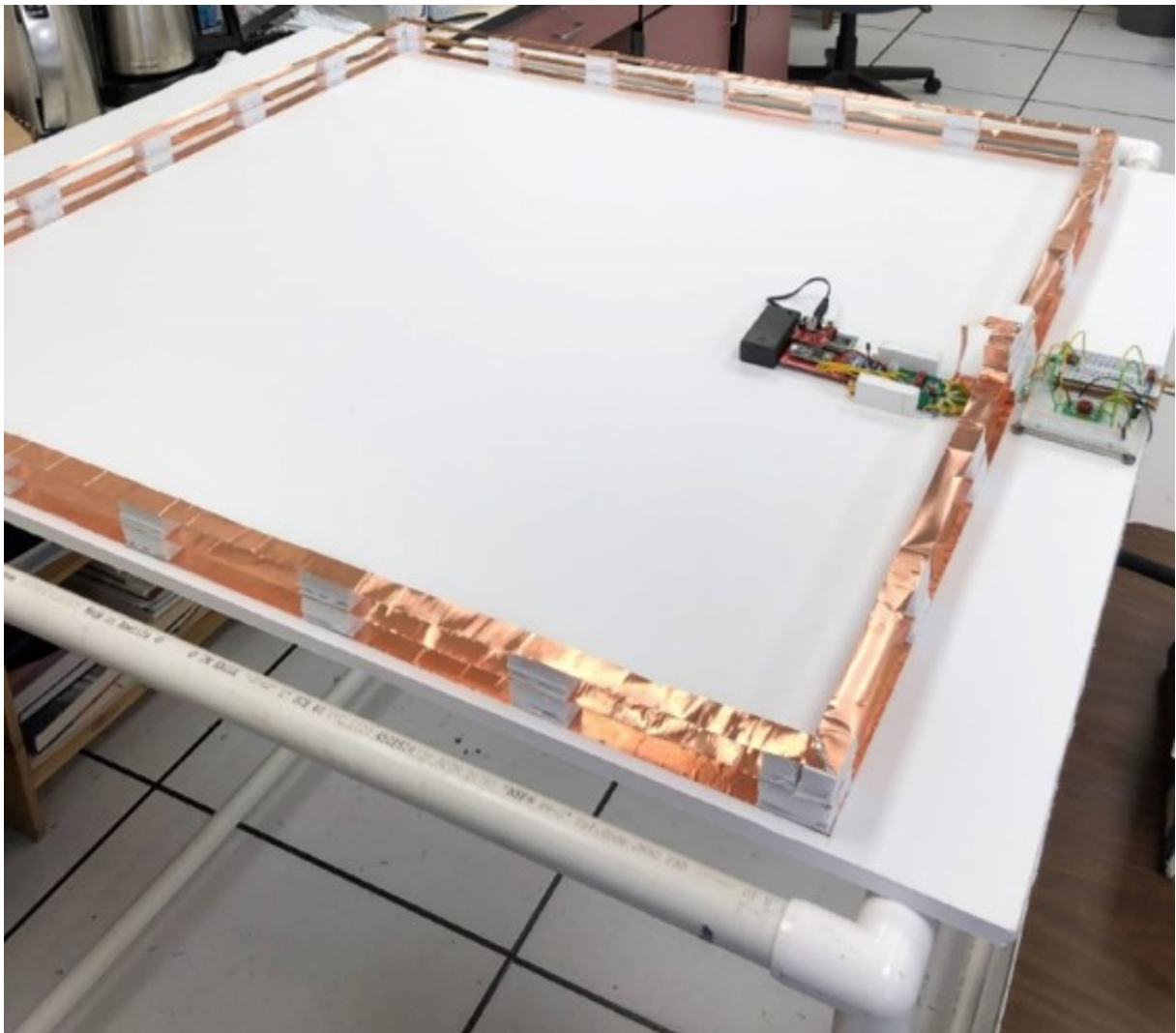


Figure 4.8: Overview of the fabricated reconfigurable multi-turn loop antenna and the receiver PCB board using fixed capacitors as the tuning element.

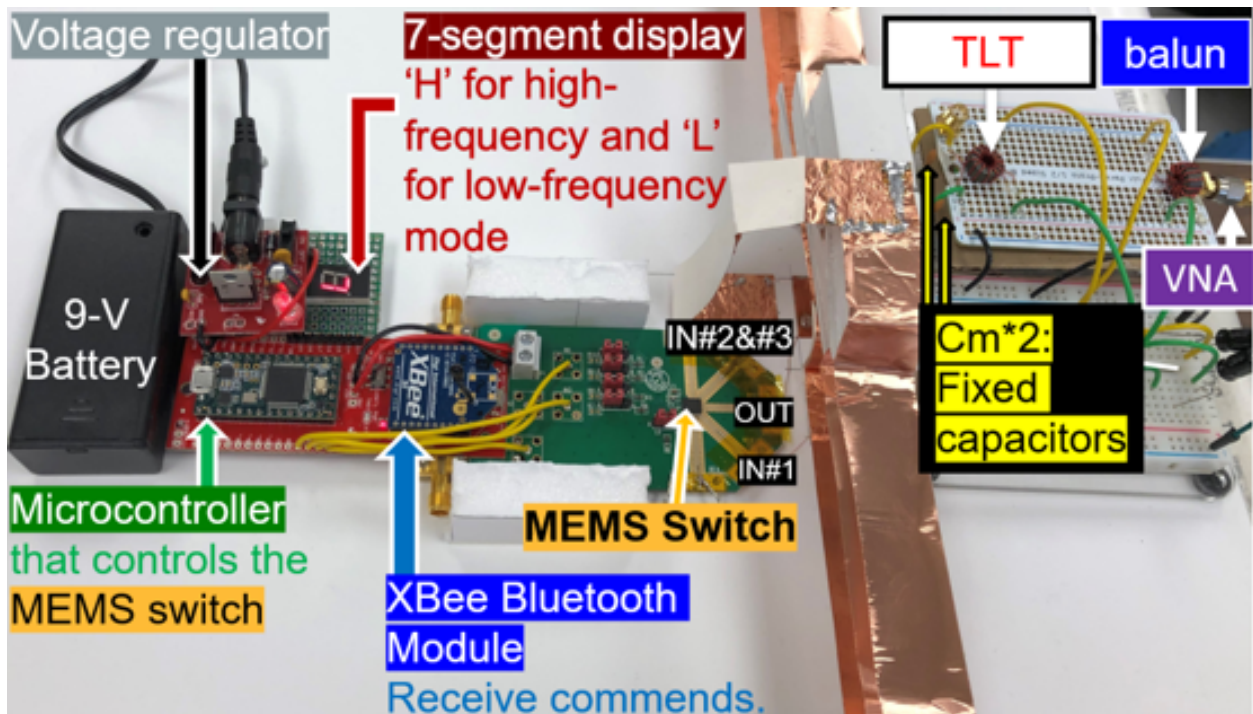


Figure 4.9: Closed-up view of the MEMS switch, the controller unit, the impedance matching network, and the tuning capacitors. The name of the components are labeled. "TLT" in the figure stands of transmission-line transformers. The implementation corresponds to the schematic shown in Figure 3.9.

4.2.1 Measurement Using Fixed Capacitors as the Tuning Element

The fabricated prototype of the proposed reconfigurable multi-turn electrically small loop antennas with electrical frequency tuning capability is shown in the Figure 4.8. Bifilar 7- turn and 14-turn #30 AWG wire wound around Ferrite 73-2401 core Guanella transmission line transformer (TLT) and RF balun are used. An Arduino microcontroller is used to control the MEMS switch to switch between the high-frequency (HF) mode 2 and low-frequency (LF) mode 1 of the loop antenna. A pair of Xbee Bluetooth modules is used to send commands to the micro-controller from the computer through a 2.4GHz communication channel.

The S11 measurements have been performed for the prototype and the results are shown in Figure 4.10. The maximum over minimum ratio of the tuning capacitance is 28.7, which agrees with that of the simulated results, 28.3.

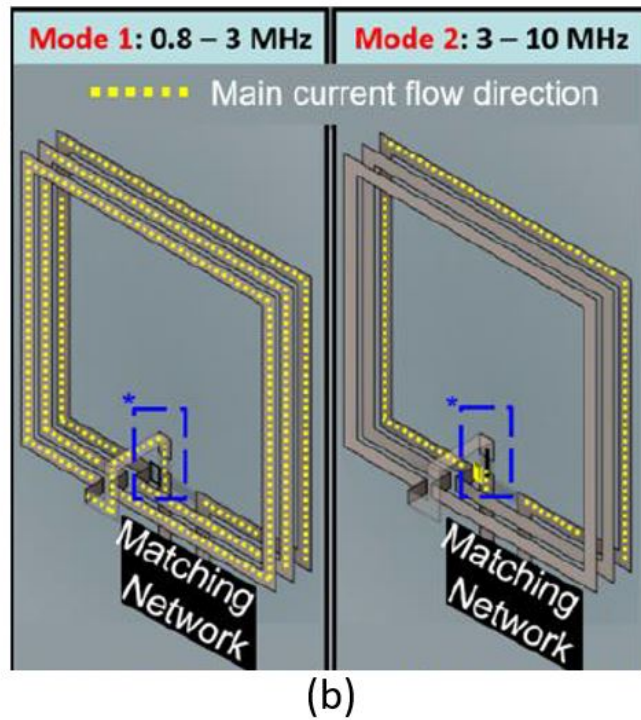
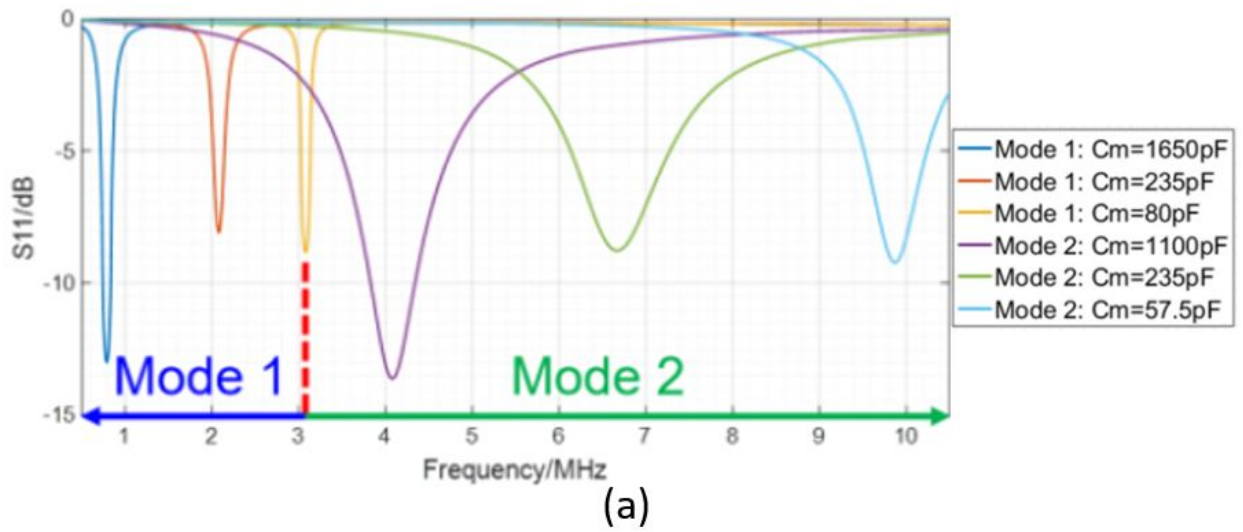


Figure 4.10: (a) Measured S_{11} of the vertically stacked multi-turn loop antenna in mode 1 and mode 2 with 6 representative C_m values. (b) Illustrations of the current flow along the loop antenna under mode 1 and mode 2.

4.2.2 Measurement on the Reconfigurable Multi-Turn Loop Antenna Using Varactors

Last but not least, varactors and the proposed biasing structure are built and measured with surface mount inductors as the load for proof of concept. Shown in Figure 4.11, three air-core $1\mu H$ inductors connected in series mimics the impedance of the proposed reconfigurable multi-turn electrically small loop antenna in Chapter 3. Conventional transformers T1 and T2 are wound on a single FT-150A-K ferrite core that has a 3.8-cm outer diameter. The core has a K-type ferrite core that has a permeability less than the one used for the balun and the transmission line transformer. Given the dimensions and the permeability of the ferrite core, the inductance of a single winding can be estimated through Faraday's law,

$$L \approx \frac{\mu N^2 A}{2\pi r} = 3.5\mu H \quad (4.1)$$

where μ is the permeability of the magnetic core, A is the cross-sectional area, N is the number of turns, and r is the radius of the toroid to the center axis. Using Equation 3.28, the required capacitance range for tuning the resonant frequency through 3 to 10MHz can be readily calculated assuming a coupling coefficient of 0.7 to be,

$$C_{1,initial} = \frac{1}{4\pi^2 [3MHz]^2 * 3.43\mu H * \left(1 - \frac{3.43\mu H}{\frac{2*3.43\mu H + 3.5\mu H}{2*0.7^2}}\right)} = 1198.2pF \quad (4.2)$$

$$C_{1,end} = \frac{1}{4\pi^2 [10MHz]^2 * 3.43\mu H * \left(1 - \frac{3.43\mu H}{\frac{2*3.43\mu H + 3.5\mu H}{2*0.7^2}}\right)} = 107.8pF \quad (4.3)$$

Thus, a capacitance of 1198.2pF to 107.8pF is required, which can be achieved by fifteen SMV1801-079LPF varactors (the capacitance vs. bias voltage of which is a listed in the Table 4.2).

For proof of electrical frequency tunability, in the experiment eight varactors are put in parallel biased from 0V to 12V, which corresponds to a capacitance range of 701.28pF to 44pF. Given the capacitance values, the tuned resonant frequency can also be predicted by using Equation 3.29 as,

Table 4.2: Capacitance vs. Bias Voltage Levels of the Varactors

From datasheet of SMV1801-079LF [21]		
Bias Voltage Levels/V	Capacitance/pF	Total Capacitance of 8 in parallel/pF
0	87.66	701.28
1	58.25	466
2	44.14	353.12
4	26.9	215.2
6	14.8	118.4
10	5.69	45.52
15	3.91	31.28
25	2.81	22.48
30	2.65	21.2

$$f_{initial} = \frac{1}{2\pi} \sqrt{\frac{1}{701.28pF * 3.43\mu H * \left(1 - \frac{3.43\mu H}{\frac{2*3.43\mu H + 3.5\mu H}{2*0.7^2}}\right)}} = 3.9MHz \quad (4.4)$$

$$f_{end} = \frac{1}{2\pi} \sqrt{\frac{1}{44pF * 3.43\mu H * \left(1 - \frac{3.43\mu H}{\frac{2*3.43\mu H + 3.5\mu H}{2*0.7^2}}\right)}} = 15.5MHz \quad (4.5)$$

Thus, a tuned resonant frequency range of 3.9MHz to 15.5MHz is predicted. From the S11 measurement Results shown in Figure 4.12, the resonant frequency is successfully tuned and the measured frequency tuning range is from 3.7MHz to 8.7MHz. It is relatively smaller than the prediction. This result is reasonable because the mathematical predictions done in the design phase only consider ideal models of the varactors. The parasitic inductance and resistance of actual varactor components can contribute to a narrower frequency tuning range in practice. Luckily, there is a large bias voltage range for the varactors in use. Thus, the measurement results support that with a larger DC bias voltage range, leading to a wider tuning capacitance range of the varactors, the resonant frequency of the fabricated reconfigurable electrically small multi-turn loop antenna can be electrically tuned through the desired bandwidth.

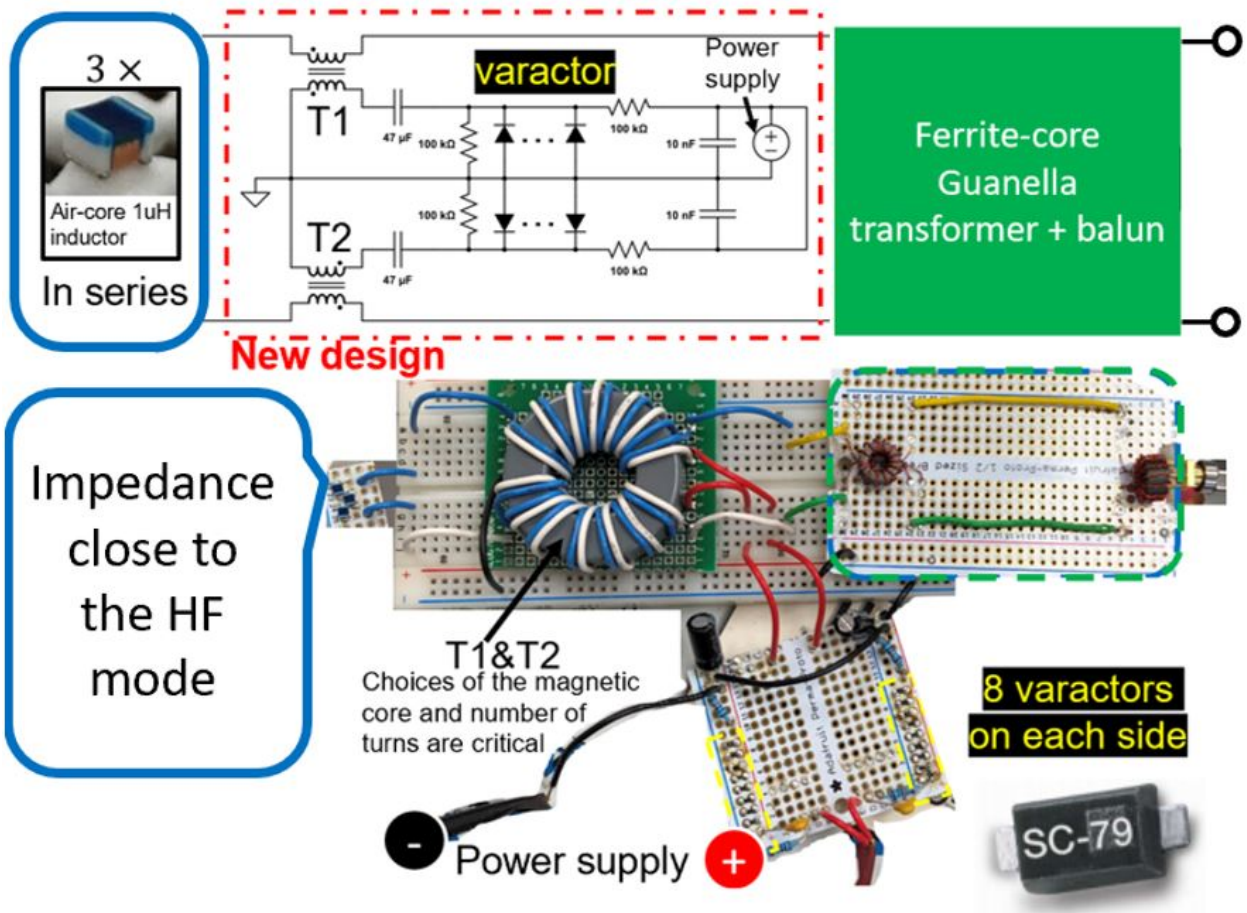


Figure 4.11: Schematic of varactors and the biasing network implementation. The load is consisted of three air-core $1\mu H$ inductors in series mimicking the impedance of the antenna in the HF mode. T1 and T2 in the figure are the conventional transformers for DC isolation. Eight Skyworks Solutions, Inc. SMV1801-079LF varactors are used at each one of the two tuning points.

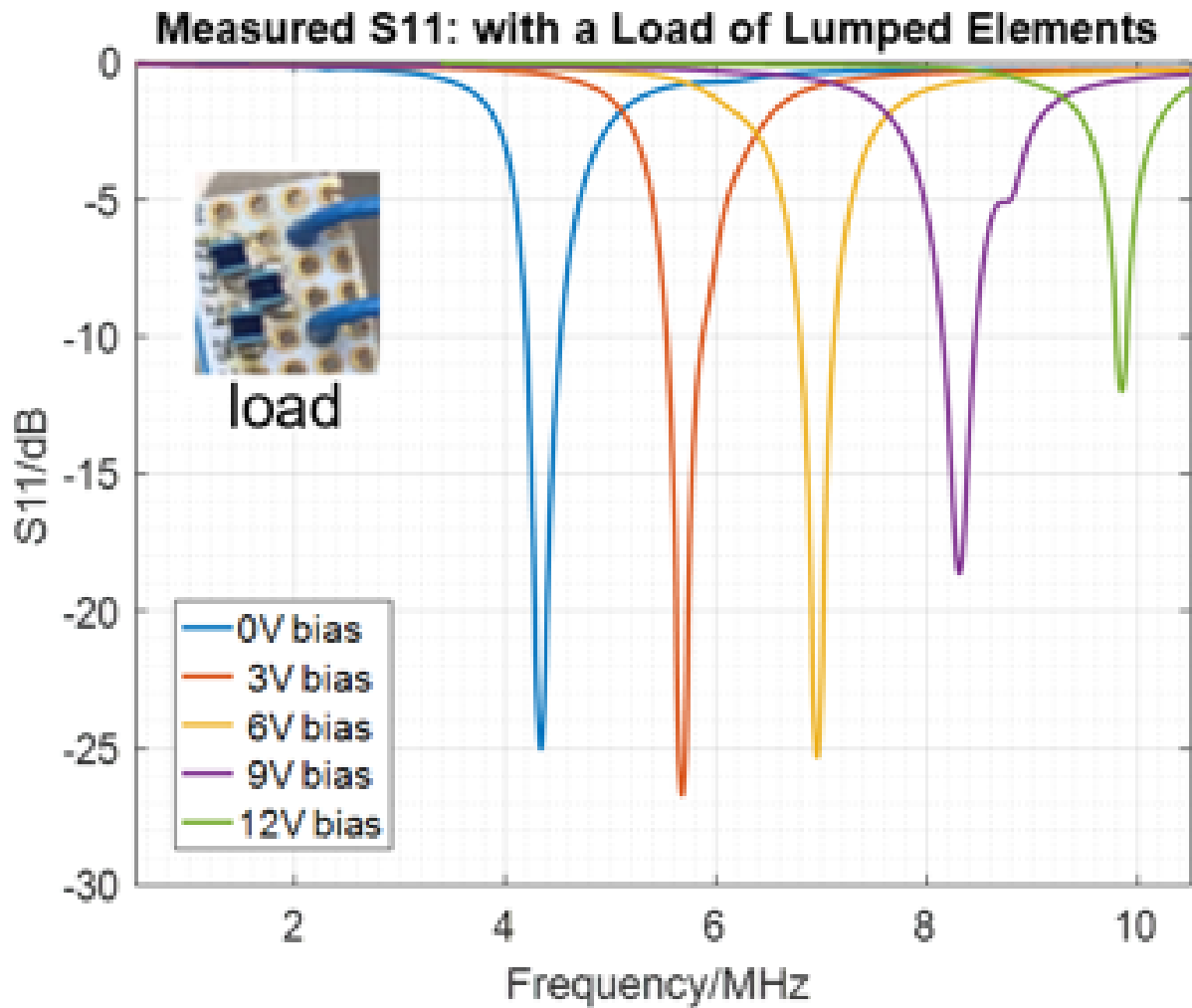


Figure 4.12: Measured S11 of the setup shown in Figure 4.11. The resonant frequency is electrically tuned through a wide range of frequencies with different bias voltage levels from 0V to 12V.

CHAPTER 5

Conclusions and Future Works

Electrically small loop antenna, with its unique linear frequency response and current distribution, has become a popular option for resonators. Its presence can be found in a variety of commercial devices, such as MRI receive coils, magnetic field probes and antenna tuners. Seeking through the heart of the applications, however, reveals that electrically small loop antenna has been monotonically used in a narrow-band operation with a mechanically tuned linear frequency response. This research aims to investigate the unprecedented wide-band electrical frequency tuning capability of an electrically small loop antenna through the lens of Mars exploration. More specifically, usage on a 0.8 — 10MHz wide-band dielectric spectrometer for hydration detection in the Martian subsurface is targeted for the design goals.

In the first part of the research work, a single-turn 1m by 1m electrically small loop antenna with mechanical frequency tunability is systematically studied. T-type impedance matching network is thoroughly investigated, mathematically derived and specifically designed for matching the antenna's input impedance. The proposed antenna design with continuous tuning frequency 0.8 — 10MHz is simulated and measured with fixed capacitors. The near-field electric and magnetic fields at 1MHz are simulated and are successfully matched with a modified analytical model to prove the impact of current distribution on the near-field radiation of an electrically small loop antenna. Additionally, two loop antennas, either coupled or decoupled, are investigated. Furthermore, a targeting 0.8 — 10MHz (1:12.5 ratio) continuous electrical resonance tuning has been demonstrated to be extremely difficult, through an exhaustive optimisation of the proposed T-type impedance network.

Yet, another novel and feasible design that tackles the aforementioned problems is presented in the second part of the research work: usage of a non-linear component and electri-

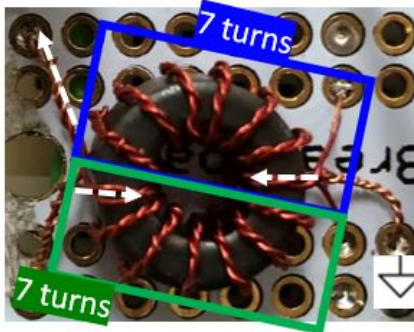
cally variable capacitors are at the core of the design. A wide-band reconfigurable electrically small multi-turn loop antenna has been designed, fabricated and measured for 0.8 — 10MHz operation to prove its accuracy and effectiveness. MEMS switch, is modeled and successfully integrated with the multi-turn loop antenna to achieve reconfigurability. Measured and simulated tuning capacitance max-to-min ratio agree well and satisfy the maximum achievable ratio of off-the-shelf varactors. Thus, an excellent electrical frequency tuning capability is proven through the simulation and the measurement. The simulated 6-meter deep electric and magnetic field patterns at 1MHz in air have the same peak magnitudes respectively as those in sand. Varactors and biasing circuitry have been designed and prototypes have been fabricated and tested for proof of concept.

For the future work in the scope of the application for Mars exploration, a more rigid conducting material than copper sheet (e.g., copper tube) needs to be considered for the reconfigurable electrically small multi-turn loop antenna design. Field tests using the proposed antennas need to be conducted to evaluate their signal sensitivity in a Mars-like environment. Beyond the scope of this application, the proposed electrical frequency tuning mechanism and reconfigurability of small loop using the MEMS switch have merits that are unique in the academia and industry of electrically small loop antennas. The same methodologies are also suitable for other applications at different frequencies of operation. For example, re-configuring the coil aperture size of MRI receive coils is often desired in certain clinical applications. MEMS switch is a winning option for achieving such reconfigurability. In addition, the presented varactor biasing structure in this work can be readily adapted for detuning MRI receive coil during RF transmission.

APPENDIX A

Transformer Fabrication

Upper half of the core: the left end of the bifilar #1 comes out from bottom of the core

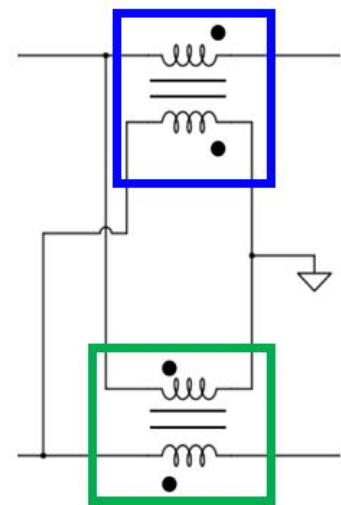


Upper half of the core: the right end of the bifilar #1 comes out from top of the core

Connections between two bifilar windings are twisted.

Lower half of the core: The left end of the bifilar #2 comes out from top of the core

Lower half of the core: the right end of the bifilar #2 comes out from bottom of the core



(b)

(a)

Figure A.1: Winding details of the 1:4 transmission-line transformer. (a) Illustration of the two pairs of 7-turn # 30 AWG bifilar windings on a ferrite core, and (b) corresponding schematic.

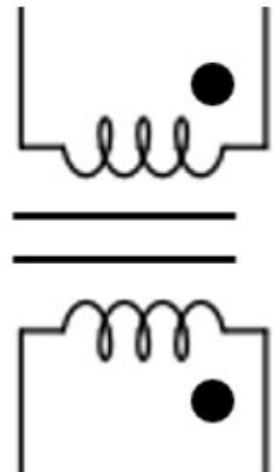
Appendix A emphasizes on the fabrication aspect of the transformers utilized in the impedance matching network proposed in Chapter 3. Pictorial illustrations of the winding positioning and phasing of the transmission-line transformers and RF current balun are available in Figures A.1 and A.2. Due to the deliberate design of the opposite phases on the two transformers in the 1:4 transmission-line transformer, the two pairs of windings (indi-

cated as blue and green in Figure A.1(a)) can share a single ferrite core without interference. The choices of the type of the wire, the number of turns, and the number of twists per inch are elaborated in Chapter 3.4.1. For operating near the lower cutoff frequency of the transmission-line transformer, the characteristic impedance of the winding is trivial and not necessarily needed to be 50-Ohm.

Figure A.3 shows the detailed steps taken to wind the transformer. It is crucial to ensure that the magnetic flux is confined within the toroidal structure of the transformer instead of leaking out, which would otherwise give rises to a high leaky loss. Ferrite core has an excellent performance on the transducer loss at the low frequencies, a much lower transducer loss than that of a core with less of a permeability (e.g., iron-powdered toroid). Also, use of a high-permeability magnetic core reduces the number of turns and length of wire needed to achieve the same magnitude of inductance, which would minimize the loss in the wire too.



14 turns
spread out
the entire
ferrite core.



(a)

(b)

Figure A.2: Winding details of the RF balun. (a) Illustration of the 14-turn # 30 AWG bifilar winding on a ferrite core, and (b) corresponding schematic.

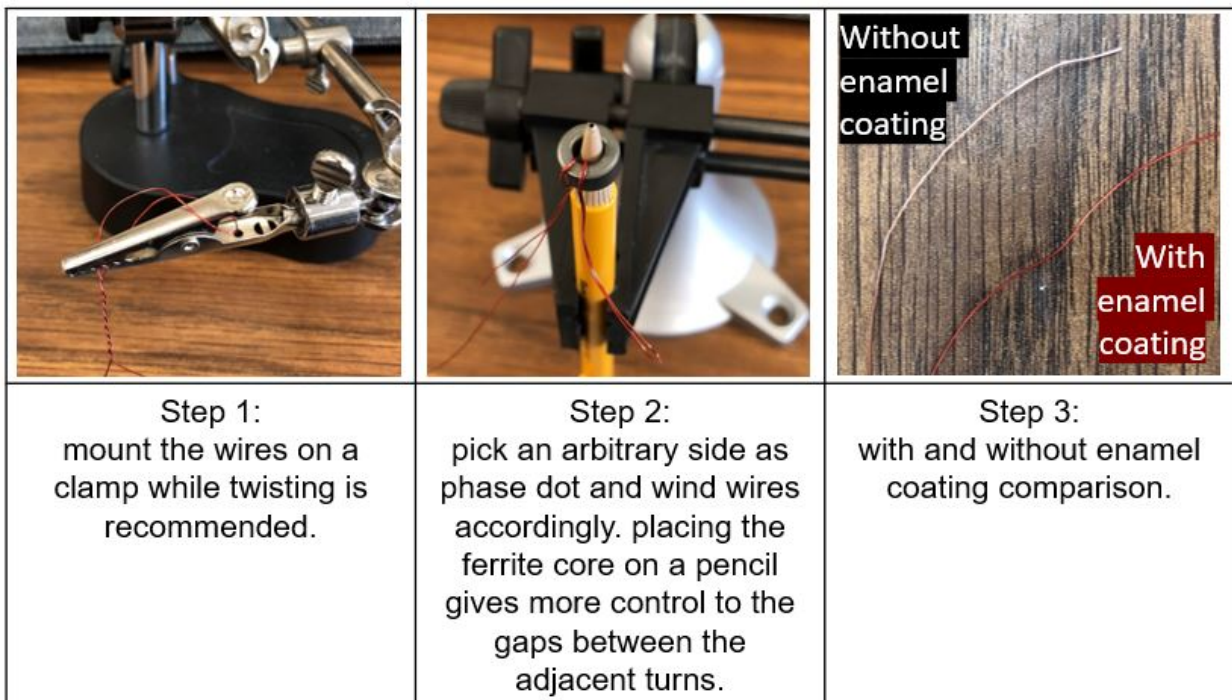


Figure A.3: Sequential steps of fabricating a transformer with an winding optimal layout, using #30 AWG wires and a ferrite core.

APPENDIX B

Efforts Toward Directional Radiation Pattern

A fundamental characteristic of electrically small loop antennas (the perimeter of which is less than one fifth of the wavelength) is that its radiated electric or magnetic field in the near-field region is symmetrical between the top and the bottom with respect to the plane of the loop. It is not a favorable characteristic in the application of this work because 1) the bidirectional radiation would interfere with the Mars rover chassis that the loops are mounted underneath and 2) in terms of the power efficiency, it means that we need to waste half of the input power. A tremendous amount of efforts has been taken in investigating potential solutions to alter the near-field radiation pattern of the electrically small loop antenna to make it more directional.

Small loop antenna duality states that a small loop of electric current I and of area A creates an electromagnetic field equivalent to that of an infinitesimal magnetic dipole (magnetic current element) with current equaling to $I_m \Delta l$ such that $j\omega\mu IA = I_m \Delta l$. Conceptually, according to image theory, as shown in Figure B.1 if we had a vertical infinitesimal magnetic dipole sitting above an infinite perfect electric conductor (PEC), the radiated fields in the upper half of the space would be numerically the same as removing the PEC and instead having a virtual magnetic dipole radiating along with the original dipole [1]. Applying image theory to the modified analytical model derived in Section 2.4.2 leads to analytical models of a copper tube electrically small loop antenna sitting 30 cm above an infinite PEC or PMC plane. A pictorial demonstration is shown in Figure B.2. To validate the image theorem, the aforementioned cases are simulated in CST. The simulation setup is shown in Figure B.3. The infinite PEC and PMC planes are implemented by boundary conditions of electric (tangential $E = 0$) and magnetic (tangential $H = 0$) respectively.

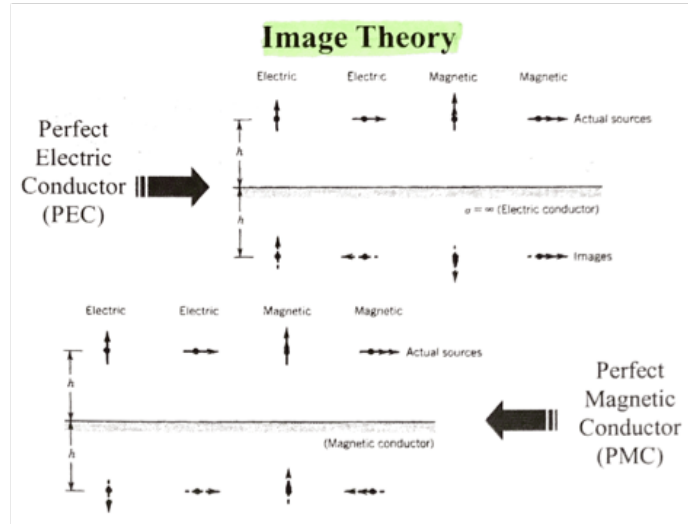


Figure B.1: Illustration of image theory [1].

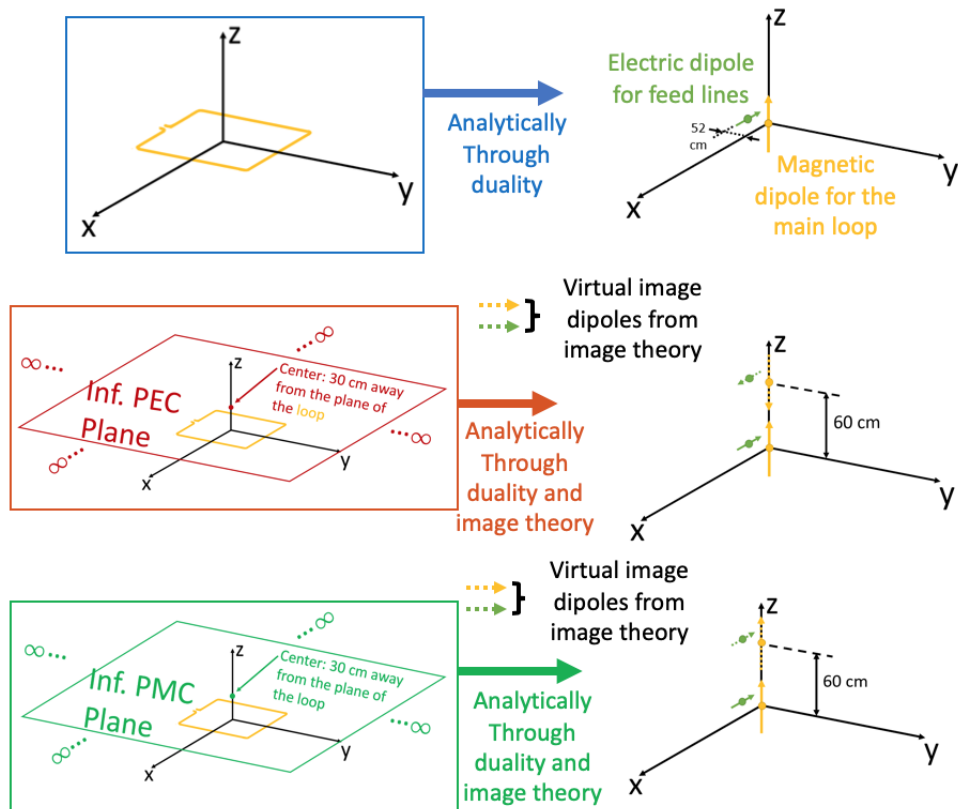


Figure B.2: Analytical models of an electrically small loop antenna in (a) free space, (b) 30 cm above an infinite PEC plane, and (c) 30 cm above an infinite PMC plane.

The simulated S11 is shown in Figure B.4. With the presence of an infinite PEC plane, the resonant frequency of the loop antenna is shifted up by 0.1 MHz. Whereas with an infinite PMC plane, the frequency is shifted down by 0.08 MHz.

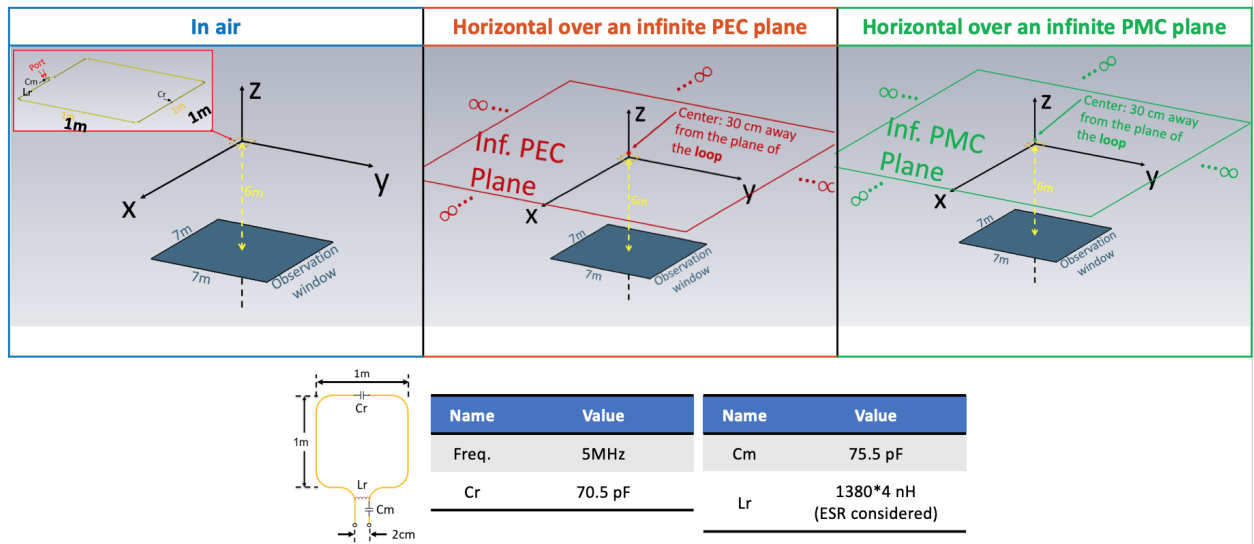


Figure B.3: CST simulation setups of 6-meter deep 7m-by-7m observation plane. The infinite PEC or PMC plane is implemented in CST by setting electric (tangential $E = 0$) or magnetic (tangential $H = 0$) boundary conditions.

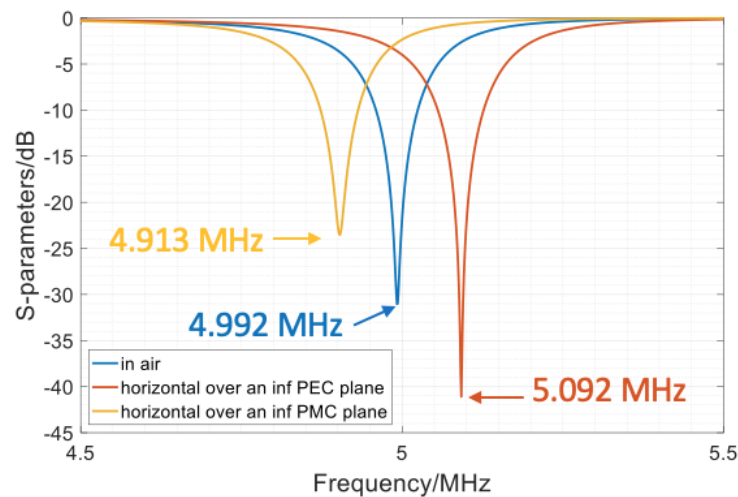


Figure B.4: Simulated S11 of an electrically small loop antenna in (a) free space, (b) 30 cm above an infinite PEC plane, and (c) 30 cm above an infinite PMC plane.

Horizontal over an infinite PEC plane

Frequency: 5.092 MHz

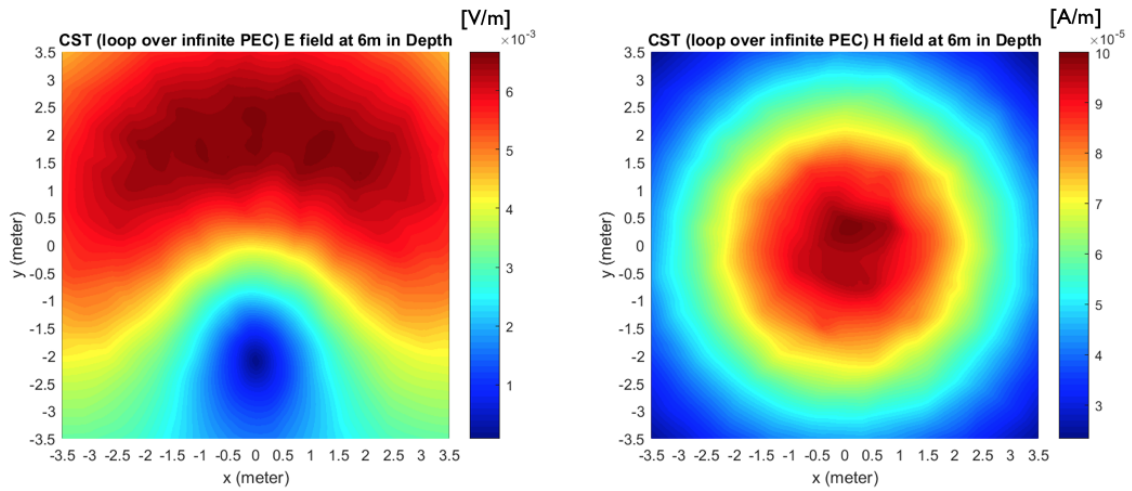


Figure B.5: Simulated 6-meter deep electric and magnetic fields of an electrically small loop antenna placed 30 cm above an infinite PEC plane.

Horizontal over an infinite PMC plane

Frequency: 4.913 MHz

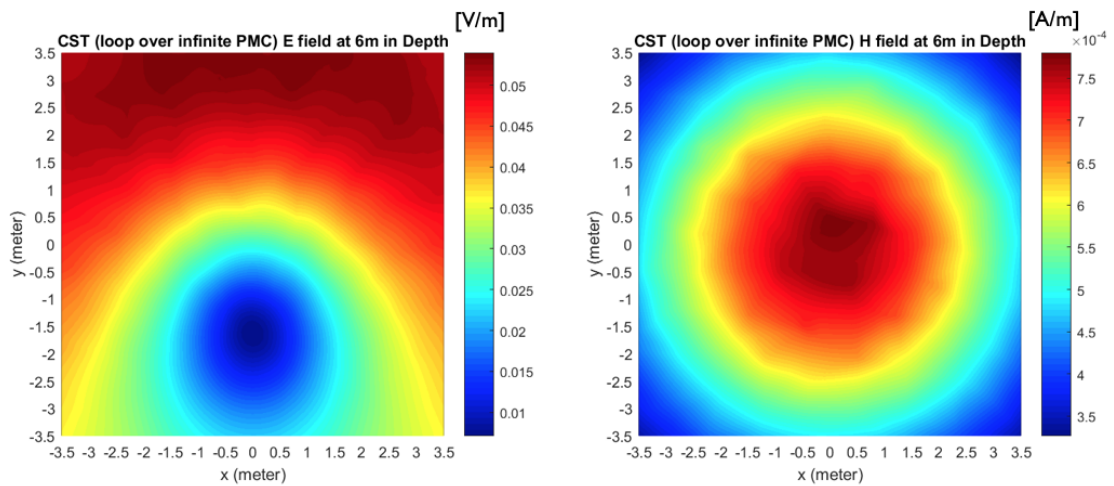


Figure B.6: Simulated 6-meter deep electric and magnetic fields of an electrically small loop antenna placed 30 cm above an infinite PMC plane.

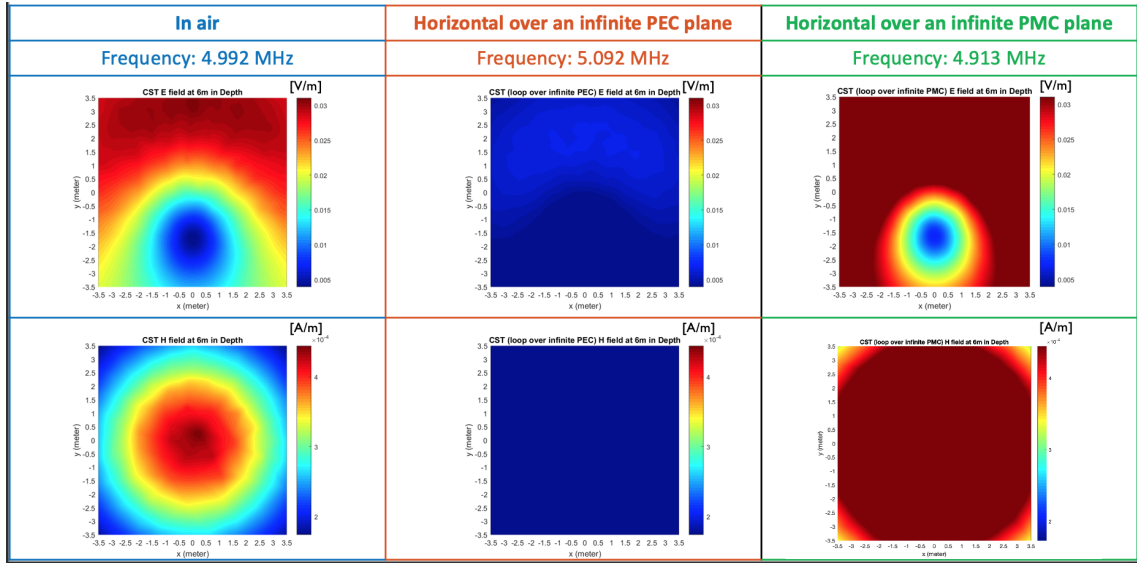


Figure B.7: Same-scale comparison of simulated 6-meter deep electric and magnetic fields of an electrically small loop antenna placed in (a) free space, (b) 30 cm above an infinite PEC plane, and (c) 30 cm above an infinite PMC plane.

Figure B.5, B.6 and B.7 show the simulated 6-meter deep electric and magnetic fields of the electrically small copper tube loop antenna 1) in air, 2) horizontal over an infinite PEC plane and 3) horizontal over an infinite PMC plane. For the PEC case, since the virtual dipoles (Figure B.2) are all pointing in the opposite direction as the original ones, part of the radiated electric or magnetic field at the observation point below the plane of the loop is cancelled out (determined via right-hand rule). Thus, in the CST simulation results, we see that the electrically small copper tube loop antenna's radiated electric and magnetic fields observed at 6m away are very minimal with the presence of the infinite PEC plane, compared to when it is in the air. For PMC however, the radiated electric and magnetic fields are larger than the loop antenna in the air case. It is consistent with the expectation through duality and image theory: the virtual dipoles are pointing in the same directions as the original dipoles, leading to addition of E and H fields from the original dipoles and the virtual dipoles.

Questions about power consumption may be raised: since the simulated S11 magnitude of the loop with the presence of the infinite PEC or PMC plane is maintained while the electric

and the magnetic fields are different, where does the power go at the resonant frequency? A tremendous effort has been taken to study the power distribution in a reactive near-field region around the loop antenna with an infinite PEC 30cm away. CST simulated electric and magnetic field results are shown in Figure B.8-B.18. From the simulated S11 results, with the same amount of input power, the electrically small 1m by 1m loop antenna radiates out of the loop a similar amount of power with or without the presence of an infinite PEC plate 30cm away. Note that the resonant frequency is affected and shifted up with the introduction of the infinite PEC. However, the power distribution around a sphere of same radius around the loop antenna is different between the cases of in or out the presence of the infinite PEC. When the loop antenna is in vacuum, the power is evenly distributed upward and downward with respect to the plane of the loop. Whereas when the loop antenna is 30cm away from an infinite PEC plate, most power is distributed between the plate and the loop, while less power is distributed in the space below the loop. The E and H vector fields are different with the introduction of the infinite PEC, which is expected due to the enforcement of PEC's boundary conditions. If an infinite PMC is used instead of PEC, more power will be distributed in the space below the loop rather than between the plate and the loop. Image theory still holds in the perspective of power consumption.

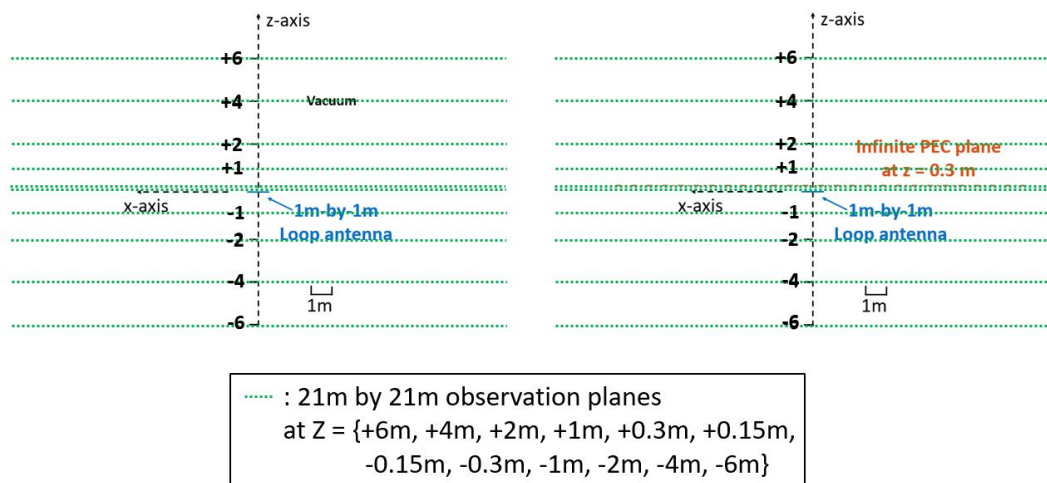


Figure B.8: Pictorial demonstration of the observation planes of electric and magnetic fields in Table B.1

Table B.1: Electric and Magnetic Fields Comparison

Horizontal cuts	E field maximum magnitude [V/m]		H field maximum magnitude [A/m]	
Vertical distance (Z=)	In air	Inf. PEC plate 30 cm away	In air	Inf. PEC plate 30 cm away
+6m	0.0438	0	0.0007	0
+4m	0.1174	0	0.0020	0
+2m	0.7283	0	0.0130	0
+1m	4.1451	0	0.0755	0
+0.3m	35.4063	62.7133	0.4506	0.6166
+0.15m	89.0516	92.6041	0.8499	0.9170
Loop antenna is positioned at Z = 0				
-0.15m	84.6944	78.1424	0.8150	0.7148
-0.3m	34.3965	30.1072	0.4420	0.3552
-1m	4.1012	3.0109	0.0743	0.0505
-2m	0.7227	0.4073	0.0130	0.0068
-4m	0.1174	0.0396	0.0019	0.0006
-6m	0.0457	0.0099	0.0007	0.0001

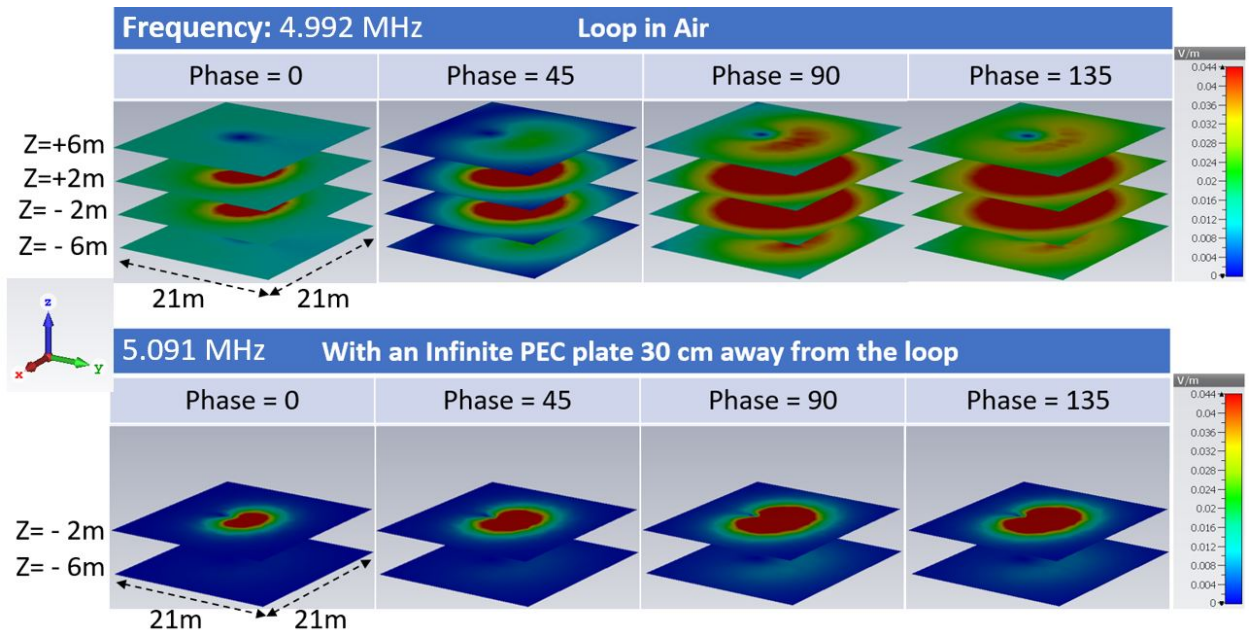


Figure B.9: E Field at $Z= +6, +2, -6, -2$ m

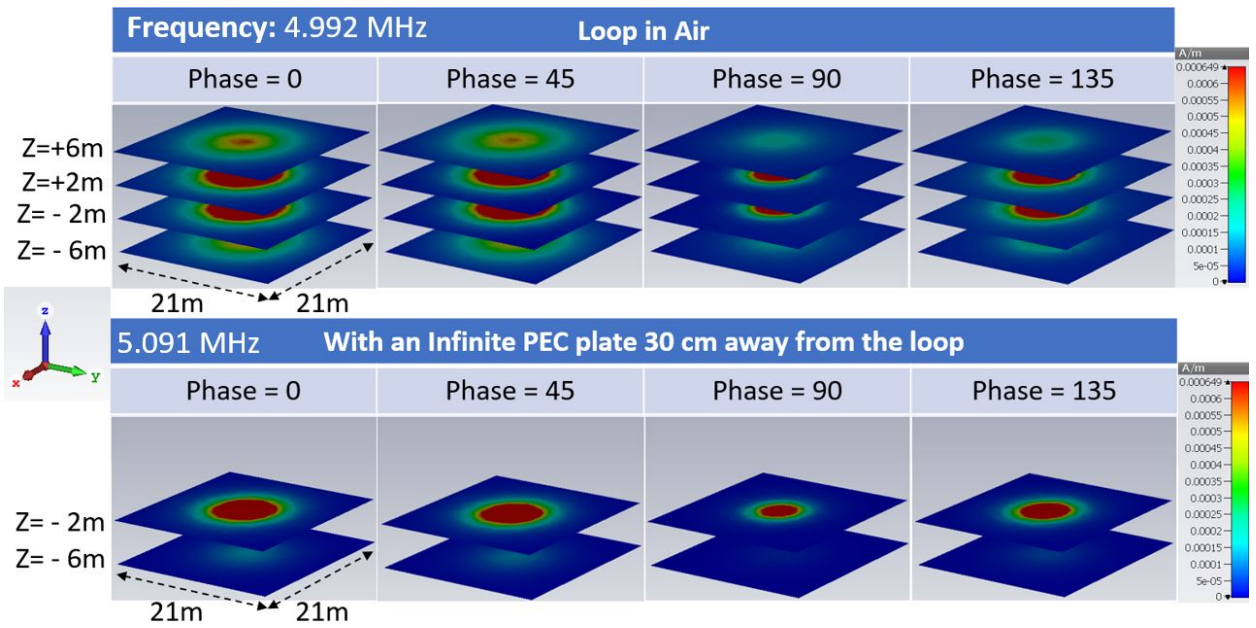


Figure B.10: H Field at $Z= +6, +2, -6, -2$ m

E Field of the Loop in Air at Z=+0.3m

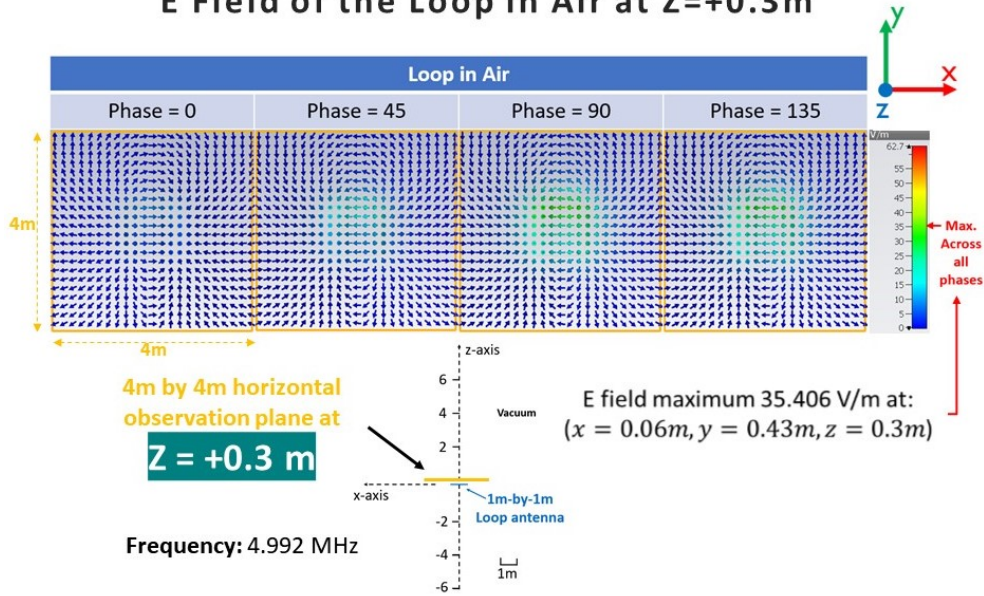


Figure B.11: E Field of the Loop in Air at Z=+0.3m

E Field of the Loop with an Infinite PEC at Z=+0.3m

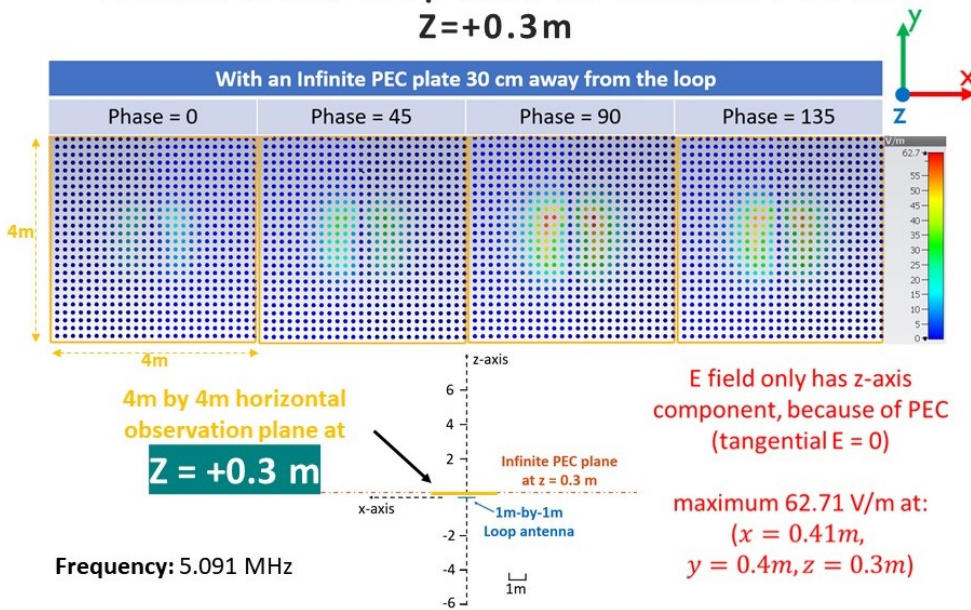


Figure B.12: E Field of the Loop with an Infinite PEC at Z=+0.3m

H Field of the Loop in Air at Z=+0.3m

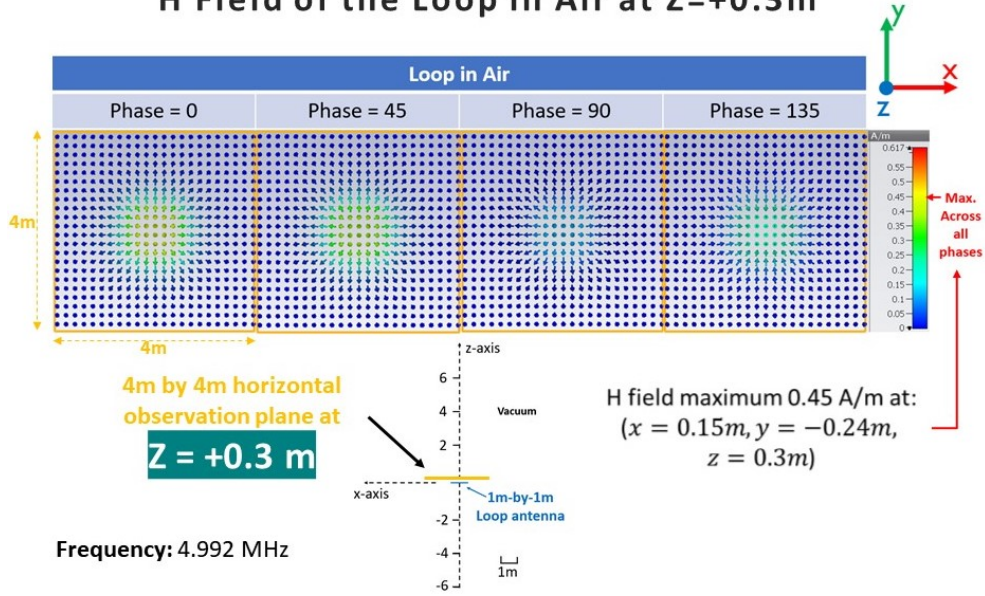


Figure B.13: H Field of the Loop in Air at Z=+0.3m

H Field of the Loop with an Infinite PEC at Z=+0.3m

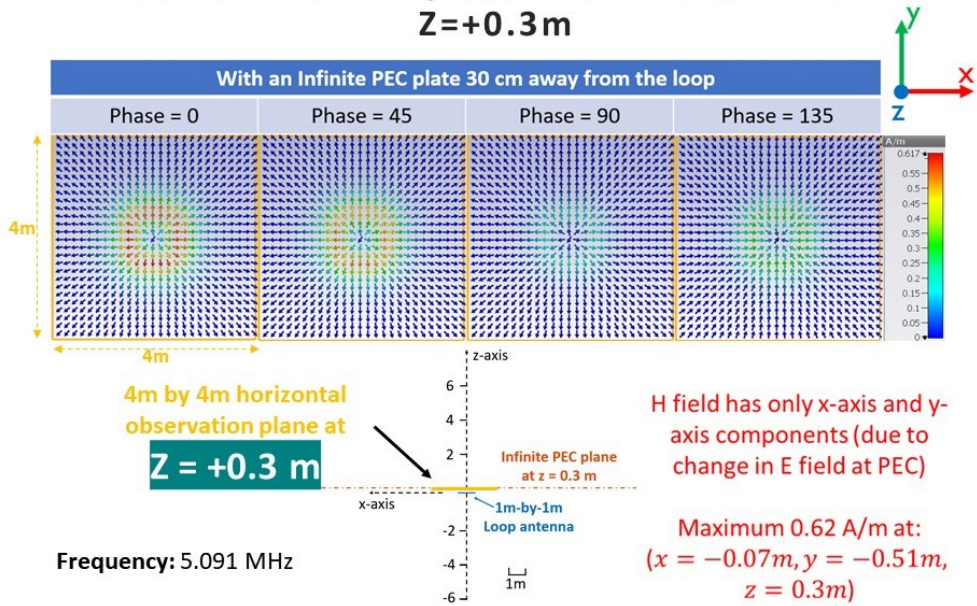


Figure B.14: H Field of the Loop with an Infinite PEC at Z=+0.3m

E Field of the Loop in Air at $Z=+0.15\text{m}$

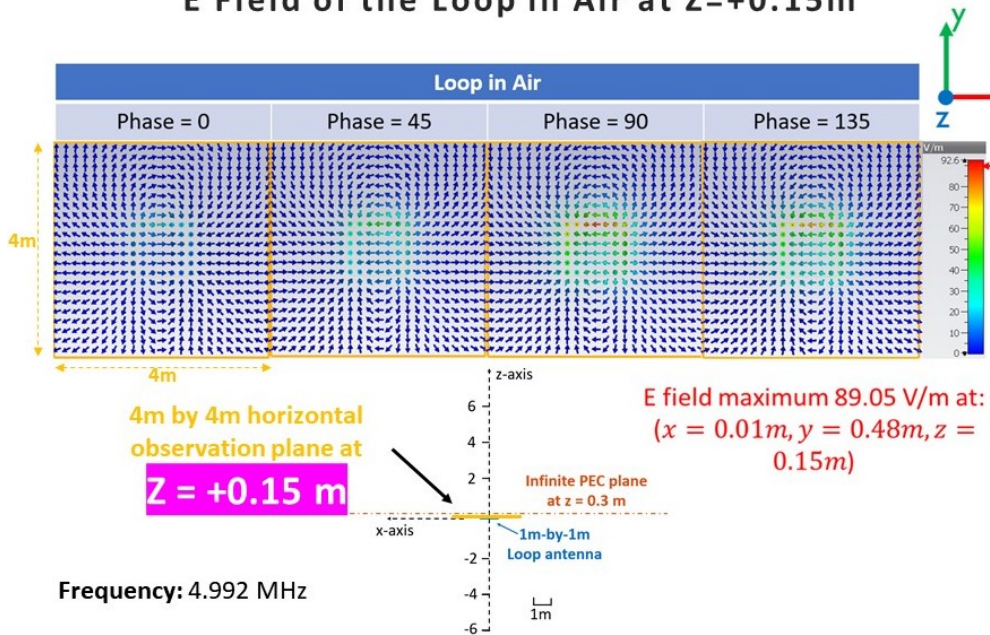


Figure B.15: E Field of the Loop in Air at $Z=+0.15\text{m}$

E Field of the loop with an Infinite PEC at $Z=+0.15\text{m}$

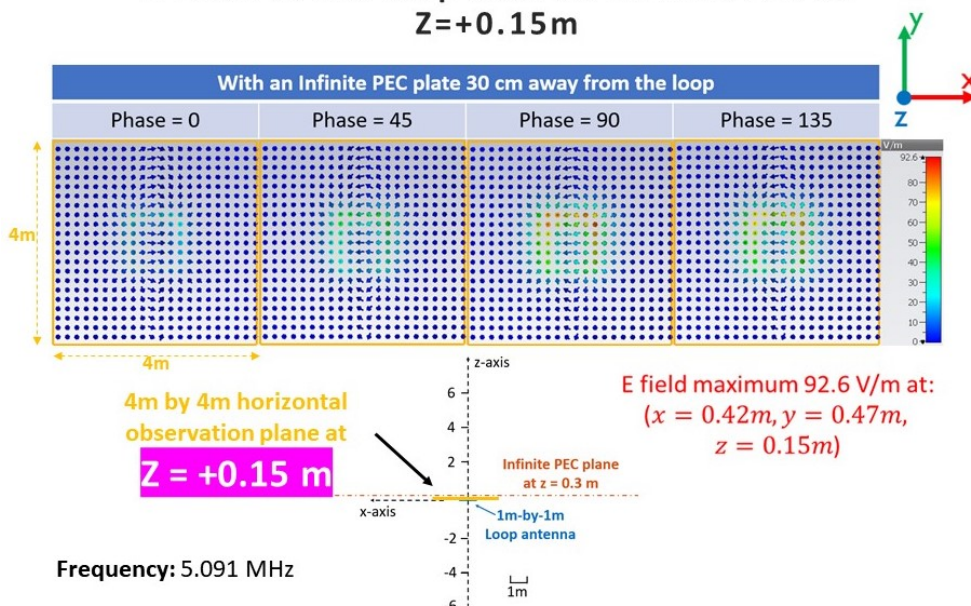


Figure B.16: E Field of the loop with an Infinite PEC at $Z=+0.15\text{m}$

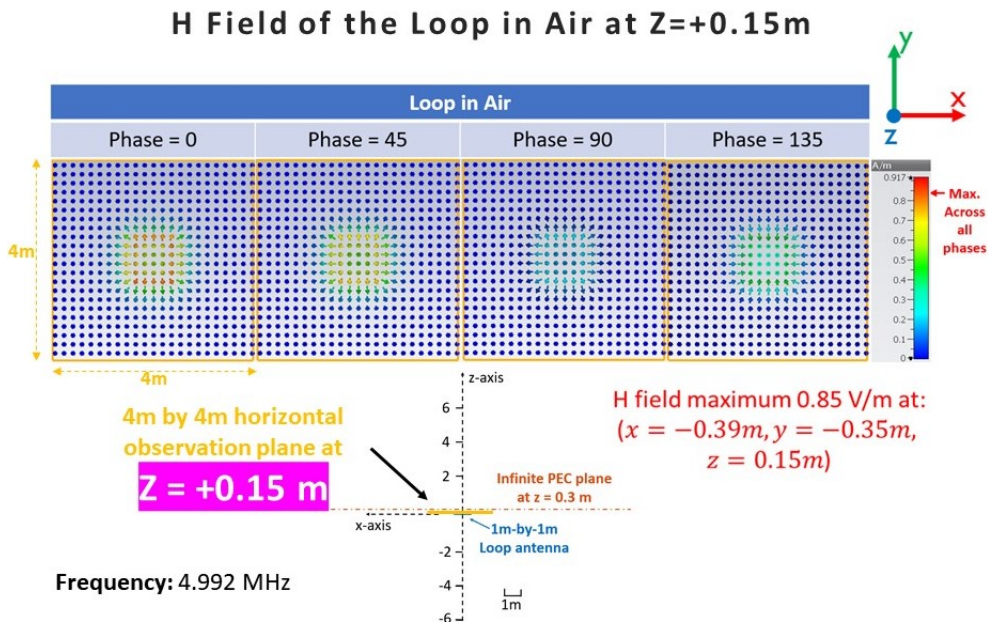


Figure B.17: H Field of the Loop in Air at $Z=+0.15\text{m}$

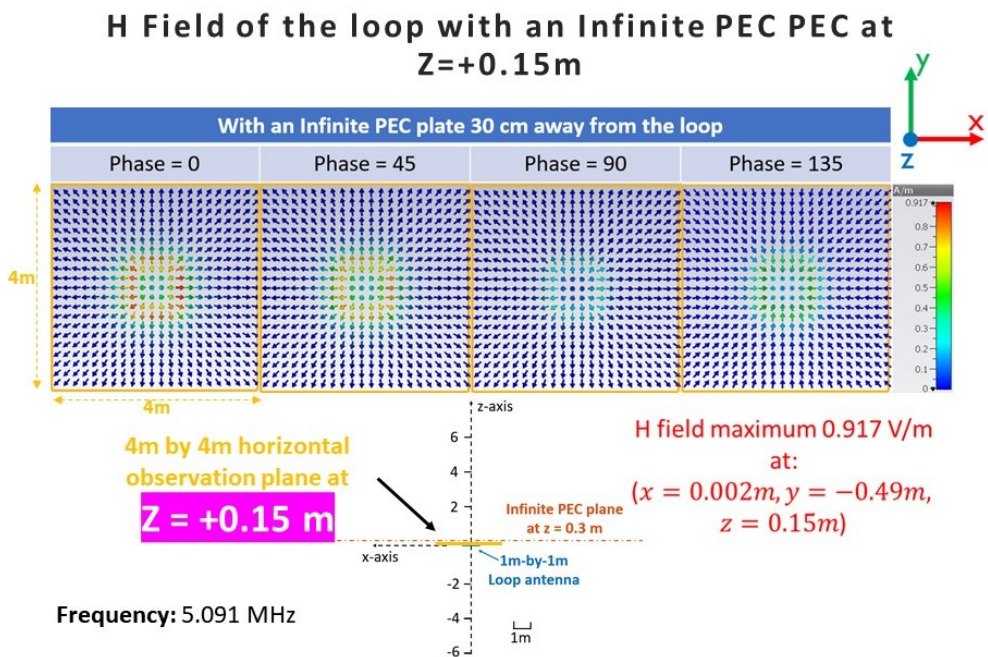


Figure B.18: H Field of the loop with an Infinite PEC at $Z=+0.15\text{m}$

However, in reality such setup is nearly impossible to achieve, because 1) PMC is a hypothetical artificial material that can be made possible through an electromagnetic band-gap structure, which would be impractically humongous, if it were to be implemented to operate

in a frequency as low as 1—10MHz, and 2) usually an infinite plane can be approximated to be finite sized but sufficiently large (e.g., several wavelengths), whereas in this application, a single wavelength is already impractically large in a range of 30 to 375 meters. Although the problem is conceptually unsolvable, a more quantitative understanding of it is desired, relying on the CST full-wave electromagnetic simulation.

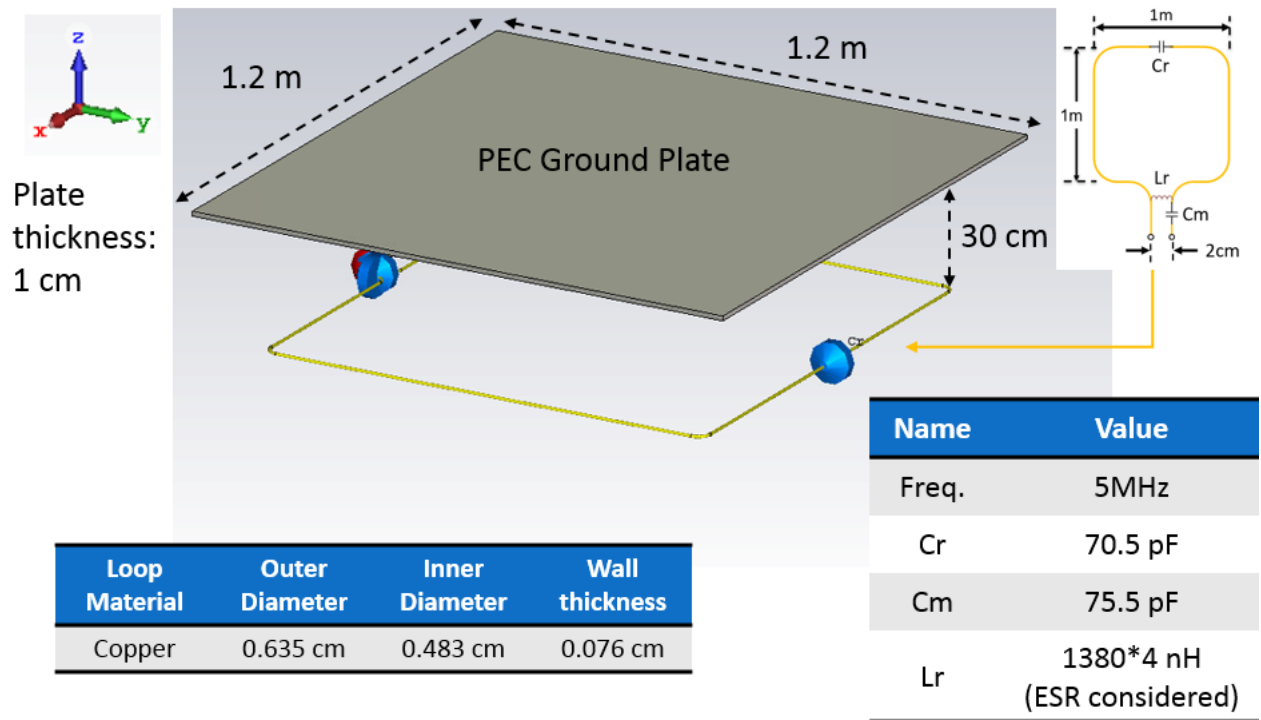


Figure B.19: CST full-wave electromagnetic simulation setup of a copper tube single-turn loop antenna resonating at 5MHz in the presence of a PEC ground plate. The dimensions of the copper tube are tabulated. The capacitance and inductance used for resonant frequency tuning are also shown.

For the purpose of preliminary investigation, the copper tube single-turn loop antenna proposed in Chapter 2 is investigated. 5MHz, at the center of the desired 0.8 — 10MHz operation, is chosen as the primary frequency of interest. The wavelength at 5MHz is 60 meters, whereas the perimeter of the loop antenna is roughly 4 meters — corresponding to one fifteenth of the wavelength. The first attempt in enforcing a more directional radiation of the electrically small loop antenna is to have a perfect electric conductor (PEC) ground plane

in vicinity of the antenna. Modeled in CST, a 1.2m by 1.2m meter 1-cm thick PEC ground plate is positioned 0.3m away from the plane of the loop antenna (shown in Figure B.19). With the presence of the PEC plate the S11 performance of the loop antenna is nearly unchanged, compared to the without case. The simulated near-field electric and magnetic field at zero phase results are shown in Figure B.20, the top and bottom observation windows generate almost the same field pattern and order of magnitude. The results show that with such a PEC plane underneath the electrically small loop antenna, its electric and magnetic field patterns observed in the near-field region are unaltered.

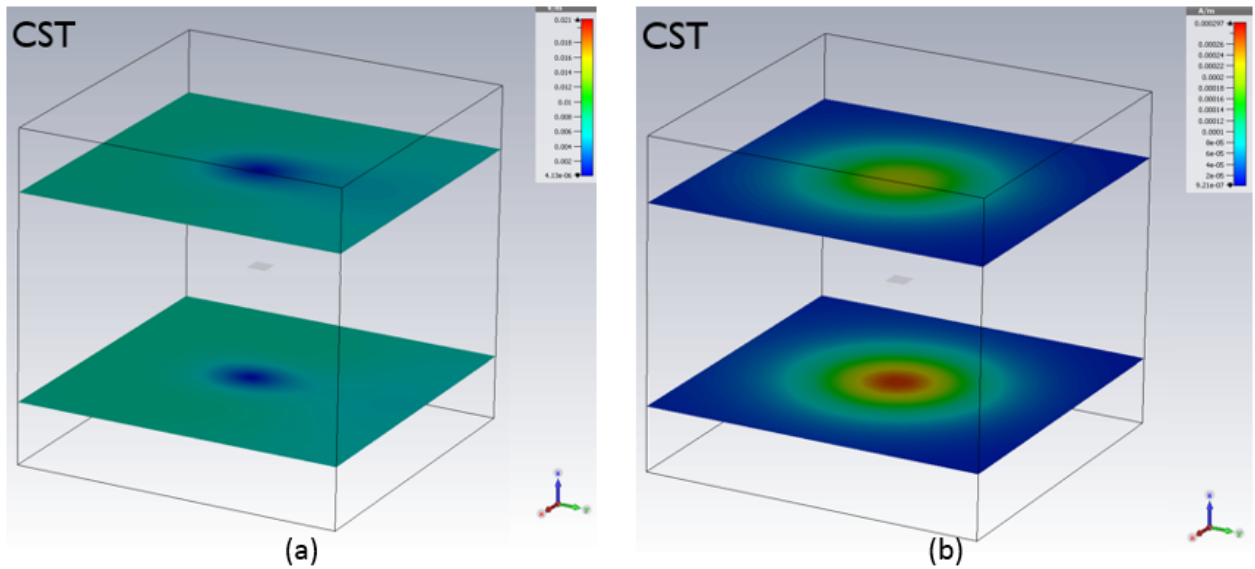


Figure B.20: Simulated fields at 5MHz, zero-phase, with a 21.2m by 21.2m planar observation window. Top window is 6m away from the PEC plate and the bottom window is 6m away from the loop. (a) near-field electric field, and (b) near-field magnetic field.

Furthermore, an idea of having a parasitic PEC plate or box with cutouts is investigated. Three case studies are presented hereafter: a copper-tube single-turn loop antenna simulated 1) with a parasitic 1mm-thick $1.2m \times 1.2m$ PEC plate with 18-degree apart slots, 2) with a parasitic 1mm-thick $1.4m \times 1.4m \times 0.3m$ bottom-open box with 18-degree apart slots, and 3) with a parasitic 1mm-thick $1.4m \times 1.4m \times 0.3m$ bottom-open box with 9-degree apart slots. The thickness and the size choices of the simulated PEC plate or box are from a standpoint of practicality. From the results shown in Figure B.21— B.29, the effects of the parasitic

plane and box on the near-field bidirectional radiation of the electrically small loop have shown to be very minimal. The limited physical space available around the loop antenna, relative to the wavelength, makes it extremely difficult to alter the inherent radiation pattern of the electrically small loop antenna. In this part of the work, although only curved 1/4 in-diameter copper tube loop at 5MHz operation is considered, it is a good representation of the performance of other design variations of the electrically small loop antenna, as long as its footprint is still within 1m by 1m.

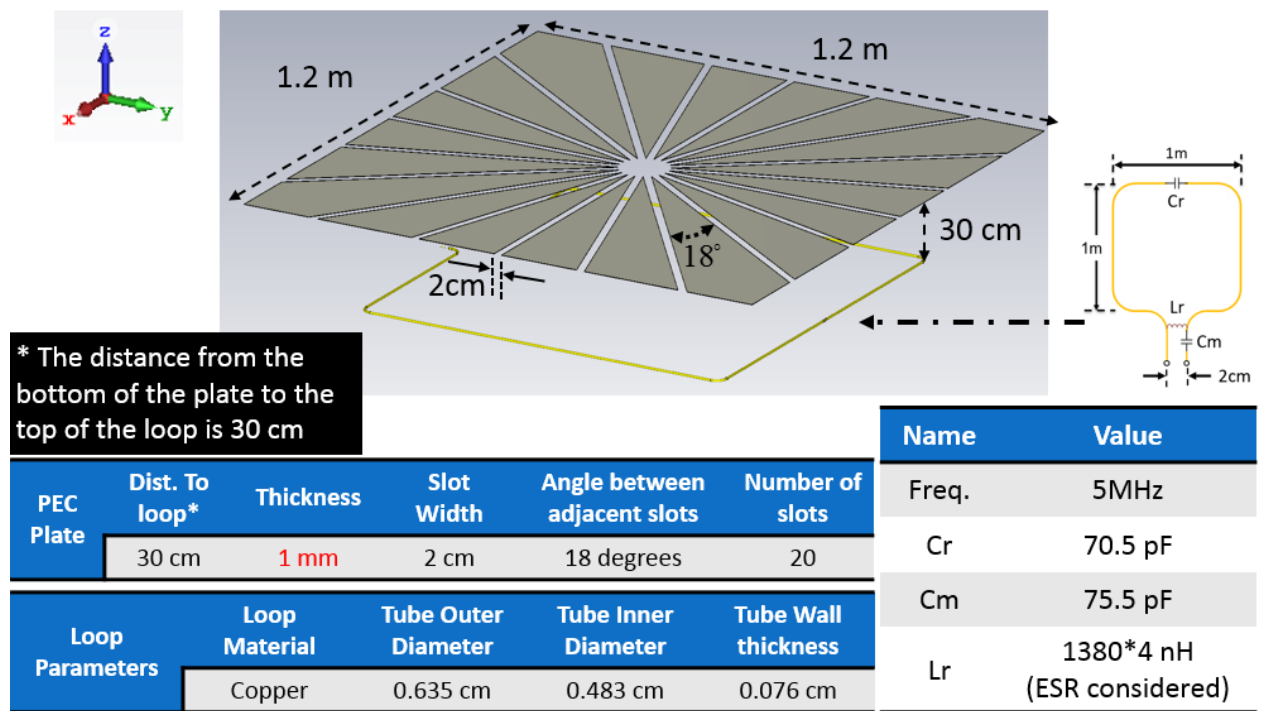


Figure B.21: Simulation setup of a copper tube single-turn loop antenna resonating at 5MHz in the presence of a PEC plate with 18-degree slots. The dimensions of the copper tube are tabulated. The capacitance and inductance used for resonant frequency tuning are also shown.

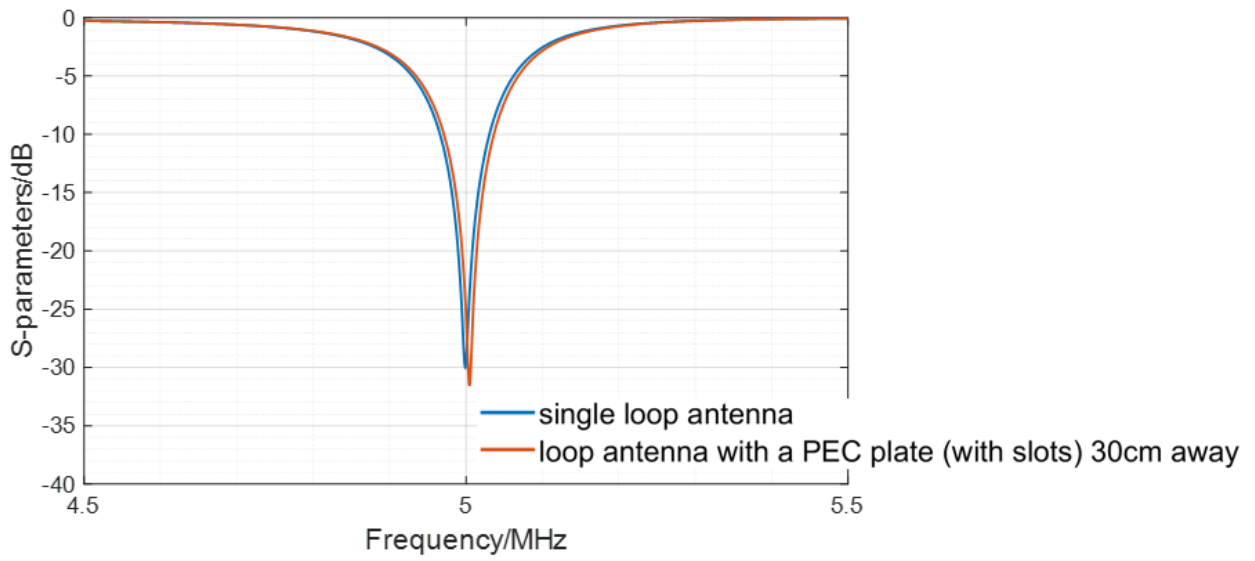


Figure B.22: Simulated S11 comparison of the loop antenna with and without the presence of a PEC plate with slots. Simulation setup is shown in Figure B.21.

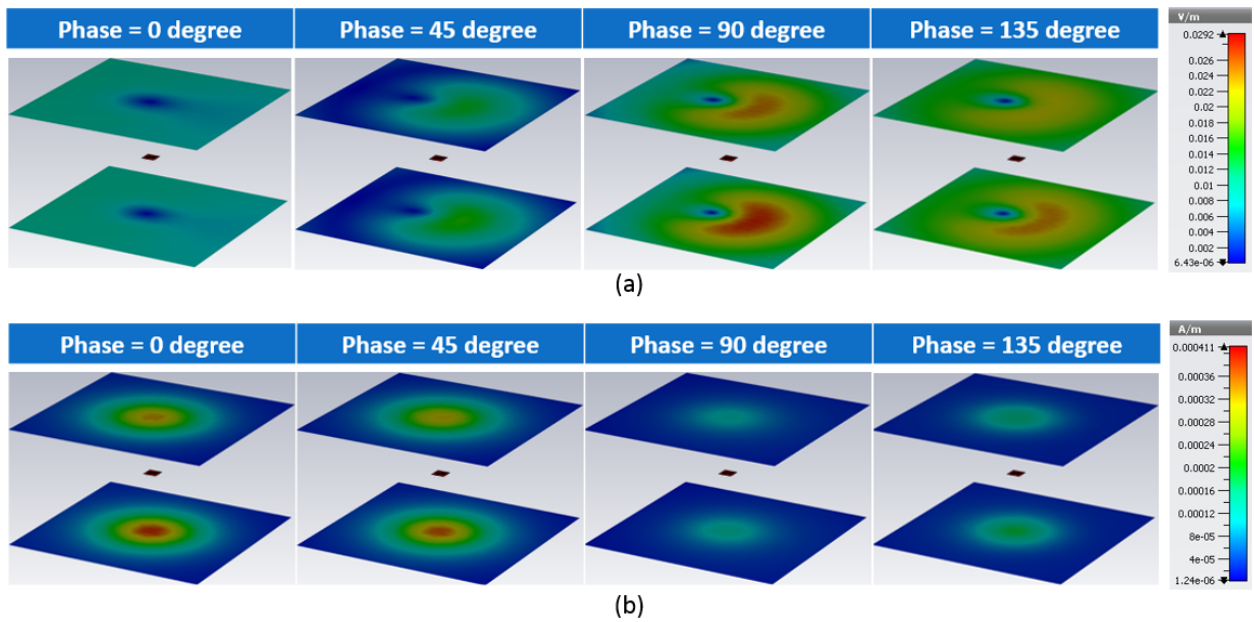
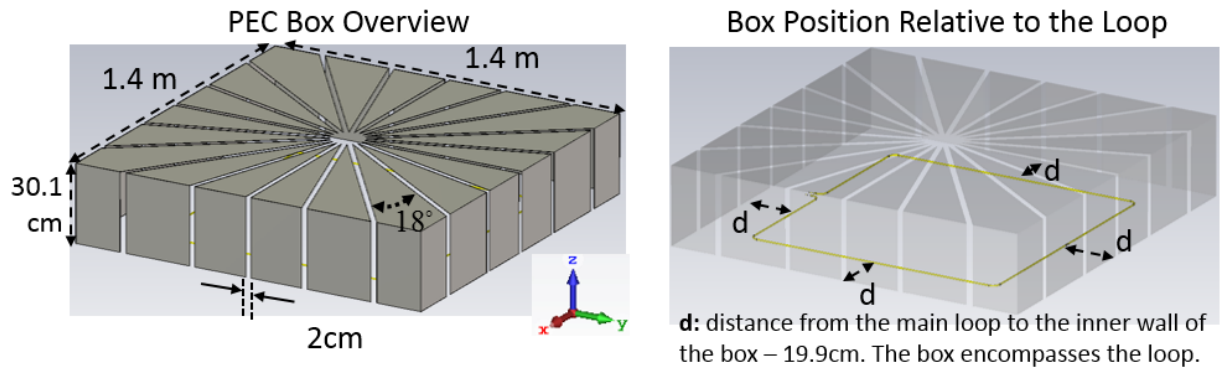


Figure B.23: Simulated fields at 5MHz with a 21.2m by 21.2m planar observation window. Top window is 6m away from the PEC plate and the bottom window is 6m away from the loop. (a) near-field electric field, and (b) near-field magnetic field.



PEC Box						Value	
Size of the box	Sheet Thickness	Slot Width	Angle between adjacent slots	Number of slots		Freq	5MHz
	140cm*140cm*30.1cm	1 mm	2 cm	18 degrees	20	Cr	70.5 pF
Loop Parameters	Loop Material	Tube Outer Diameter	Tube Inner Diameter	Tube Wall thickness		Cm	75.5 pF
	Copper	0.635 cm	0.483 cm	0.076 cm		Lr	1380*4nH (ESR considered)

Figure B.24: Simulation setup of a copper tube single-turn loop antenna resonating at 5MHz in the presence of a PEC bottom-open box with 18-degree slots. The dimensions of the copper tube are tabulated. The capacitance and inductance used for resonant frequency tuning are also shown.

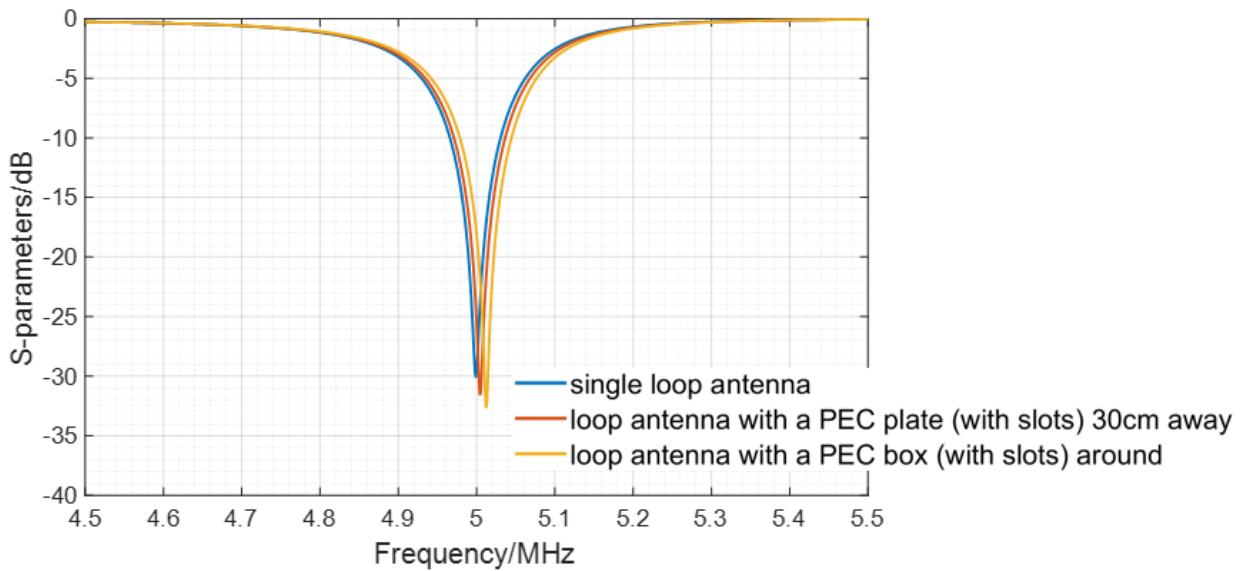
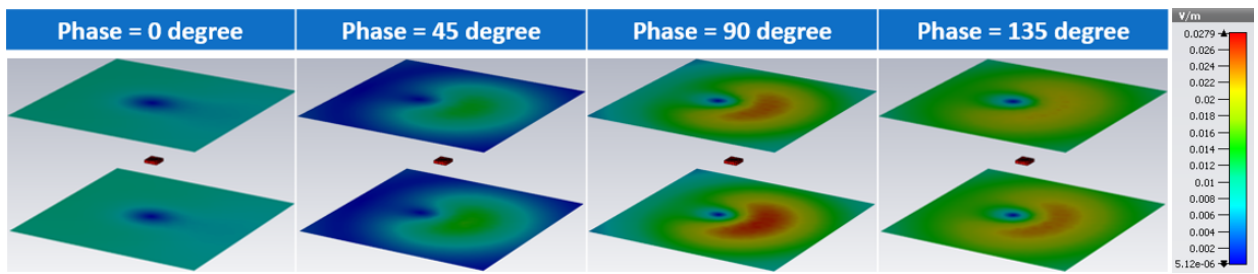
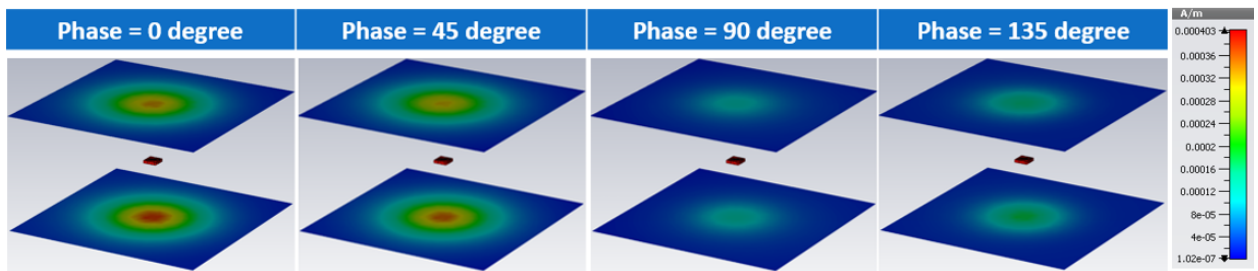


Figure B.25: Simulated S11 comparison of the loop antenna with and without the presence of a PEC bottom-open box with 18-degree slots. Simulation setup is shown in Figure B.24.



(a)



(b)

Figure B.26: Simulated fields at 5MHz with a 21.2m by 21.2m planar observation window. Top window is 6m away from the PEC box and the bottom window is 6m away from the loop. (a) near-field electric field, and (b) near-field magnetic field.

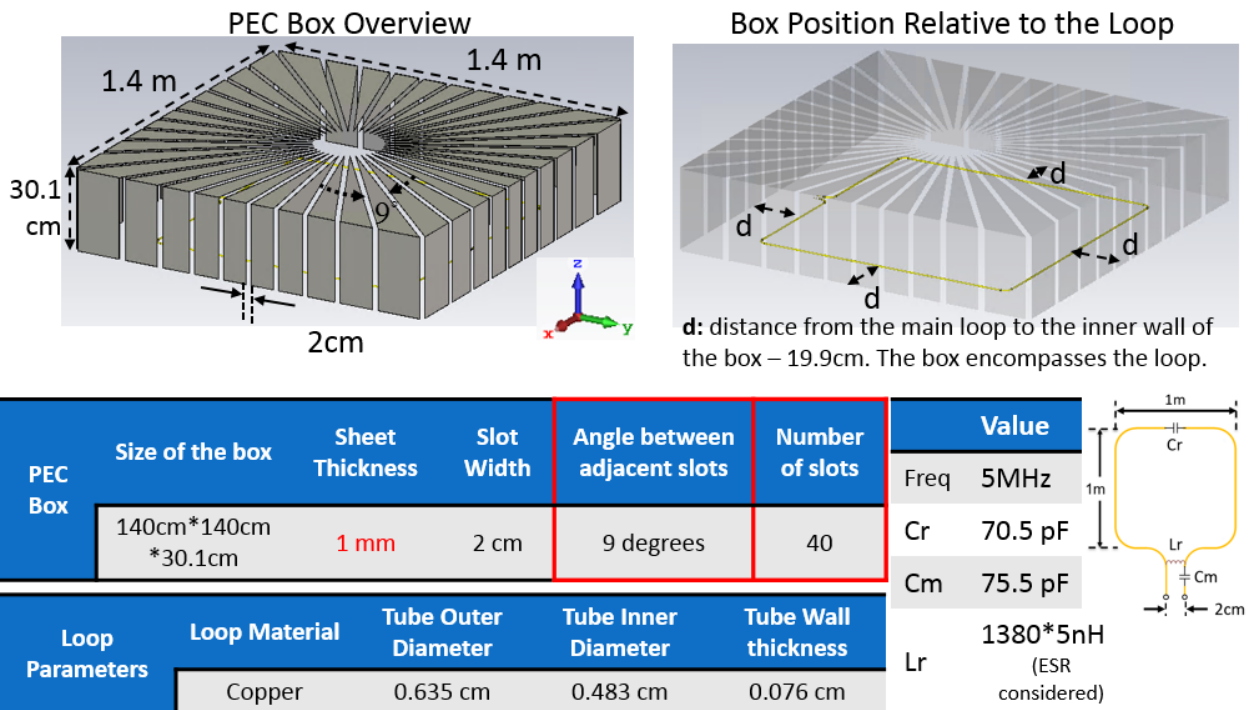


Figure B.27: Simulation setup of a copper tube single-turn loop antenna resonating at 5MHz in the presence of a PEC bottom-open box with 9-degree slots. The dimensions of the copper tube are tabulated. The capacitance and inductance used for resonant frequency tuning are also shown.

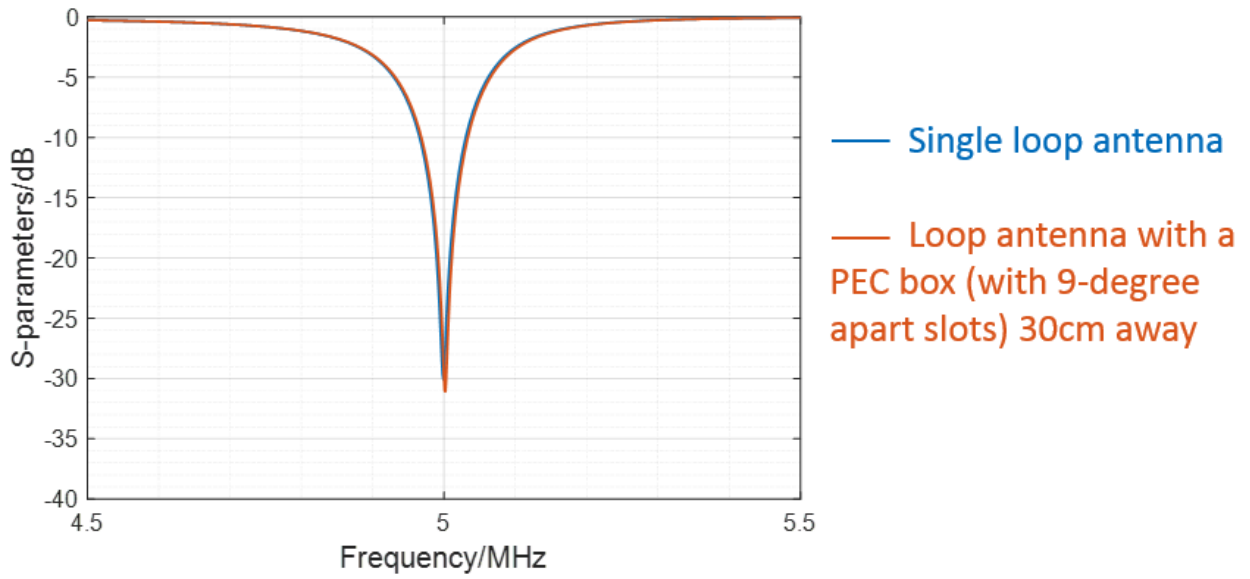


Figure B.28: Simulated S11 comparison of the loop antenna with and without the presence of a PEC bottom-open box with 9-degree slots. Simulation setup is shown in Figure B.27.

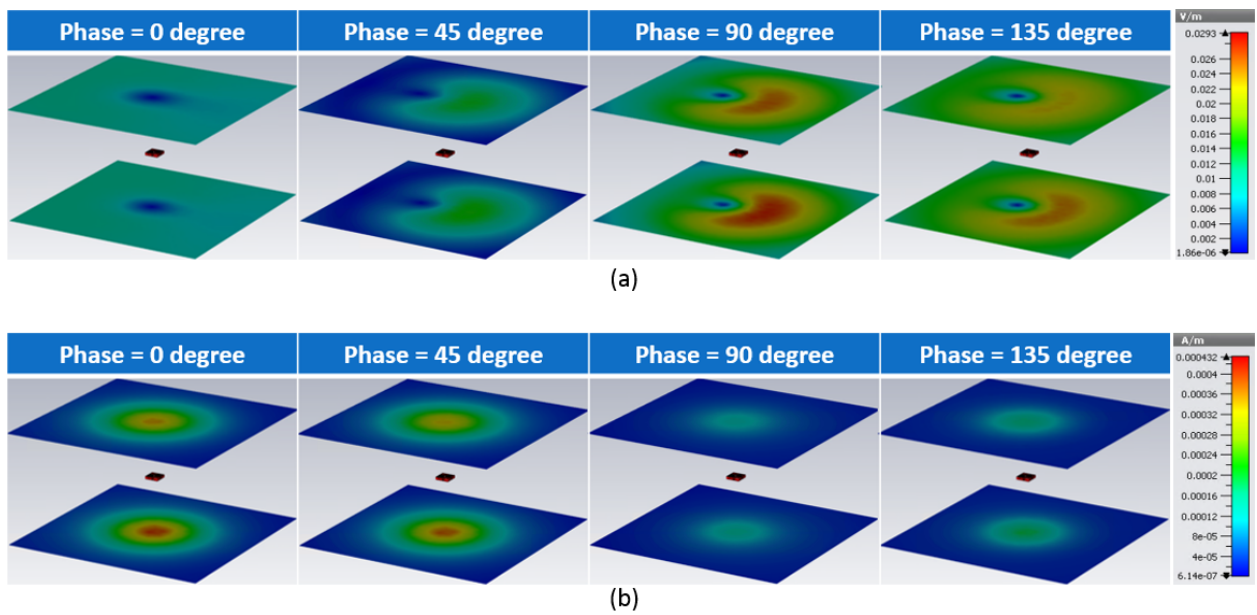


Figure B.29: Simulated fields at 5MHz with a 21.2m by 21.2m planar observation window. Top window is 6m away from the PEC box and the bottom window is 6m away from the loop. (a) near-field electric field, and (b) near-field magnetic field.

REFERENCES

- [1] C. A. Balanis, *Antenna Theory Analysis and Design*. Wiley Online Library, 2005.
- [2] C.M. Dundas, A. M. Bramson, L. Ojha, J. J. Wray, M. T. Mellon, S. Byrne, A. S. McEwen, N. E. Putzig, D. Viola, S. Sutton, E. Clark, and J. W. Holt, “Exposed Subsurface Ice Sheets in the Martian Mid-Latitudes,” *Science*, vol. 359, issue 6372, pp. 199-201, Jan. 2018.
- [3] E.M. Cheng¹, M. F. Abdul Malek², S. F. Khor³, K. Y. You⁴, K.Y. Lee⁵, M. A. Rojan¹, S. Abu Bakar¹, N. F. Mohd Nasir¹, Z. Zakaria¹, and W. H. Tan¹, “Reflection and Dielectric Measurement for Salinity of Water Using Microstrip Loop Antenna and Dielectric Probe,” *International Journal of GEOMATE*, Aug., 2016, Vol. 11, Issue 24, pp. 2335-2340.
- [4] H. F. Morrison, A. Ratti, E. Gasperikova, “System and method for groundwater detection and evaluation,” U.S. Patent 10126456B2, Jan 7, 2016.
- [5] J. T. Vaughan, and J. R. Griffiths, *RF Coils for MRI*. Wiley Online Library, 2012.
- [6] Keck Institute for Space Studies at California Institute of Technology, [Online]. Available: <http://kiss.caltech.edu/>.
- [7] A. Grebennikov, *RF and Microwave Transmitter Design*. Wiley Online Library, 2011.
- [8] Questions and Answers in MRI, “Receive-only RF coils,” Elster LLC, [Online]. Available: <http://mriquestions.com/receive-only-coils.html>.
- [9] HF-automatic antenna tuner, Palstar, [Online]. Available: <http://www.palstar.com/en/hf-auto/>.
- [10] LF-R 400 H-Field Probe 100 kHz up to 50 MHz, “Receive-only RF coils,” Langer EMV-Technik, [Online]. Available: <https://www.langer-emv.de/en/product/lf-passive-100-khz-50-mhz/36/lf-r-400-h-field-probe-100-khz-up-to-50-mhz/2>.
- [11] B. Gruber, M. Froeling, T. Leiner, and D. W. J. Klomp, “RF Coils: A Practical Guide for Nonphysicists,” *Journal of magnetic resonance imaging*, vol. 48-3, pp. 590–604, Jun. 2018.
- [12] J. M. Kovitz, and K. W. Allen, “Recent developments toward reconfigurable mmWave apertures and components using vanadium dioxide RF switches,” *2018 IEEE 19th Wireless and Microwave Technology Conference (WAMICON)*, Sand Key, FL, pp. 1-4, 2018.
- [13] E. Carty, P. Fitzgerald, and P. McDaid, “The Fundamentals of Analog Devices’ Revolutionary MEMS Switch Technology,” Analog Device, Inc., [Online]. Available: <https://www.analog.com/en/technical-articles/fundamentals-adi-revolutionary-mems-switch-technology.html>

- [14] G. Guanella, "New Method of Impedance Matching in Radio-Frequency Circuits," *The Brown Boveri Review*, pp. 327-3, Sep. 1944.
- [15] J. Sevick, *Transmission Line Transformers*, Norcross: Noble Publishing, 2001.
- [16] C. Trask, "Transmission Line Transformers: Theory, Design and Applications," *High Frequency Electronics*, vol. 4, pp. 46–53, Dec. 2005, vol. 5, pp. 26–33, Jan. 2006.
- [17] E. Rotholz, "Transmission-Line Transformers," *IEEE Trans. Microwave Theory Tech.*, vol. MTT-29, pp. 148–154, Apr. 1981.
- [18] J. Horn and G. Boeck, "Design and Modeling of Transmission Line Transformers," *Proc. IEEE SBMO/MTT-S Int. Microwave and Optoelectronics Conf.*, vol. 1, pp. 421–424, Sept. 2003.
- [19] G. D. Vendelin, A. M. Pavio, and U. L. Rohde, *Microwave Circuit Design Using Linear and Nonlinear Techniques*. Wiley Online Library, 2005.
- [20] M. H. Norwood, and E. Shatz, "Voltage variable capacitor tuning: A review," in *Proceedings of the IEEE*, vol. 56, no. 5, pp. 788-798, May 1968.
- [21] Skyworks Solutions, Inc., [Online]. Available:
https://www.skyworksinc.com/-/media/SkyWorks/Documents/Products/301-400/SMV1801_079LF_200915G.pdf